DYNAMIC SCAFFOLDING IN A G-PROTEIN SIGNALING CASCADE

APPROVED BY SUPERVISORY COMMITTEE

Rama Ranganathan, M.D., Ph.D.

Leon Avery, Ph.D.

Ege Kavalali, Ph.D.

Elliott M. Ross, Ph.D.

DYNAMIC SCAFFOLDING IN A G-PROTEIN SIGNALING CASCADE

by

PRASHANT MISHRA

DISSERTATION / THESIS

Presented to the Faculty of the Graduate School of Biomedical Sciences

The University of Texas Southwestern Medical Center at Dallas

In Partial Fulfillment of the Requirements

For the Degree of

DOCTOR OF PHILOSOPHY

The University of Texas Southwestern Medical Center at Dallas

Dallas, Texas

May, 2009

ACKNOWLEDGEMENTS

I would like to thank Dr. Rama Ranganathan, first and foremost, for his continual support, encouragement and insight during the completion of this body of work. In addition, I would like to thank all the members of the Ranganathan lab for useful comments, discussions and criticism. Specific acknowledgements go to Dr Mark Wall and Michael Socolich for crystallography data, as well as Drs. Zifen Wang and Jennifer Graves for construction and analysis of transgenic fly lines. Acknowledgements also go to Drs. F. El-Mazouni, D. DeCamp, M. Mumby, A. Huber, A. Fayyazuddin and P. Heisinger for assistance with various experiments performed in this thesis. Financial support from the UT Southwestern Medical Scientist Training Program and DCMB training grant was greatly appreciated. Lastly, I would like to thank my wife and my family for continued encouragement during my PhD years.

DYNAMIC SCAFFOLDING IN A G-PROTEIN SIGNALING CASCADE

Prashant Mishra, Ph.D.

The University of Texas Southwestern Medical Center at Dallas, Graduation Year

Supervising Professor: Rama Ranganathan, M.D., Ph.D.

The InaD scaffold organizes a multi-protein complex that is essential for proper visual signaling in *Drosophila* photoreceptor cells. Here we show that one of the InaD PDZ domains (PDZ5) exists in a redox-dependent equilibrium between two conformations– a reduced form which is similar to the structure of other PDZ domains, and an oxidized form in which the ligand-binding site is distorted through formation of a strong intramolecular disulfide bond. We demonstrate transient light-dependent formation of this disulfide bond *in vivo*, and find that transgenic flies expressing a mutant InaD in which PDZ5 is locked in the reduced state display severe defects in termination of visual responses and visually-mediated reflex behavior. These studies demonstrate a novel conformational switch mechanism for PDZ domain function and suggest that InaD

behaves more like a dynamic machine rather than a passive scaffold, regulating signal transduction at the millisecond timescale through cycles of conformational change.

TABLE OF CONTENTS

LIST OF FIGURES

LIST OF TABLES

LIST OF APPENDICES

N/A

LIST OF DEFINITIONS

AC – adenylyl cyclase

AKAP – A-kinase anchoring protein

AMS – 4-acetamido-4’-maleimidylstilbene-2,2’-disulfonic acid (molecular weight =536.44Da)

Arr2 – βarrestin 2

C645S – Cys645Ser mutation

Ca2+ - calcium

cam - calmodulin

cAMP – cyclic adenosine monophosphate

Cdc42 – cell division cycle 42

Cy3m – Cy3 maleimide

DTT - dithiothreitol

Fus3 – cell fusion 3

GPCR – G-protein coupled receptor

Gβ – heterotrimeric G-protein β

Gq – heterotrimeric Gq-protein α

GRIP – glutamate receptor interacting protein

GST – glutathione-S-transferase

inaC – inactivation no afterpotential C

InaD – inactivation no afterpotential D

K+ - potassium

L1, L2 – large monopolar cells

LMC – large monopolar cell

MAPK – mitogen-activated protein kinase

Na+ - sodium

NinaC – neither inactivation nor afterpotential C

ninaE – neither inactivation nor afterpotential E

NorpA – no receptor potential A

PAGE – polyacrylamide gel electrophoresis

Par-6 – partitioning defective 6

Pd - palladium

PDE4D3 – type 4 phosphodiesterase

PDZ – post-synaptic density 95, discs large, zona occludens 1

PDZ1 – 1st PDZ domain of InaD

PDZ5 – 5th PDZ domain of InaD

pegM – pegylated maleimide (molecular weight = 5kD)

PIP2 – phosphatidylinositol-4,5,-bisphosphate

PITP – phosphatidylinositol transfer protein

PKA – protein kinase A

PKC – protein kinase C

PLC-β – phospholipase C β

PP2B – protein phosphatase 2 B

PSD – post-synaptic density

PSD-95 – post-synaptic density 95

PSD95-PDZ3 – 3rd PDZ domain of PSD-95

Pt - platinum

pY - phosphotyrosine

Se - selenium

R1, R2, R3, … R8 – photoreceptor cells

rdgB – retinal degeneration B

Rh1 – Rhodopsin isoform 1

Rim1α - Rab3-interacting molecule 1α

RMSD – root mean square deviation

SDS – sodium dodecyl sulfate

SH3 – Src homology 3

Shank – SH3 domain and ankyrin repeat containing protein

Ste5 – sterile 5

Ste11 – sterile 11

TCA – trichloroacetic acid

TCEP – Tris(2-carboxyethyl)phosphine hydrochloride

TRP – transient receptor potential

Chapter One
Introduction

Scaffolding and signaling

Proper subcellular localization of signal transduction proteins is critical for cellular information processing. One primary mechanism for localizing components is the use of scaffolding molecules – proteins which bind and organize three or more members of a common catalytic pathway into macromolecular complexes (Bhattacharyya et al., 2006b). The importance of scaffolding has been demonstrated in numerous signaling pathways; examples include the Ste5 scaffold in the mitogen-activated protein kinase (MAPK) cascade (Morrison and Davis, 2003), the A-kinase anchoring proteins (AKAPs) involved in protein kinase A signaling (Wong and Scott, 2004), the RIM proteins involved in organization of the neuronal pre-synaptic active zone (Schoch et al., 2002), and the numerous scaffolds (e.g., PSD-95, GRIP, Shank) involved in organization of the neuronal post-synaptic density. By concentrating appropriate signaling proteins to local environments within cells, scaffolds reduce cross-talk and increase reaction kinetics, thereby promoting efficient and specific cellular signaling. The above examples highlight the generality of this mechanism in biology.

Having successive members of a signaling cascade arranged in close spatial proximity should certainly enhance the speed and specificity of signaling. But do scaffolds have other roles important for cellular physiology? Data from multiple systems suggest that this may be the case; scaffolds are also important for maintenance of cellular identity, morphology and polarity (Hardy et al., 2007; Hung et al., 2007), for feedback regulation of the signaling cascade itself (Bhattacharyya et al., 2006a; Lonart et al.,

2003), and, likely, for evolution of novel signaling cascades (Bhattacharyya et al., 2006b). These data, though recent, suggest that much may be learned through a detailed analysis of scaffolding proteins, from an atomic to organismal scale.

The Drosophia eye

The *Drosophila melanogaster* phototransduction system, has served as a prototypical model for understanding scaffolding (Hardie and Raghu, 2001; Huber et al., 1996a; Montell, 2005; Tsunoda and Zuker, 1999). Visual signaling initiates in the retina, which is composed of an ordered array of a large number of hexagonal ommatidia; each ommatidium is composed of eight photoreceptor cells (R1-R8), the first order neurons responsible for sensing light. The photoreceptor cells are arranged concentrically around the outer edge of the ommatidia and each projects a specialized organelle, known as the rhabdomere, into the central canal (Figure 1-1A-C). The rhabdomere is a collection of ~30,000 microvilli; each about 1μm long and 50nm in diameter, containing a single actin filament (allowing visualization by standard staining methods (Figure 1-1B)). Light absorption takes place in these microvilli, leading to a depolarization signal which is transmitted via the cell body and axon to 2nd order neurons.

Absorption of light in a microvillus is achieved via molecules of rhodopsin, a member of the class A G-protein coupled receptors (GPCRs), containing a chromophore (3-hydroxyretinal) which isomerizes upon light absorption. Signaling initiated by rhodopsin activation triggers a depolarization signal in the photoreceptor (see below) which is passed on to 2nd order neurons. The R1-R6 photoreceptors express the major rhodopsin of the eye, the blue-light sensitive Rh1, and are responsible for motion

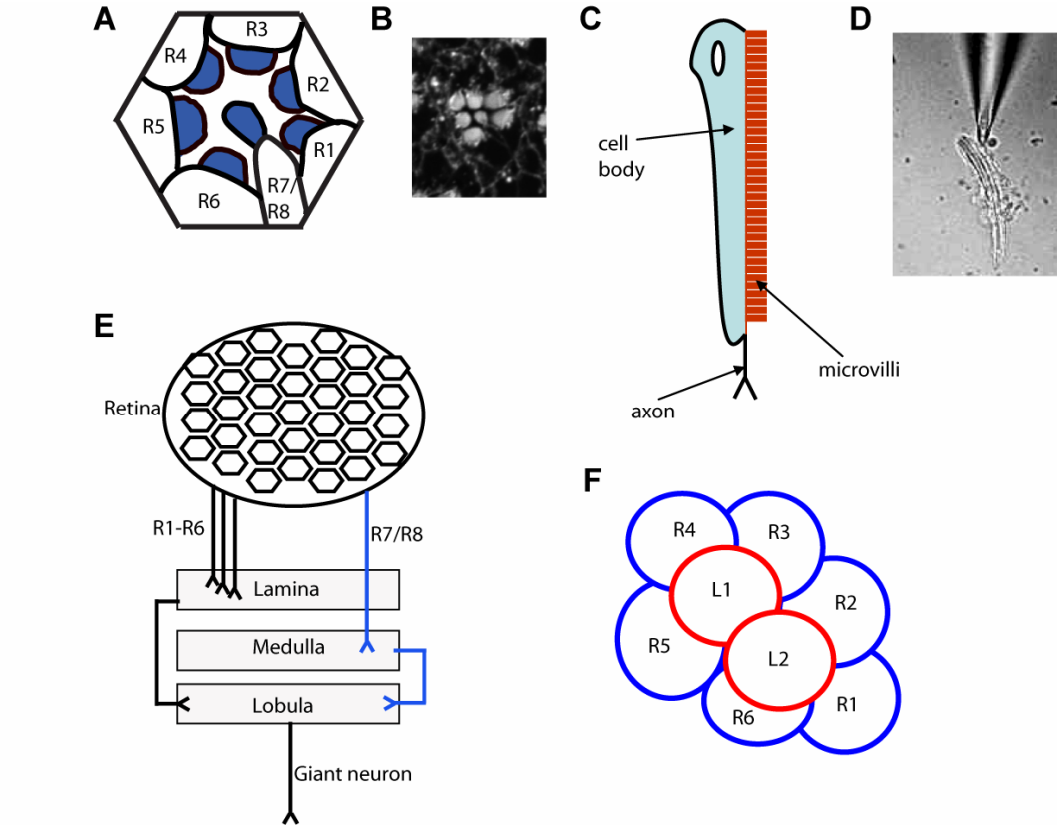

Figure 1-1 Organization of the *Drosophila* visual signaling system. (A) Schematic of a *Drosophila* ommatidium. Photoreceptor cell bodies (R1-R8) are arranged concentrically around a central canal; each photoreceptor projects a collection of microvilli (rhabdomeres, blue) into the central canal to sense light. (B) Cross-section of an ommatidium stained with rhodamine-conjugated phalloidin (which preferentially binds actin). The actin-rich rhabdomeres of the R1-R7 cells can be visualized. (C) Schematic of a photoreceptor cell. Light absorption takes place in the microvilli; light-induced depolarization is transmitted via the cell body and axon to downstream neurons. (D) An isolated ommatidium; whole-cell path clamping can be performed via direct access to a photoreceptor cell membrane. (E) Axons from R1-R6 photoreceptors project to the lamina for image processing. R7/R8 axons bypass the lamina and project to the medulla for color vision. Neurons from the lamina and medulla synapse in the lobula for higher-order processing and signaling to the giant neurons. (F) Schematic of a laminar cartridge. Axons from R1-R6 photoreceptors (blue) synapse with L1 and L2 large monopolar cells (red) in a stereotypic pattern.

detection and image processing in the fly. Axons from the R1-R6 cells project to the lamina (Figure 1-1E), where they synapse with 2nd order neurons (large monopolar cells,

or LMCs) in a stereotypical, ordered arrangement (Figure 1-1F) (Morante and Desplan, 2004). These "laminar cartridges" each receive inputs from six photoreceptor axons (one each from a R1-R6 cell), and are organized in a manner according to the principle of neural superposition – that is, axons from photoreceptor cells oriented toward the same point in visual space converge on the same laminar cartridge (Franceschini et al., 1981; Zeil, 1979). In contrast, the R7 and R8 cells express rhodopsins with different spectral sensitivity (UV, blue or green) (Feiler et al., 1992; Salcedo et al., 1999) and are responsible for color vision in the fly. Axons from R7 and R8 cells bypass the lamina and synapse in the medulla. 2nd order neurons from the lamina and medulla synapse with 3rd order neurons in the lobula, where higher order information processing and activation of the giant neurons takes place (Figure 1-1E) (Morante and Desplan, 2004).

Visual signaling in Drosophila

As mentioned earlier, the intital steps of visual signaling take place in the individual microvilli of the 1st order photoreceptor cell. The scaffolding protein, InaD (inactivation, no after-potential D), plays an important role in localizing a number of signaling proteins to this specialized organelles and assembling them into a specifc macromolecular complex (Hardie and Raghu, 2001). Figure 1-2 summarizes the signaling reactions organized by InaD.

Signaling begins with the absorption of a photon of light by the G-protein coupled receptor rhodopsin and then proceeds via sequential activation of a Gq-isoform of heterotrimeric G protein and a phospholipase C (the NorpA PLC-β). Through a currently unknown mechanism, PLC-β activity triggers the opening of cation-selective

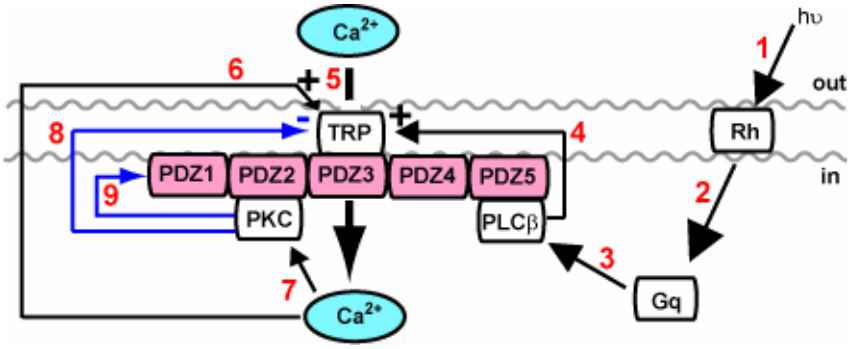

Figure 1-2 Visual signaling in *Drosophila* at the microvillar membrane. Photon absorption by rhodopsin (1) sequentially activates Gqα (2) and PLC-β (3). Through an unknown mechansism, PLC-β activity activates the TRP cation channels (4). Calcium influx (5) activates positive feedback mechanisms (promoting the opening of more TRP channels (6)) as well as an eye-specific kinase (eye-PKC) (7), which then feedback phosphorylates both the TRP channel (8) and the InaD scaffold (in red, 9). Through its PDZ domains, InaD assembles a core macromolecular complex involving PLC-β, TRP and eye-PKC.

TRP (Transient Receptor Potential) channels in the microvillar membrane. Ca^{2+} influx then triggers both positive and negative feedback regulation that is essential for the extraordinary speed and sensitivity of invertebrate vision (Henderson et al., 2000; Ranganathan et al., 1991). The mechanism of Ca^{2+}-dependent positive feedback is yet unclear, but negative feedback operates at least in part through activation of an eye-specific isoform of protein kinase C (eye-PKC) (Hardie et al., 1993; Ranganathan et al., 1991; Smith et al., 1991). This visual signaling pathway has served as a general model system for G-protein signaling; for example, the core components of the pathway (rhodopsin, Gq, PLC, PKC, TRP) are known to mediate various biological processes in organisms ranging from flies to mammals.

Visual signaling in *Drosophila* can be extremely sensitive; in dark-adapted animals, reliable single photon responses (also known as quantum bumps) can be measured (Figure 1-3, top panel). This electrical response is an inward current resulting

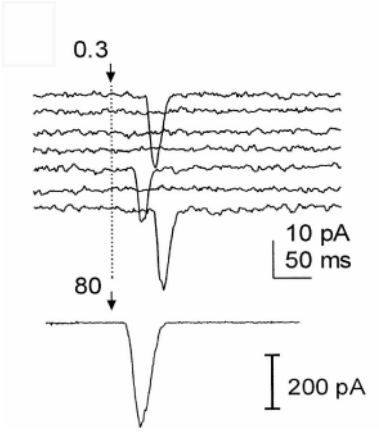

Figure 1-3 The *Drosophila* visual response. (Top) A single photon response (quantum bump) from a *Drosophila* photoreceptor. In response to flashes containing ~0.3 photons on average, transient inward currents representing the opening (and closing) of TRP cation channels can be measured. (Bottom) A multi-photon (macroscopic) response from a flash containing ~80 photons. The electrical response is a linear sum of the appropriate number of quantum bumps. Taken from (Hardie, 2003).

from the opening of TRP channels in a single microvillus (Henderson et al., 2000). Each microvillus is thought to act independently as a fundamental unit of signaling; the multiphoton response (or macroscopic response) has thus been shown to be composed of a linear sum of numerous quantum bumps (Figure 1-3, lower panel) (Henderson et al., 2000). Such measurements (taken in voltage-clamp mode in isolated cells) represent the opening of TRP channels in the microvillus without contamination from voltage-sensitive channels in the cell body and axon. In the whole organism, the opening of TRP channels causes depolarization of the photoreceptor membrane; this signal is transmitted as a graded potential (via voltage-gated K^+ channels) down the axon to trigger synaptic vesicle release at the photoreceptor-LMC synapse.

InaD plays an essential role in both activation and termination of the electrical response to light (Scott and Zuker, 1998; Shieh and Zhu, 1996; Tsunoda et al., 1997). InaD is a concatemer of five PDZ (Post-synaptic density 95, Discs Large, Zona Occludens 1) domains, a diverse and nearly ubiquitous family of protein interaction modules that bind the C-terminal residues of target proteins (Hung and Sheng, 2002). Through PDZ-mediated interactions, InaD assembles a core complex involving at least

three proteins: the NorpA PLC-β (the main effector for rhodopsin-mediated signaling), the TRP channel (the main mechanism of membrane depolarization and Ca^{2+} entry), and eye-PKC (the primary effector for Ca^{2+}-dependent negative feedback regulation) (Figure 1-2) (Chevesich et al., 1997; Huber et al., 1996a; Li and Montell, 2000; Shieh et al., 1997; Tsunoda et al., 1997). The scaffolding of PLC-β to the InaD complex is critical for maintaining the high efficiency and speed of visual signaling (Scott and Zuker, 1998), and scaffolding of eye-PKC directs feedback phosphorylation reactions within the complex that are required for fast response termination (Henderson et al., 2000; Popescu et al., 2006).

InaD as a model system

According to definition (Bhattacharyya et al., 2006b), InaD certainly qualifies as a typical scaffold – it binds and organizes at least three members (TRP, PLC-β, PKC) of a catalytic pathway and perhaps more (Montell, 1998; Montell, 2005), playing an essential role for efficient signaling (see above). More recently though, reports have surfaced implicating scaffolds in more complex roles related to cellular physiology (see below); interestingly, InaD (and *Drosophila* phototransduction) potentially provides a good model system for studying such properties.

Co-localization of both activating and inactivating proteins into a single complex has profound effects on the kinetics and spatial regulation of the stimulus response. The AKAP family of scaffolds (involved in protein kinase A (PKA) signaling) provides a good example of this (Figure 1-4). The muscle specific AKAP (mAKAP) binds both PKA and a type 4 phosphodiesterase (PDE4D3). Hormonal stimulation leads to

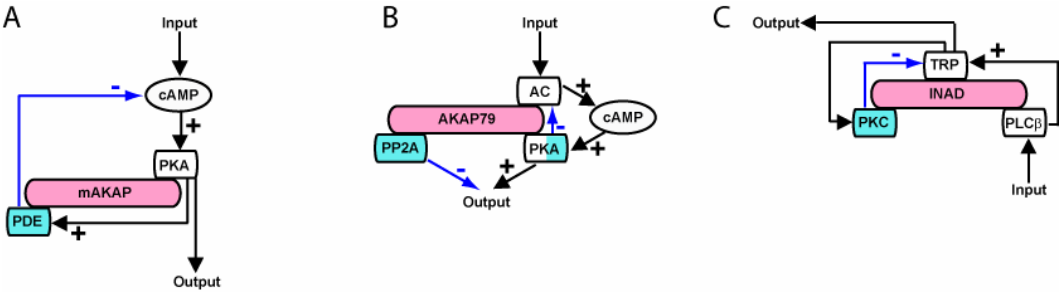

Figure 1-4 Scaffolding co-localizes activating and inactivating components. (A) The muscle-specific AKAP co-localizes PKA and PDE. PKA is activated by local increases in cAMP concentration; however, phosphorylation of the co-localized PDE increases phosphodiesterase activity and subsequently attenuates signaling. (B) The neuron specific AKAP79 co-localizes adenylyl cyclase (AC), with PKA and PP2B. Activation of AC leads to PKA activity; however, PKA serves to negatively regulate AC in order to prevent uncontrolled signaling. In addition, the phosphatase PP2B is co-localized, thereby competing with PKA and preventing excessive signaling. (C) InaD co-localizes the activating elements (PLC-β and TRP) with the negative feedback regulator (PKC). TRP channel opening leads to PKC activation (via Ca^{2+} influx); PKC susbsequently phosphorylates TRP, promoting channel closure and a transient electrical response. Scaffolds are shown in pink; proteins involved in negative feedback in blue.

increased cAMP levels, thereby activating PKA. The local proximity of PDE4D3 allows PKA to efficiently phosphorylate it, resulting in enhanced phosphodiesterase activity which subsequently lowers cAMP levels (Figure 1-4A) (Dodge et al., 2001). This mechanism generates pulses of PKA activity and prevents unattenuated signaling. A similar mechanism is utilized by the neuron specific AKAP79 (Figure 1-4B) which binds adenylyl cyclase (AC), PKA and the protein phosphatase PP2B. AC leads to activation of PKA (via the generation of cAMP); however, PKA negatively regulates AC to limit the spatio-temporal dynamics of cAMP generation (Bauman et al., 2006). In addition, co-localization of the PP2B phosphatase prevents excessive PKA signaling. InaD utilizes a similar mechanism to generate a transient electrical response to light (Figure 1-4C). By co-localizing TRP and PKC, InaD promotes activation of PKC (via Ca^{2+} influx through

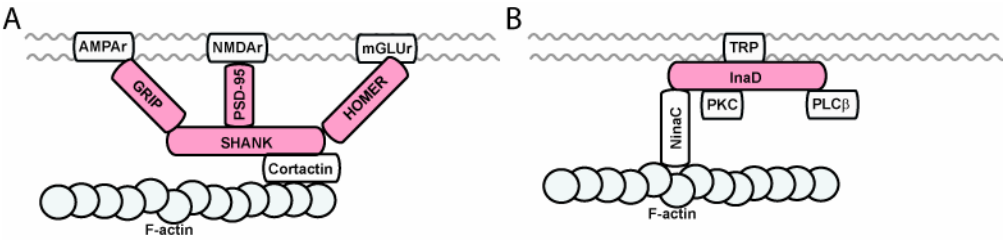

Figure 1-5 Scaffolding and cytoskeletal regulation. (A) A simplified view of the scaffolding interactions in the post-synaptic density. Shank, through an interaction with the actin-binding protein cortactin, organizes other scaffolds around actin filaments, thereby providing a potential link between signaling and cytoskeletal remodeling. (B) InaD, through a proposed interaction with the atypical myosin kinase NinaC, organizes complexes around the single actin filament in each microvilli; thus, playing a potential role in microvilli morphology and protein trafficking.

TRP) and subsequent PKC-mediated negative feedback regulation, via phosphorylation of TRP and channel closure. Indeed, InaD mutants in which TRP is mislocalized (*inaD*^{215}) show a specific delay in deactivation of channels (Henderson et al., 2000).

In other systems, scaffolds are hypothesized to provide an important link between signaling molecules and cytoskeletal elements – thereby playing an important role in cellular identity and morphology. One particular example involves the organization of the post-synaptic density (PSD) (Figure 1-5A). Numerous scaffolds have been identified in the PSD, including PSD-95, GRIP, Homer and Shank; these scaffolds interact with various signaling molecules, neurotransmitter receptors, as well as each other. Interestingly, Shank has been reported to colocalize with cortactin (Naisbitt et al., 1999), which in turn interacts with filamentous actin. These data raise the possibility that scaffolding (in the PSD) is involved with cytoskeletal regulation that may be important for neurite outgrowth, local cytoskeletal remodeling in response to receptor activity, and trafficking between the cell body and the synapse (Sheng and Kim, 2000). Interestingly,

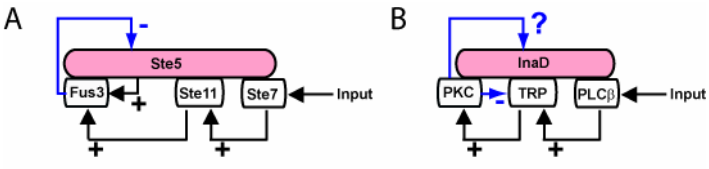

Figure 1-6 Scaffolding-mediated feedback regulation. (A) The Ste5 scaffold organizes a MAPK cascade via co-localization of Ste7, Ste11 and Fus3. In addition, Ste5 allosterically activates the Fus3 kinase, and the activated Fus3 feedback phosphorylates the Ste5 scaffold to downregulate signal output via an unknown mechanism. (B) InaD is also feedback phosphorylated (by PKC) in a signaling-dependent manner; however, the effect of this phosphorylation is currently unknown.

InaD has been reported to interact with NinaC, a chimeric protein consisting of a protein kinase domain and a myosin head domain, which in turn interacts with actin (Figure 1-5B). In addition, NinaC has been shown to play an essential role in the trafficking of proteins between the cell body and the rhabdomere (Cronin et al., 2004; Lee and Montell, 2004; Meyer et al., 2006). How the proposed InaD-NinaC interaction is related to trafficking and rhabdomere morphology is still unclear.

In many signaling cascades, feedback regulation plays an important role by controlling the spatio-temporal properties of the input-output relationship. Scaffolds usually promote efficient feedback regulation through co-localization of the involved parties. However, there are examples where the scaffold is directly involved in such regulation. For instance, the Ste5 scaffold co-localizes a MAPK cascade (Ste7→Ste11→Fus3) for the mating (pheromone) response in yeast (see Figure 1-6A). In addition, Ste5 itself activates Fus3 in an allosteric manner, and the allosterically activated Fus3 feedback phosphorylates the Ste5 scaffold in order to downregulate signaling output (through an unknown mechanism) (Bhattacharyya et al., 2006a). The InaD scaffold also has the potential to regulate signaling output (Figure 1-6B); in addition to co-localizing

PLC-β, TRP and PKC, InaD is also multiply phosphorylated by PKC in a light-regulated manner (Huber et al., 1996b; Matsumoto et al., 1999; Matsumoto et al., 1982; Matsumoto and Pak, 1984). Unfortunately, the precise phosphorylation sites and the resultant effect on InaD (and visual signaling) is not currently known.

In summary, InaD (and *Drosophila* visual signaling) serves as an excellent model system to study scaffolding, a mechanism ubiquitous in biology for cellular signaling. InaD plays an essential role in organizing a G-protein signaling cascade which mediates the visual response in flies; in addition, the *Drosphila* visual system displays many interesting properties suggesting that scaffolding serves purposes other than simple co-localization of catalytic proteins. Practically speaking, the fruitfly has longed served as a tractable genetic organism for studying biology, and mutants are readily available for the majority of the visual signaling proteins. Lastly, techniques have been developed to study visual signaling at high resolution – the use of whole-cell patch clamp allows us to obtain time-resolved data on TRP channel opening in response to a wide range of light stimulation. In this thesis, we will take advantage of these properties in order to examine InaD's role as a scaffold in detail.

References

Bauman, A. L., Soughayer, J., Nguyen, B. T., Willoughby, D., Carnegie, G. K., Wong, W., Hoshi, N., Langeberg, L. K., Cooper, D. M., Dessauer, C. W., and Scott, J. D. (2006). Dynamic regulation of cAMP synthesis through anchored PKA-adenylyl cyclase V/VI complexes. Mol Cell *23*, 925-931.

Bhattacharyya, R. P., Remenyi, A., Good, M. C., Bashor, C. J., Falick, A. M., and Lim, W. A. (2006a). The Ste5 scaffold allosterically modulates signaling output of the yeast mating pathway. Science *311*, 822-826.

Bhattacharyya, R. P., Remenyi, A., Yeh, B. J., and Lim, W. A. (2006b). Domains, motifs, and scaffolds: the role of modular interactions in the evolution and wiring of cell signaling circuits. Annu Rev Biochem *75*, 655-680.

Chevesich, J., Kreuz, A. J., and Montell, C. (1997). Requirement for the PDZ domain protein, INAD, for localization of the TRP store-operated channel to a signaling complex. Neuron *18*, 95-105.

Cronin, M. A., Diao, F., and Tsunoda, S. (2004). Light-dependent subcellular translocation of Gqalpha in Drosophila photoreceptors is facilitated by the photoreceptor-specific myosin III NINAC. J Cell Sci *117*, 4797-4806.

Dodge, K. L., Khouangsathiene, S., Kapiloff, M. S., Mouton, R., Hill, E. V., Houslay, M. D., Langeberg, L. K., and Scott, J. D. (2001). mAKAP assembles a protein kinase A/PDE4 phosphodiesterase cAMP signaling module. Embo J *20*, 1921-1930.

Feiler, R., Bjornson, R., Kirschfeld, K., Mismer, D., Rubin, G. M., Smith, D. P., Socolich, M., and Zuker, C. S. (1992). Ectopic expression of ultraviolet-rhodopsins in the blue photoreceptor cells of Drosophila: visual physiology and photochemistry of transgenic animals. J Neurosci *12*, 3862-3868.

Franceschini, N., Hardie, R., Ribi, W., and Kirschfeld, K. (1981). Sexual dimorphism in a photoreceptor. Nature *291*, 241-244.

Hardie, R. C. (2003). Regulation of TRP channels via lipid second messengers. Annu Rev Physiol *65*, 735-759.

Hardie, R. C., Peretz, A., Suss-Toby, E., Rom-Glas, A., Bishop, S. A., Selinger, Z., and Minke, B. (1993). Protein kinase C is required for light adaptation in Drosophila photoreceptors. Nature *363*, 634-637.

Hardie, R. C., and Raghu, P. (2001). Visual transduction in Drosophila. Nature *413*, 186-193.

Hardy, W. R., Li, L., Wang, Z., Sedy, J., Fawcett, J., Frank, E., Kucera, J., and Pawson, T. (2007). Combinatorial ShcA docking interactions support diversity in tissue morphogenesis. Science *317*, 251-256.

Henderson, S. R., Reuss, H., and Hardie, R. C. (2000). Single photon responses in Drosophila photoreceptors and their regulation by Ca2+. J Physiol *524 Pt 1*, 179-194.

Huber, A., Sander, P., Gobert, A., Bahner, M., Hermann, R., and Paulsen, R. (1996a). The transient receptor potential protein (Trp), a putative store-operated Ca2+ channel essential for phosphoinositide-mediated photoreception, forms a signaling complex with NorpA, InaC and InaD. Embo J *15*, 7036-7045.

Huber, A., Sander, P., and Paulsen, R. (1996b). Phosphorylation of the InaD gene product, a photoreceptor membrane protein required for recovery of visual excitation. J Biol Chem *271*, 11710-11717.

Hung, A. Y., and Sheng, M. (2002). PDZ domains: structural modules for protein complex assembly. J Biol Chem *277*, 5699-5702.

Hung, W., Hwang, C., Po, M. D., and Zhen, M. (2007). Neuronal polarity is regulated by a direct interaction between a scaffolding protein, Neurabin, and a presynaptic SAD-1 kinase in Caenorhabditis elegans. Development *134*, 237-249.

Lee, S. J., and Montell, C. (2004). Light-dependent translocation of visual arrestin regulated by the NINAC myosin III. Neuron *43*, 95-103.

Li, H. S., and Montell, C. (2000). TRP and the PDZ protein, INAD, form the core complex required for retention of the signalplex in Drosophila photoreceptor cells. J Cell Biol *150*, 1411-1422.

Lonart, G., Schoch, S., Kaeser, P. S., Larkin, C. J., Sudhof, T. C., and Linden, D. J. (2003). Phosphorylation of RIM1alpha by PKA triggers presynaptic long-term potentiation at cerebellar parallel fiber synapses. Cell *115*, 49-60.

Matsumoto, H., Kahn, E. S., and Komori, N. (1999). The emerging role of mass spectrometry in molecular biosciences: studies of protein phosphorylation in fly eyes as an example. Novartis Found Symp *224*, 225-244; discussion 244-228.

Matsumoto, H., O'Tousa, J. E., and Pak, W. L. (1982). Light-induced modification of Drosophila retinal polypeptides in vivo. Science *217*, 839-841.

Matsumoto, H., and Pak, W. L. (1984). Light-induced phosphorylation of retina-specific polypeptides of Drosophila in vivo. Science *223*, 184-186.

Meyer, N. E., Joel-Almagor, T., Frechter, S., Minke, B., and Huber, A. (2006). Subcellular translocation of the eGFP-tagged TRPL channel in Drosophila photoreceptors requires activation of the phototransduction cascade. J Cell Sci *119*, 2592-2603.

Montell, C. (1998). TRP trapped in fly signaling web. Curr Opin Neurobiol *8*, 389-397.

Montell, C. (2005). TRP channels in Drosophila photoreceptor cells. J Physiol *567*, 45-51.

Morante, J., and Desplan, C. (2004). Building a projection map for photoreceptor neurons in the Drosophila optic lobes. Semin Cell Dev Biol *15*, 137-143.

Morrison, D. K., and Davis, R. J. (2003). Regulation of MAP kinase signaling modules by scaffold proteins in mammals. Annu Rev Cell Dev Biol *19*, 91-118.

Naisbitt, S., Kim, E., Tu, J. C., Xiao, B., Sala, C., Valtschanoff, J., Weinberg, R. J., Worley, P. F., and Sheng, M. (1999). Shank, a novel family of postsynaptic density proteins that binds to the NMDA receptor/PSD-95/GKAP complex and cortactin. Neuron *23*, 569-582.

Popescu, D. C., Ham, A. J., and Shieh, B. H. (2006). Scaffolding protein INAD regulates deactivation of vision by promoting phosphorylation of transient receptor potential by eye protein kinase C in Drosophila. J Neurosci *26*, 8570-8577.

Ranganathan, R., Harris, G. L., Stevens, C. F., and Zuker, C. S. (1991). A Drosophila mutant defective in extracellular calcium-dependent photoreceptor deactivation and rapid desensitization. Nature *354*, 230-232.

Salcedo, E., Huber, A., Henrich, S., Chadwell, L. V., Chou, W. H., Paulsen, R., and Britt, S. G. (1999). Blue- and green-absorbing visual pigments of Drosophila: ectopic expression and physiological characterization of the R8 photoreceptor cell-specific Rh5 and Rh6 rhodopsins. J Neurosci *19*, 10716-10726.

Schoch, S., Castillo, P. E., Jo, T., Mukherjee, K., Geppert, M., Wang, Y., Schmitz, F., Malenka, R. C., and Sudhof, T. C. (2002). RIM1alpha forms a protein scaffold for regulating neurotransmitter release at the active zone. Nature *415*, 321-326.

Scott, K., and Zuker, C. S. (1998). Assembly of the Drosophila phototransduction cascade into a signalling complex shapes elementary responses. Nature *395*, 805-808.

Sheng, M., and Kim, E. (2000). The Shank family of scaffold proteins. J Cell Sci *113 (Pt 11)*, 1851-1856.

Shieh, B. H., and Zhu, M. Y. (1996). Regulation of the TRP Ca2+ channel by INAD in Drosophila photoreceptors. Neuron *16*, 991-998.

Shieh, B. H., Zhu, M. Y., Lee, J. K., Kelly, I. M., and Bahiraei, F. (1997). Association of INAD with NORPA is essential for controlled activation and deactivation of Drosophila phototransduction in vivo. Proc Natl Acad Sci U S A *94*, 12682-12687.

Smith, D. P., Ranganathan, R., Hardy, R. W., Marx, J., Tsuchida, T., and Zuker, C. S. (1991). Photoreceptor deactivation and retinal degeneration mediated by a photoreceptor-specific protein kinase C. Science *254*, 1478-1484.

Tsunoda, S., Sierralta, J., Sun, Y., Bodner, R., Suzuki, E., Becker, A., Socolich, M., and Zuker, C. S. (1997). A multivalent PDZ-domain protein assembles signalling complexes in a G-protein-coupled cascade. Nature *388*, 243-249.

Tsunoda, S., and Zuker, C. S. (1999). The organization of INAD-signaling complexes by a multivalent PDZ domain protein in Drosophila photoreceptor cells ensures sensitivity and speed of signaling. Cell Calcium *26*, 165-171.

Wong, W., and Scott, J. D. (2004). AKAP signalling complexes: focal points in space and time. Nat Rev Mol Cell Biol *5*, 959-970.

Zeil, J. (1979). A new kind of neural superposition eye: the compound eye of male Bibionidae. Nature *279*, 249-250.

Chapter Two
A two-state model for the 5th PDZ domain of InaD.

InaD – a tandem array of PDZ domains

The primary sequence of InaD indicates that it is composed of 5 PDZ domains, separated by linkers of varying lengths. A typical PDZ domain consists of 90-100 amino acids and adopts a five-stranded β-sandwich with two flanking α helices (Fig. 2-1B); the target peptide canonically binds in the groove between the β2 strand and the α2 helix (Doyle et al., 1996). PDZ domains are generally thought of as static modules, which can be mixed and matched to create molecules with multiple binding partners (Bhattacharyya et al., 2006; Dueber et al., 2004; Dueber et al., 2003; Harris and Lim, 2001; Park et al., 2003; Sallee et al., 2007; Yeh et al., 2007). However, there are isolated examples of PDZ domains playing more "active" roles; for instance, the binding affinity of the PDZ domain from Par-6 (a protein involved in establishment of cell polarity) is allosterically controlled via an interaction with the Rho GTPase Cdc42 on the backside of the domain (via the α1 helix and β1 strand) (Garrard et al., 2003; Penkert et al., 2004; Peterson et al., 2004).

Being composed solely of PDZ domains, InaD is considered a prototypical example of a scaffolding molecule which binds its protein partners (thereby co-localizing them) but does little else. In fact, localization of InaD's binding partners (TRP, PLC-β, and eye-PKC) is **not** known to be dynamic (Bahner et al., 2002; Kiselev et al., 2000), in stark contrast to other phototransduction proteins (e.g., arrestin, rhodopsin, Gqα, and the TRPL channel) which do **not** bind InaD and whose subcellular localization **is**

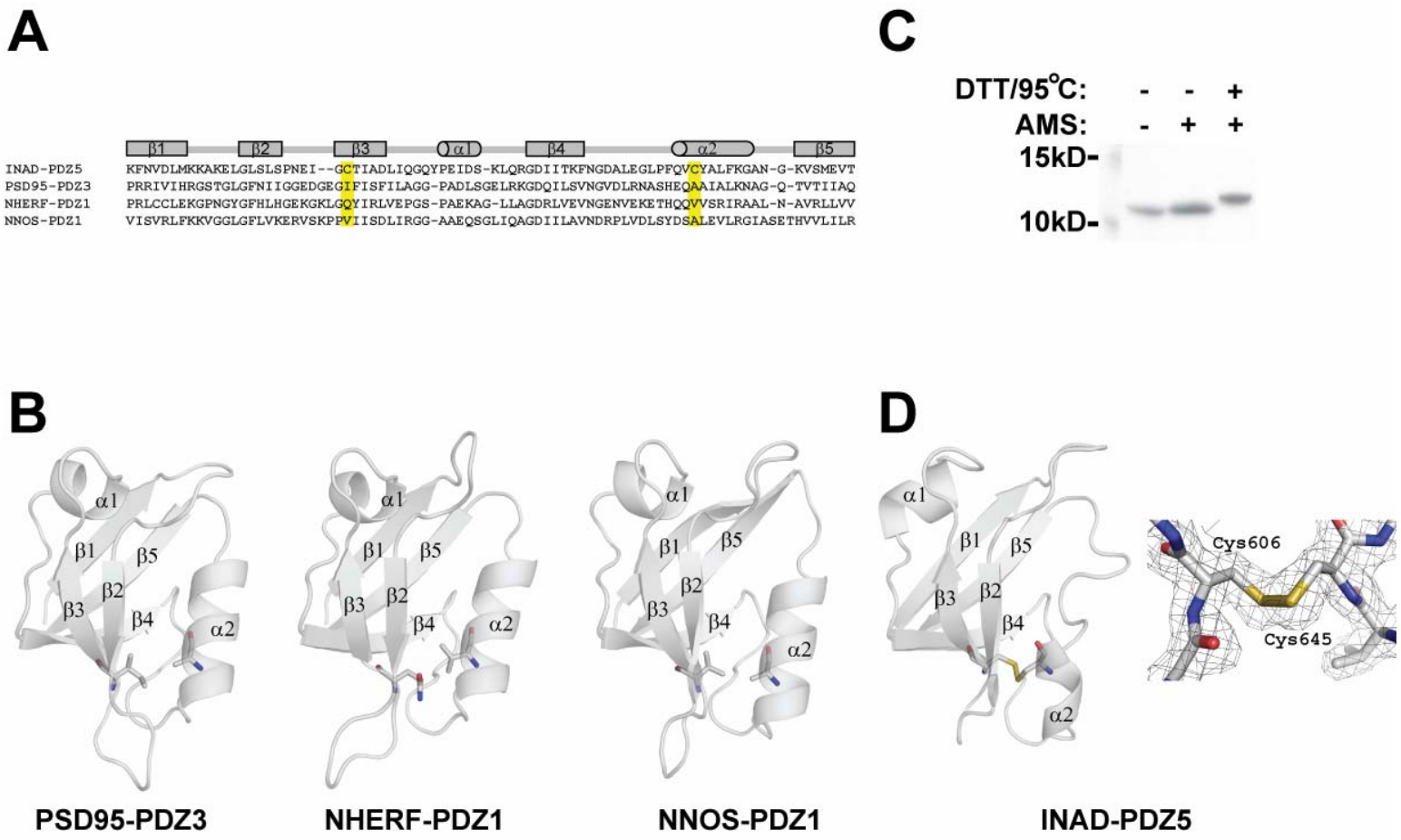
A
β1 β2 β3 α1 β4 α2 β5
INAD-PDZ5 KFNVDLMKKAKELGLSLSPNEI--GCTIADLIQGQYPEIDS-KLQRGDIITKFNGDALEGLPFQVCYALFKGAN-G-KVSMEVT
PSD95-PDZ3 PRRIVIHRGSTGLGFNIIGGEDGEGIFISFILAGG-PADLSGELRKGDQILSVNGVDLRNASHEQAAIALKNAG-Q-TVTIIAQ
NHERF-PDZ1 PRLCCLEKGPNGYGFHLHGEKGKLGQYIRLVEPGS-PAEKAG-LLAGDRLVEVNGENVEKETHQQVVSRIRAAL-N-AVRLLVV
NNOS-PDZ1 VISVRLFKKVGGLGFLVKERVSKPPVIISDLIRGG-AAEQSGLIQAGDIILAVNDRPLVDLSYDSALEVLRGIASETHVVLILR
C
DTT/95°C: - - +
AMS: - + +
15kD-
10kD-
B
α1
β1
β5
β2
β3
β4
α2
PSD95-PDZ3
NHERF-PDZ1
NNOS-PDZ1
D
Cys606
Cys645
INAD-PDZ5

Figure 2-1 The 5th PDZ domain of InaD contains an intramolecular disulfide bond. (A) Sequence alignment of a sample of PDZ domains: 5th PDZ domain from *D.melanogaster* Inactivation-No Afterpotential-D (InaD-PDZ5); 3rd PDZ domain from *R.norvegicus* synaptic protein PSD-95 (PSD95-PDZ3); 1st PDZ domain from *H.sapiens* Na^+/H^+ Exchange Factor (NHERF-PDZ1); 1st PDZ domain from *R.norvegicus* Neuronal Nitric Oxide Synthase (NNOS-PDZ1). Rectangles indicate β sheets, cylinders indicate α helices. Highlighted columns indicate positions corresponding to cysteines 606 and 645 (INAD numbering). (B) Backbone ribbon representations of PDZ domains from (A) with residues homologous to cysteines 606 and 645 depicted in stick format. (PDB accession numbers: 1BE9, 1G9O, and 1QAU). (C) Cysteine-labeling assay performed on recombinant PDZ5 protein incubated with varying amounts of DTT and/or heat. Reactivity is probed via a molecular weight shift due to AMS (MW=536.44Da) incorporation. (D) (left) The crystal structure of PDZ5 (in the absence of DTT) is shown using a backbone ribbon representation. Cysteines 606 and 645 are depicted in stick format. (right) $2F_o$-F_c electron density map contoured at 1σ around cysteines 606 and 645.

dynamically regulated by light conditions (Cronin et al., 2004; Cronin et al., 2006; Kiselev et al., 2000; Meyer et al., 2006). Nevertheless, InaD does play a critical, though possibly static, role in phototransduction; InaD-null mutants show dramatic defects in the speed and efficiency of visual signaling (Tsunoda et al., 1997; Tsunoda and Zuker, 1999).

An intramolecular disulfide bond in InaD

A sequence alignment of PDZ domains reveals that the 5th PDZ domain of InaD (PDZ5) has two cysteines (residues 606 and 645, InaD numbering) located in the β3 strand and the α2 helix, respectively (Figure 2-1A). Despite considerable sequence divergence (Fig 2-1A), homologous positions in other PDZ domains are in close proximity and have sidechains oriented toward one another (Figure 2-1B); this suggests that PDZ5 may possess an intramolecular disulfide bond. To test this, cysteine-reactivity of recombinant PDZ5 was probed with a maleimide deriviative (AMS, see Methods) which specifically labels free thiol groups, adding approximately 500 daltons per thiol.

The labeled species can then be identified by separation via SDS-PAGE. The data indicate that neither cysteine is reactive unless the domain is treated with a reducing agent (dithiothreitol (DTT)) (Figure 2-1C), suggesting that a disulfide bond is formed *in vitro*.

Atomic structures of PDZ5 in the absence of DTT (solved by M. Socolich and R. Ranganathan) confirm the presence of an intramolecular disulfide bond (Figure 2-1D). The isolated domain was crystallized in space group $P4_12_12$, and its structure was solved at 2.1Å resolution (R=.224, R_{free}=.242) by multiple isomorphous replacement with very good stereochemistry (Table 2-1). The electron density difference map ($2F_o$-F_c) clearly indicates the presence of a disulfide bond (Figure 2-1D, right; S-S distance = 2.0Å). Thus, PDZ5 provides the first example of an intramolecular disulfide bond within a PDZ domain; previous examples of redox chemistry in the family have involved either intramolecular bonds within the ligand (van den Berk et al., 2005), or intermolecular bonds between the domain and its ligand (Kimple et al., 2001; von Ossowski et al., 2006). In fact, a search of currently known PDZ domains (PF00595 from PFAM (Bateman, 2004)) indicates that no other family members, other than some InaD orthologs in flying insects, contain cysteines at both positions homologous to 606 and 645 from InaD.

The overall structure of PDZ5 is similar to that of a typical PDZ domain (Figure 2-2) with two novel exceptions: First, the α1 helix is oriented at an alternate angle relative to the rest of the domain; it has rotated nearly 70° relative to its position in other known PDZ structures. Second, the α2 helix is unwound at its C-terminus, more tightly wound at its N-terminus, and displaced towards the β3 strand (presumably to

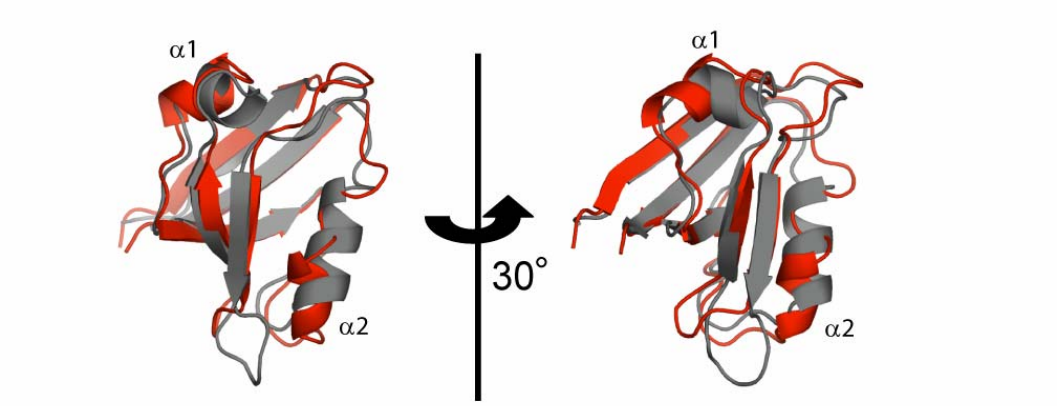

Figure 2-2 Structural alignment of the 3rd PDZ domain from *R.norvegicus* synaptic protein PSD-95 (PSD95-PDZ3; gray) and the 5th PDZ domain from *D.melanogaster* InaD. Overall, the structures are quite similar; however significant deviations are seen in the position of the α1 helix, as well as the conformation of the α2 helix.

accommodate the disulfide bond). As residues from the α2 helix typically participate in specificity and formation of the binding pocket (Doyle et al., 1996), this conformation is inconsistent with the canonical mode of ligand binding (see below).

The reduced structure of InaD-PDZ5

To ascertain the structure of the reduced form, PDZ5 was crystallized (by M. Wall and M. Socolich) in the presence of reducing agent. Crystals were obtained in 10mM DTT in a different space group ($P4_322$) and the structure was solved at 2.2Å resolution (R=.205, R_{free}=.231) by seleno-methionine multi-wavelength anomalous dispersion (Table 2-2). Three distinct molecules were found in the asymmetric unit (Figure 2-3A), each representing a distinct form of the protein. One molecule (red) is in the oxidized state (Figures 2-3F and 2-3G; S-S distance = 2.1Å) and shows identical structural distortions in the α2 helix as observed above (Figures 2-1D, 2-2). The other

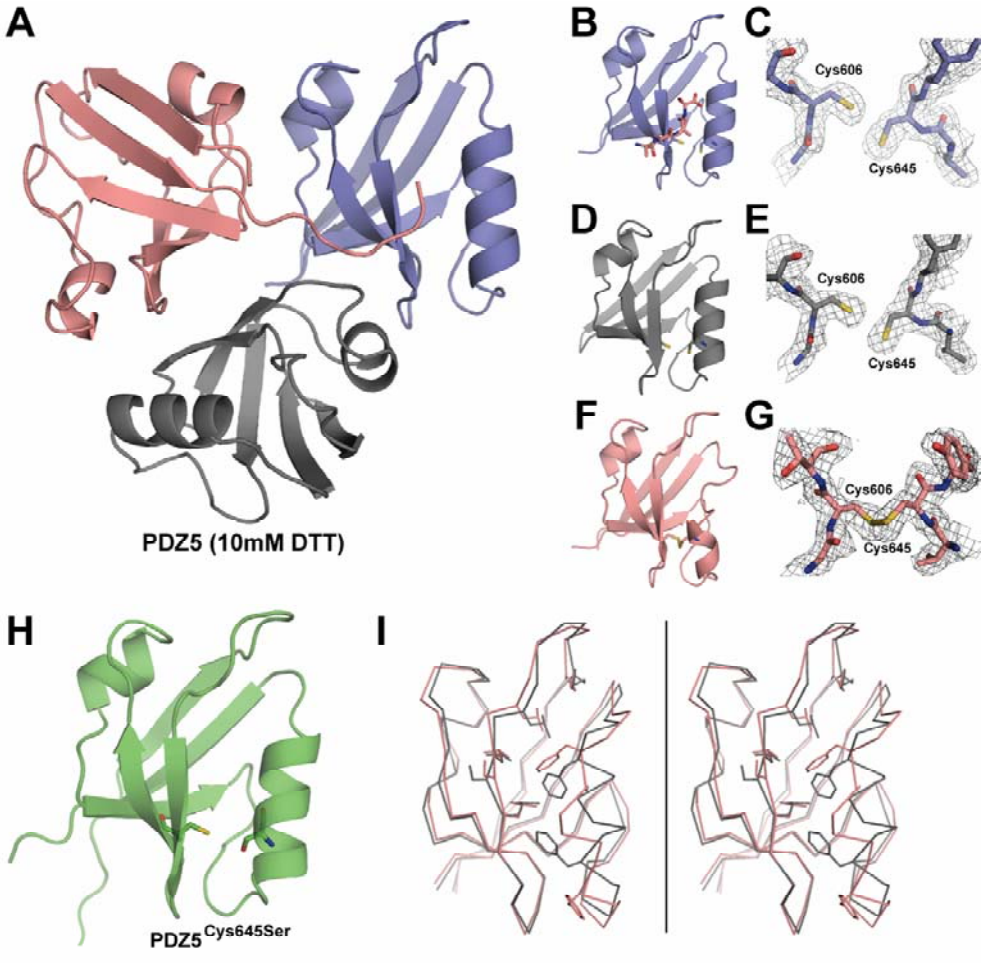

Figure 2-3. The oxidized and reduced forms of PDZ5 differ in the orientation of the α2 helix. (A) The asymmetric unit of PDZ5 crystals grown in 10mM DTT. Three distinct molecules are observed; note that the red molecule has its C-terminus inserted into the binding pocket of the blue molecule. (B,D,F) Backbone ribbon representations of the three monomers in (A). Cysteines 606 and 645 and the four C-terminal residues of the red monomer are shown in stick format. Only the red molecule is distorted in the α2 helix. (C,E,G) Electron density ($2F_o$-F_c maps contoured at 1σ) around cysteines 606 and 645 for the three monomers in (A). Only the red molecule is in an oxidized state. (H) Backbone ribbon representation of the crystal structure of $PDZ5^{Cys645Ser}$. The α2 helix is in the same orientation as the reduced forms of the domain. (I) Stereo view of an overlay of the α-carbon traces of oxidized (red) and reduced (gray) PDZ5. Sidechains of residues Lys590, Leu595, Leu597, Ser598, Leu599, Phe642 and Phe649 are displayed.

two molecules (blue and gray) are in a reduced state as evidenced by the electron density (Figures 2-3C and 2-3E; S-S distance = 3.8Å, 3.7Å respectively). Additionally, the blue molecule has the C-terminus of a neighboring monomer present in its binding site.

Interestingly, the α2 helices of the two reduced molecules are not distorted (Figures 2-3B and 2-3D), suggesting that the disulfide bond is necessary to "lock" the helix in an alternate conformation. As an independent test of this hypothesis, the disulfide bond was perturbed via a cysteine to serine mutation at position 645. Crystals of PDZ5^{Cys645Ser} grew in the absence of DTT in a third space group ($P4_332$); the structure was solved (by M. Socolich) at a resolution of 2.0Å resolution (R=.246, R_{free}=.270) by seleno-methionine single-wavelength anomalous dispersion (Table 2-3). The overall structure (Figure 2-3H) is very similar to that of the reduced form (all atom RMSD = 0.962Å) and the α2 helix adopts a canonical conformation. Thus, data from three different structures, in three different space groups, indicate that only the oxidized form of the domain takes on the alternate α2 conformation.

A two-state model for InaD-PDZ5

A quantitative comparison of the Cα positions of reduced, oxidized and mutant PDZ5 with previously known PDZ domain structures reveals that while all three species significantly differ in the α1 helix orientation, only oxidized PDZ5 differs in the α2 helix (Figure 2-4, Table 2-4). Both deviations are novel for the PDZ family. A closer comparison of the oxidized and reduced structures (Figures 2-3I, 2-4) indicates that there is little conformational difference between the two species outside of the α2 helix (all

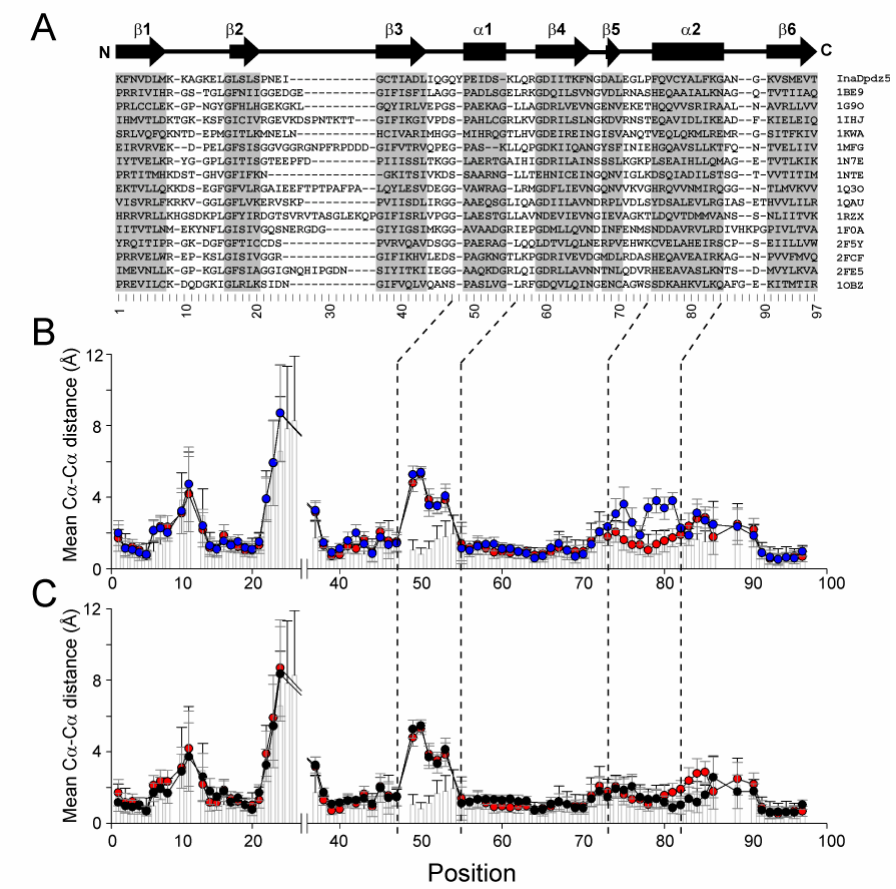

Figure 2-4. Comparison between InaD-PDZ5 and known PDZ domain structures. (A) The RCSB protein data bank (http://www.rcsb.org/pdb) was searched for PDZ domain crystal structures with resolution < 2.5 angstroms and R_{free}<0.30. Sixteen manually aligned sequences (including PDZ5) are shown with their PDB accession codes listed on the right. (B) Pairwise structural alignment of Cα atoms from the domains listed in (A) was performed in PyMol (DeLano Scientific, http://pymol.sourceforge.net/) using the 'fit' command. Cα-Cα distances were calculated from the fits and averaged. In gray columns are the distances calculated from all pairwise alignments of domains not including PDZ5. In blue, the oxidized form of PDZ5 is compared with other PDZ domains. In red, the reduced form of PDZ5 is compared. Both forms show significant deviations in the region of the α1 helix; however, only the oxidized form shows deviations in the α2 helix. Bars indicate standard deviations. (C) Similar calculations as in (B). In gray columns are the distances calculated from all pairwise alignments of domains not including PDZ5. In red, the reduced form of PDZ5 is compared with other PDZ domains; in black, $PDZ5^{C645S}$ is compared. Both the reduced form of PDZ5 and $PDZ5^{C645S}$ show significant deviations in the α1 helix, but not in the α2 helix. Bars indicate standard deviations.

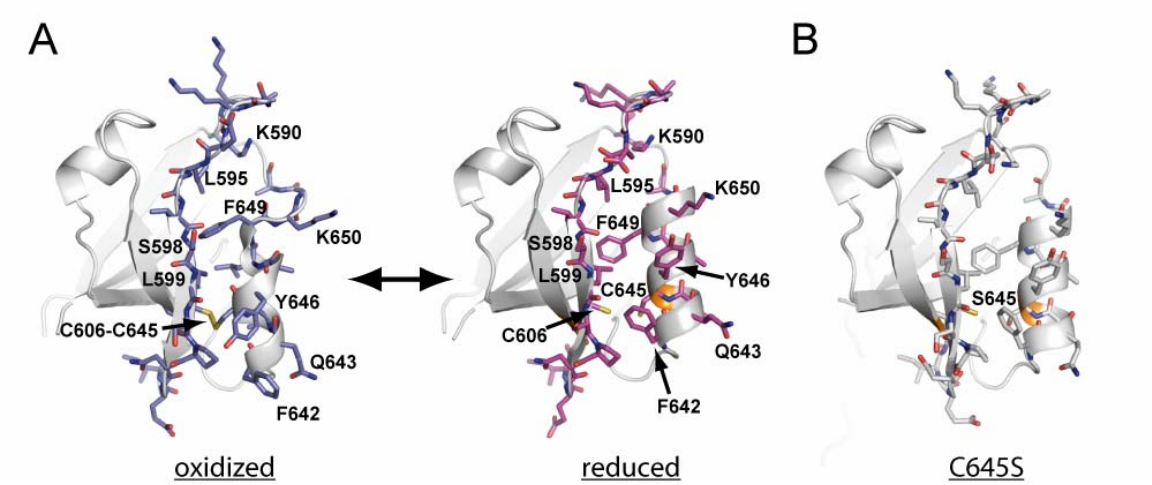

Figure 2-5. Detailed view of the binding pocket in the oxidized and reduced states of PDZ5 (A) and in the C645S mutant structure (B). The data show that key specificity determining residues (F642 and F649) on the α2 helix adopt significantly different conformations in the oxidized and reduced states, and that the C645S mutant is effectively locked in the reduced state structure.

atom RMSD of the α2 helix (residues 642-650) = 2.16Å, all atom RMSD of the remainder of the domain = 0.65Å). Of the residues known to contact the ligand (Doyle et al., 1996), those contributed by the β strands (Lys590, Leu595, Leu597, Ser598, Leu599) have only minor differences in their atomic positions (Figures 2-3I, 2-4, 2-5A, Table 2-4). In contrast, Phe642 and Phe649 (ligand specificity determinants from the α2 helix) adopt distinct conformations in the two states; their positions in the reduced state are consistent with known modes of PDZ binding, while their positions in the oxidized state are not. In fact, the presence of a C-terminus in the active site of the blue molecule (Figures 2-3A and 2-3B) suggests that the reduced form is competent for ligand binding. These results suggest a two-state model for PDZ5 whereby the activity of the domain can be controlled via its redox state.

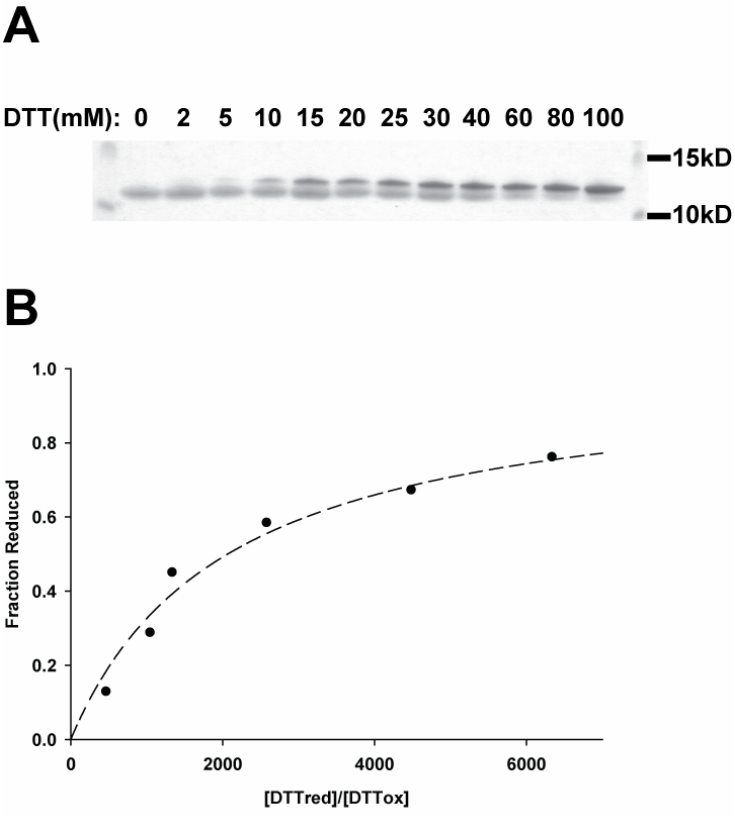

Figure 2-6. Standard redox potential of InaD-PDZ5. (A) Sample redox titration of InaD-PDZ5 with DTT. Purified PDZ5 was incubated with the indicated concentration of DTT for 4 hours at 30°C. Cysteine-labeling assays were performed with AMS (see Methods) to determine fraction of reduced protein. Here, AMS specifically reacts with the reduced species, causing a molecular weight shift visible on a 16.5% Tris-Tricine SDS-PAGE gel. (B) Sample redox titration of PDZ5 fit to a standard Langmuir isotherm. Titrations were done in triplicate yielding $E'_{0(PDZ5)} = -424.5 \pm 2.0$ mV at pH 7 and 30ºC.

Previous suggestions for dynamic control of PDZ activity have involved changes in the ligand itself, including phosphorylation (Cao et al., 1999; Chetkovich et al., 2002; Cohen et al., 1996) or disulfide-mediated cyclization of the C-terminal residues (van den Berk et al., 2005). The few examples of plasticity within the domain itself have involved changes in the flexible β1-β2 loop, along with small shifts in the positions of the α1 and

α2 helices (Penkert et al., 2004; Peterson et al., 2004). In contrast, PDZ5 shows significant plasticity in its ability to rewind the α2 helix between two rigid states (the average temperature factor is 16.7Å^2 for the reduced state and 17.0Å^2 for the oxidized state). These results challenge the assertion that protein interaction modules are static entities and similar dynamic behavior may exist in other families of modular domains.

In addition, titration of PDZ5 with reducing agent reveals a standard redox potential of -425±2 mV (Figure 2-6), indicating that though the bond is quite stable, two distinct species can be formed *in vitro*. With such a highly negative reducing potential, the disulfide bond in PDZ5 may actually form within the normally reducing cytosolic conditions (E_0 = -230 to -300mV (Hanson et al., 2004; Hwang et al., 1995; Hwang et al., 1992; Keese et al., 1999; Ostergaard et al., 2004; Schafer and Buettner, 2001)) *in vivo*. In the next chapter, we will specifically examine the redox state of InaD in the *Drosophila* eye.

Methods

Protein expression and purification

PDZ5 (residues 580-665 from *D.melanogaster* InaD) was cloned as a GST-fusion in pGEX-5X-3 (GE Healthcare) and expressed in *E.Coli* BL21-DE3 cells (Stratagene). Cells were grown at 37ºC in Terrific Broth to OD_{600} of ~1.2, induced with 100μm IPTG at 18ºC overnight, resuspended in PBS (10mM Na_2HPO_4, 1.8mM KH_2PO_4, 140mM NaCl, 2.7mM KCl, pH7.4) + 0.1% Tween-20, and lysed by sonication. The lysate was cleared by centriguation at 50,000g for 1 hour and incubated with glutathione

sepharose (GE) at 4°C for 1 hr. The resin was then washed with 20 bed volumes of PBS+0.1%Tween-20 followed by 20 bed volumes of PBS and eluted in PBS + 10mM reduced glutathione. To cleave the GST tag, Factor Xa protease (GE) was added at 1:50 (w/w) and the sample was dialyzed overnight into buffer A (50mM Tris, 100mM NaCl, pH7.5). Following rebinding to glutathione sepharose to remove undigested protein, the sample was subjected to size exclusion chromatography (Superdex 75, GE) in buffer A; fractions containing PDZ5 were pooled and concentrated in a Centricon YM-3 concentrator (Millipore) for crystallization trials. For the 10mM DTT structure, buffer A was supplemented with 1mM dithiothreitol (DTT) during size-exclusion chromatography.

Selenomethionyl (SeMet) protein was produced for the 10mM DTT and C645S structures by growing cells in M9 minimal media at 37ºC to OD_{600} of 1.0, then inclubating with amino acids (lysine, phenylalanine, threonine at 100mg/L; isoleucine, leucine, valine at 50mg/L, Se-methionine at 60mg/L) for 15 minutes, and finally inducing with 500μM IPTG overnight at 20ºC. Protein purification was carried out as above.

Crystallization

Purified PDZ5 was concentrated to 15mg/mL in buffer A without (oxidized and C645S structures) or with (reduced structure) 10mM DTT and crystallization trials were conducted at 4ºC using the vapor diffusion hanging drop method. Crystals grew either spontaneously or with microseeding with well-solutions containing 1.3M NaCitrate, pH 7.5 in 1-3 days. Single crystals were cryoprotected by serial equilibration into well solutions containing increasing amounts of glycerol (up to 15%) and flash frozen in

liquid propane. For the oxidized structure, heavy-atom derivatives were obtained by soaking single crystals in well-solution containing either K_2PtCl_4 (1mM) or trans-$Pd(NH_3)_2Cl_2$ (2.5mM) for 1-2 days prior to cryoprotection.

Diffraction Data Collection and Structure Determination

Data were collected at 100^{o}K either at UT Southwestern Medical Center (oxidized structure, Table S1), beamline 1-5 at the Stanford Synchrotron Radiation Laboratory, SLAC (10mM DTT structure, Table S2), beamline 19-BM at the Advanced Photon Source, Argonne National Laboratory (C645S structure, SeMet crystal, Table S3), or beamline 8.2.1 at the Advanced Light Source, Lawrence Berkeley Labs (C645S structure, native crystal, Table S3) and were indexed and scaled with DENZO/SCALEPACK (Otwinowksi, 1993). All phasing and model refinement was carried out with the Crystallography and NMR System (CNS) software (Brunger et al., 1998), and the statistics are summarized in Tables 2-1, 2-2 and 2-3.

For the oxidized structure (Fig. 2-1D), automated Patterson search methods identified two Pt sites in an anomalous Patterson map; subsequently two more Pt sites and two Pd sites were identified on difference Fourier maps using the refined initial phases. After solvent flattening and phase extension to 2.1 Å, the experimental electron density map was easily traceable and showed 2 molecules in the asymmetric unit. For this and all subsequent PDZ5 structures (see below), no non-crystallographic symmetry restraints were used during phasing or refinement, and a randomly selected set of reflections (5%) was flagged for cross-validation. Manual model building was performed in O (Jones et al., 1991) and computational refinement steps involved high-temperature

torsion angle molecular dynamics followed by positional and temperature factor minimization. After six rounds of refinement, the final model contained 85 residues for each molecule and 153 water molecules. All figures and RMSD calculations were made in PyMol (DeLano, 2002).

The 10mM DTT structure (Fig. 2-3A) was determined using selenomethionine multi-wavelength anomalous dispersion methods. Here, automated Patterson search methods (CNS) identified all 6 selenium sites in an anomalous Patterson. After solvent flattening and phase extension to 2.2 Å, the experimental electron density map was clearly traceable and showed 3 molecules in the asymmetric unit. Model building and computational refinement were as described above. After seven refinement rounds, the final model contained 85, 84 and 90 residues for the three molecules plus 266 water molecules and 2 glycerol molecules.

The PDZ5^{Cys645Ser} structure (Fig. 2-3H) was determined using selenomethionine single wavelength anomalous dispersion methods. Automated Patterson search methods (CNS) identified all 4 selenium sites in an anomalous Patterson. Following solvent flattening and phase extension to 1.55 Å using data from a native crystal, the experimental electron density map was traceable and showed 2 molecules in the asymmetric unit. Model building and refinement was as above. After six rounds of refinement, the final model contained 92 residues for both molecules plus 143 water molecules.

Cysteine-labeling assays

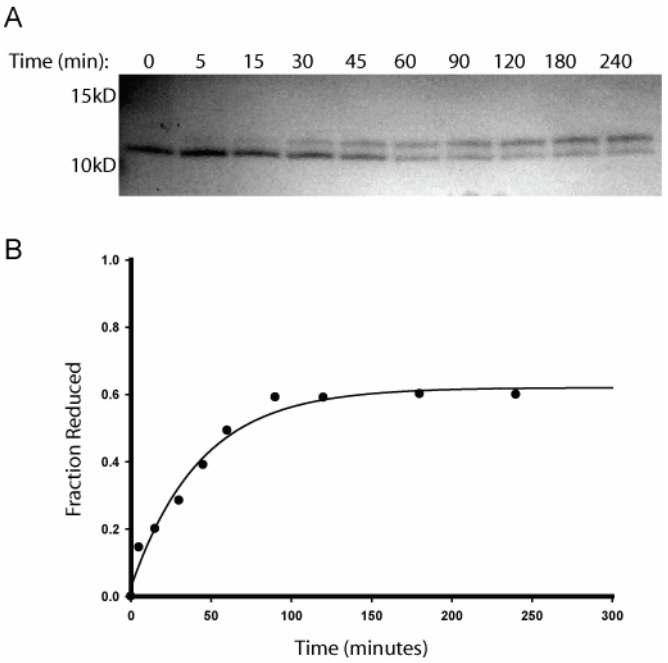

Figure 2-7. Establishment of equilibrium conditions for DTT titration of PDZ5. (A) For titrations performed in Figure 2-6, all reactions were incubated at 30°C for 4 hours to reach equilibrium. Equilibrium was usually reached within 1-2 hours; for instance, PDZ5 incubated with 15mM DTT reaches equilibrium within 90 minutes. (B) Quantitation of (A).

For *in vitro* assays, reactions were carried out with purified PDZ5 in 10mM HEPES, 50mM NaCl, pH7.0, and supplemented with various amounts of DTT. All buffers and tubes were flushed with N_2. After incubation for 4 hours at 30ºC to ensure equilibration (Figure 2-7), reactions were quenched with the addition of cold trichloroacetic acid (TCA) to 25% and precipitated on ice for >1hour. The pellet was collected by centrifugation at 13,000g for 10 minutes and washed 3x with acetone. After air-drying for 5 minutes, the pellet was resolubilized in 1%SDS, 200mM Na_2HPO_4, pH7.0 supplemented with 20mM AMS (4-acetamido-4'-maleimidystilbene-2,2'-disulfonic acid, MW = 536.44Da, Molecular Probes). The labeling reaction was allowed

to proceed for 10 minutes at room temperature and was directly loaded for separation on a 16.5% Tris-Tricine gel (Biorad) via SDS-PAGE. Protein was visualized by Coomassie staining and was imaged and quantified on an AlphaImager HP (AlphaInnotech). AMS covalently labels free cysteines, shifting the molecular weight of the reduced species by approximately 1kDa. Standard redox potentials at 30^{o}C, pH7 were calculated in triplicate as described previously (Hanson et al., 2004) using $E'_{0(DTT)}$ = -0.323V (Sajewski and Whitesides, 1980).

References

Bahner, M., Frechter, S., Da Silva, N., Minke, B., Paulsen, R., and Huber, A. (2002). Light-regulated subcellular translocation of Drosophila TRPL channels induces long-term adaptation and modifies the light-induced current. Neuron *34*, 83-93.

Bateman, A., Lachlan, C, Durbin, R, Finn, RD, Volked, H, Griffiths-Hones, S, Khanna, A, Marshall, M, Moxon, S, Sonnhammer, EL, Studholme, DJ, Yeats, C, Eddy, SR (2004). The Pfam Protein Families Database. Nucleic Acids Res *32*, D138-D141.

Bhattacharyya, R. P., Remenyi, A., Yeh, B. J., and Lim, W. A. (2006). Domains, motifs, and scaffolds: the role of modular interactions in the evolution and wiring of cell signaling circuits. Annu Rev Biochem *75*, 655-680.

Brunger, A. T., Adams, P. D., Clore, G. M., DeLano, W. L., Gros, P., Grosse-Kunstleve, R. W., Jiang, J. S., Kuszewski, J., Nilges, M., Pannu, N. S., *et al.* (1998). Crystallography & NMR system: A new software suite for macromolecular structure determination. Acta Crystallogr D Biol Crystallogr *54*, 905-921.

Cao, T. T., Deacon, H. W., Reczek, D., Bretscher, A., and von Zastrow, M. (1999). A kinase-regulated PDZ-domain interaction controls endocytic sorting of the beta2-adrenergic receptor. Nature *401*, 286-290.

Chetkovich, D. M., Chen, L., Stocker, T. J., Nicoll, R. A., and Bredt, D. S. (2002). Phosphorylation of the postsynaptic density-95 (PSD-95)/discs large/zona occludens-1 binding site of stargazin regulates binding to PSD-95 and synaptic targeting of AMPA receptors. J Neurosci *22*, 5791-5796.

Cohen, N. A., Brenman, J. E., Snyder, S. H., and Bredt, D. S. (1996). Binding of the inward rectifier K+ channel Kir 2.3 to PSD-95 is regulated by protein kinase A phosphorylation. Neuron *17*, 759-767.

Cronin, M. A., Diao, F., and Tsunoda, S. (2004). Light-dependent subcellular translocation of Gqalpha in Drosophila photoreceptors is facilitated by the photoreceptor-specific myosin III NINAC. J Cell Sci *117*, 4797-4806.

Cronin, M. A., Lieu, M. H., and Tsunoda, S. (2006). Two stages of light-dependent TRPL-channel translocation in Drosophila photoreceptors. J Cell Sci *119*, 2935-2944.

DeLano, W. L. (2002). The PyMOL Molecular Graphics System (San Carlos, CA, USA: DeLano Scientific).

Doyle, D. A., Lee, A., Lewis, J., Kim, E., Sheng, M., and MacKinnon, R. (1996). Crystal structures of a complexed and peptide-free membrane protein-binding domain: molecular basis of peptide recognition by PDZ. Cell *85*, 1067-1076.

Dueber, J. E., Yeh, B. J., Bhattacharyya, R. P., and Lim, W. A. (2004). Rewiring cell signaling: the logic and plasticity of eukaryotic protein circuitry. Curr Opin Struct Biol *14*, 690-699.

Dueber, J. E., Yeh, B. J., Chak, K., and Lim, W. A. (2003). Reprogramming control of an allosteric signaling switch through modular recombination. Science *301*, 1904-1908.

Garrard, S. M., Capaldo, C. T., Gao, L., Rosen, M. K., Macara, I. G., and Tomchick, D. R. (2003). Structure of Cdc42 in a complex with the GTPase-binding domain of the cell polarity protein, Par6. Embo J *22*, 1125-1133.

Hanson, G. T., Aggeler, R., Oglesbee, D., Cannon, M., Capaldi, R. A., Tsien, R. Y., and Remington, S. J. (2004). Investigating mitochondrial redox potential with

redox-sensitive green fluorescent protein indicators. J Biol Chem *279*, 13044-13053.

Harris, B. Z., and Lim, W. A. (2001). Mechanism and role of PDZ domains in signaling complex assembly. J Cell Sci *114*, 3219-3231.

Hwang, C., Lodish, H. F., and Sinskey, A. J. (1995). Measurement of glutathione redox state in cytosol and secretory pathway of cultured cells. Methods Enzymol *251*, 212-221.

Hwang, C., Sinskey, A. J., and Lodish, H. F. (1992). Oxidized redox state of glutathione in the endoplasmic reticulum. Science *257*, 1496-1502.

Jones, T. A., Zou, J. Y., Cowan, S. W., and Kjeldgaard (1991). Improved methods for building protein models in electron density maps and the location of errors in these models. Acta Crystallogr A *47 (Pt 2)*, 110-119.

Keese, M. A., Saffrich, R., Dandekar, T., Becker, K., and Schirmer, R. H. (1999). Microinjected glutathione reductase crystals as indicators of the redox status in living cells. FEBS Lett *447*, 135-138.

Kimple, M. E., Siderovski, D. P., and Sondek, J. (2001). Functional relevance of the disulfide-linked complex of the N-terminal PDZ domain of InaD with NorpA. Embo J *20*, 4414-4422.

Kiselev, A., Socolich, M., Vinos, J., Hardy, R. W., Zuker, C. S., and Ranganathan, R. (2000). A molecular pathway for light-dependent photoreceptor apoptosis in Drosophila. Neuron *28*, 139-152.

Meyer, N. E., Joel-Almagor, T., Frechter, S., Minke, B., and Huber, A. (2006). Subcellular translocation of the eGFP-tagged TRPL channel in Drosophila photoreceptors requires activation of the phototransduction cascade. J Cell Sci *119*, 2592-2603.

Ostergaard, H., Tachibana, C., and Winther, J. R. (2004). Monitoring disulfide bond formation in the eukaryotic cytosol. J Cell Biol *166*, 337-345.

Otwinowksi, Z. (1993). In Data collection and processing, L. Sawyer, Isaacs, N. & Bailey, S., ed. (Warrington, UK), pp. 56-62.

Park, S. H., Zarrinpar, A., and Lim, W. A. (2003). Rewiring MAP kinase pathways using alternative scaffold assembly mechanisms. Science *299*, 1061-1064.

Penkert, R. R., DiVittorio, H. M., and Prehoda, K. E. (2004). Internal recognition through PDZ domain plasticity in the Par-6-Pals1 complex. Nat Struct Mol Biol *11*, 1122-1127.

Peterson, F. C., Penkert, R. R., Volkman, B. F., and Prehoda, K. E. (2004). Cdc42 regulates the Par-6 PDZ domain through an allosteric CRIB-PDZ transition. Mol Cell *13*, 665-676.

Sajewski, R. P., and Whitesides, G. M. (1980). Rate Constants and Equilibrium Constants for Thiol-Disulfide Interchange Reactions Involving Oxidized Glutathione. J Am Chem Soc *102*, 2011-2015.

Sallee, N. A., Yeh, B. J., and Lim, W. A. (2007). Engineering modular protein interaction switches by sequence overlap. J Am Chem Soc *129*, 4606-4611.

Schafer, F. Q., and Buettner, G. R. (2001). Redox environment of the cell as viewed through the redox state of the glutathione disulfide/glutathione couple. Free Radic Biol Med *30*, 1191-1212.

Tsunoda, S., Sierralta, J., Sun, Y., Bodner, R., Suzuki, E., Becker, A., Socolich, M., and Zuker, C. S. (1997). A multivalent PDZ-domain protein assembles signalling complexes in a G-protein-coupled cascade. Nature *388*, 243-249.

Tsunoda, S., and Zuker, C. S. (1999). The organization of INAD-signaling complexes by a multivalent PDZ domain protein in Drosophila photoreceptor cells ensures sensitivity and speed of signaling. Cell Calcium *26*, 165-171.

van den Berk, L. C., Landi, E., Harmsen, E., Dente, L., and Hendriks, W. J. (2005). Redox-regulated affinity of the third PDZ domain in the phosphotyrosine phosphatase PTP-BL for cysteine-containing target peptides. Febs J *272*, 3306-3316.

von Ossowski, L., Tossavainen, H., von Ossowski, I., Cai, C., Aitio, O., Fredriksson, K., Permi, P., Annila, A., and Keinanen, K. (2006). Peptide binding and NMR analysis of the interaction between SAP97 PDZ2 and GluR-A: potential involvement of a disulfide bond. Biochemistry *45*, 5567-5575.

Yeh, B. J., Rutigliano, R. J., Deb, A., Bar-Sagi, D., and Lim, W. A. (2007). Rewiring cellular morphology pathways with synthetic guanine nucleotide exchange factors. Nature *447*, 596-600.

Table 2-1. Crystallography Statistics for InaD-PDZ5, 0mM DTT

Data Collection/Phasing:

Space Group:	$P4_12_12$			
Cell Dimensions	a=95.74 Å, b=95.74 Å, c=48.56 Å, $\alpha=\beta=\gamma=90.0^o$			
Dataset	Native	K_2PtCl_4	trans-$Pd(NH_3)_2Cl_2$	trans-$Pd(NH_3)_2Cl_2$
Source	Dip2020	RAXIS II	RAXIS II	Dip2020
Wavelength	1.54	1.54	1.54	1.54
Resolution range (Å)	20-2.05	20-2.4	20-2.05	20-2.3
Reflections (Unique)	209518 (14738)	154025 (16182)	158249 (16107)	122843 (18604)
Completeness				
All/Outer Shell	99.7/99.8	95.2/96.4	60.3/50.3	98.5/98.9
R_{sym} (%)[a]				
All/Outer Shell	4.4/15.3	7.6/23.7	4.9/37.5	5.8/22.0
I/σ				
All/Outer Shell	44.3/16.7	21.6/6.1	13.4/1.6	16.9/4.2
Heavy Atom Sites	--	4	2	2
R_{cullis}	--	0.80	0.92	0.97
Phasing Power (iso)	--	1.27	0.43	0.37
Phasing Power (ano)	--	1.23	0.71	0.30

Refinement

Dataset	Native
Resolution (Å)	2.05
Reflections working/test	13903/737
R (R_{free})[b]	0.224 (0.242)
No. of atoms	
Protein	1304
Waters	153
Mean B factor	27.5 $Å^2$
RMSD Bond Length	0.007 Å
RMSD Bond Angle	1.6^o
Ramachandran outliers	0

[a] $R_{sym} = |I_h - \langle I_h \rangle| / I_h$, where $\langle I_h \rangle$ is the average intensity over symmetry equivalent reflections.
[b] $R = \Sigma|F_{obs} - F_{calc}|/\Sigma(F_{obs})$, where the summation is over the data used in refinement. R_{free} is the same statistic caclulated for the 5% of data excluded from refinement steps.

Table 2-2. Crystallography Statistics for InaD-PDZ5, 10mM DTT.

Data Collection/Phasing:

Space Group:	$P4_322$			
Cell Dimensions	a=67.70 Å, b=67.70 Å, c=162.5 Å, $\alpha=\beta=\gamma=90.0^o$			
Source	SSRL BL 1-5			
	Peak	Edge	High remote	Low remote
Wavelength	.97965	.980035	.925256	1.06883
Resolution range (Å)	40-2.2	40-2.2	40-2.2	40-2.2
Reflections (Unique)	163831 (35925)	163970 (35987)	151097 (35471)	166696 (35921)
Completeness				
All/Outer Shell	97.9/96.2	98.0/96.3	96.9/93.3	97.9/96.0
R_{sym} (%)[a]				
All/Outer Shell	12.9/56.9	12.9/60.0	14.3/65.7	11.6/55.3
I/σ				
All/Outer Shell	9.0/1.9	9.0/1.9	7.4/1.5	10.4/2.1
No. of Se sites	6	6	6	6

Resolution	FOM[b]
4.60	0.74
3.45	0.71
3.22	0.65
3.05	0.60
2.88	0.53
2.76	0.47
2.64	0.42
2.53	0.38
2.41	0.34
2.30	0.30

Refinement

Dataset	Low remote
Resolution limit (Å)	2.2
Reflections working/test	33753/1700
R (R_{free})[c]	0.206 (0.231)
No. of atoms	
Protein	2269
Waters	266
Glycerol	12 (2 molecules)
Mean B factor	24.0 $Å^2$
RMSD Bond Length	0.006 Å
RMSD Bond Angle	1.3^o
Ramachandran outliers	0

[a] $R_{sym} = |I_h - \langle I_h \rangle| / I_h$, where $\langle I_h \rangle$ is the average intensity over symmetry equivalent reflections.
[b] Figure of Merit
[c] $R = \Sigma|F_{obs} - F_{calc}|/\Sigma(F_{obs})$, where the summation is over the data used in refinement. R_{free} is the same statistic caclulated for the 5% of data excluded from refinement steps.

Table 2-3. Crystallography Statistics for InaD-PDZ5^{C645S}, 0mM DTT.

Data Collection/Phasing:

	Native	Se-Met
Space Group	$P4_32$	$P4_32$
Cell Dimensions	a=b=c=112.04 Å, α=β=γ=90.0°	a=b=c=112.05 Å, α=β=γ=90.0°
Source	ALS 8.2.1	APS 19-BM
Wavelength (Å)	1.0	0.97940 (peak)
Resolution range (Å)	40-1.55	40-2.01
Reflections (Unique)	559574 (36464)	273593 (16616)
Completeness		
All/Outer Shell	99.9/99.9	99.8/99.1
R_{sym} (%)[a]		
All/Outer Shell	5.2/50.4	5.1/10.5
I/σ		
All/Outer Shell	51.1/4.4	72.3/23.6
No. of Se sites	--	4

Resolution (Å)	Phasing Power	FOM[b]
4.00	6.23	0.47
3.18	4.81	0.49
2.77	4.55	0.50
2.52	4.32	0.51
2.34	3.78	0.49
2.20	3.30	0.46
2.09	2.93	0.43
2.00	4.42	0.34

Refinement

Dataset	Native
Resolution limit (Å)	1.55
Reflections working/test	30072/3324
R (R_{free})[c]	0.248 (0.267)
No. of atoms	
Protein	1406
Waters	181
Mean B factor	24.66 Å^2
RMSD Bond Length	0.007 Å
RMSD Bond Angle	1.7°
Ramachandran outliers (Generously allowed / Disallowed regions)	2/0

[a] $R_{sym} = |I_h - \langle I_h \rangle| / I_h$, where $\langle I_h \rangle$ is the average intensity over symmetry equivalent reflections.
[b] Figure of Merit
[c] $R = \Sigma|F_{obs} - F_{calc}|/\Sigma(F_{obs})$, where the summation is over the data used in refinement. R_{free} is the same statistic caclulated for the 5% of data excluded from refinement steps.

Table 2-4. Structural comparison between PDZ5 structures and other PDZ domains. In order to compare InaD PDZ5 with other known PDZ domains, we constructed structural alignments between PDZ5 and available PDZ structures (see Figure 2-4). Here, we report Cα-Cα distances (mean and standard deviation) for positions involved in ligand binding (numbering according to InaD). In the "Normal" column, PDZ structures (not including InaD PDZ5) are compared against one another to determine the variability in position for each residue. In the "PDZ5" columns, the indicated structure of PDZ5 is compared against other PDZ structures. In red are PDZ5 positions which differ from the "Normal" statistics by greater than one standard deviation. The oxidized form of PDZ5 differs from other PDZ domains in the α2 helix, while the reduced and mutant (C645S) forms show no significant differences. For a complete analysis of all positions, see Figure 2-4.

		Normal	PDZ5 oxidized	PDZ5 reduced	PDZ5 C645S
β2	K590	3.84 (1.54)	3.23 (1.26)	3.11 (1.14)	2.91 (0.96)
	L595	0.99 (0.39)	1.09 (0.44)	1.15 (0.42)	1.48 (0.52)
	L597	0.91 (0.39)	1.31 (0.37)	1.39 (0.39)	1.18 (0.35)
	S598	0.98 (0.43)	1.52 (0.40)	1.23 (0.33)	1.42 (0.30)
	L599	1.00 (0.41)	1.16 (0.35)	1.03 (0.34)	1.03 (0.31)
α2	F642	1.78 (0.82)	**3.60 (0.96)**	1.62 (0.57)	1.86 (0.63)
	C645	1.35 (0.57)	**3.41 (0.55)**	1.04 (0.35)	1.34 (0.42)
	Y646	1.47 (0.61)	**3.80 (0.67)**	1.37 (0.55)	1.38 (0.48)
	F649	1.28 (0.58)	**2.27 (0.48)**	1.85 (0.49)	1.02 (0.50)

Chapter Three
In vivo characterization of the PDZ5 disulfide.

A disulfide bond in vivo

In vitro measurement of the standard redox potential of the isolated PDZ5 domain (E_0 = -425mV) in chapter two indicates the presence of an extremely strong disulfide bond that may actually be stable in the normally reducing cytosolic interior of a cell. In fact, a survey of the literature indicates that the redox potential of the cytosol is usually between -230mv and -300mV (Hanson et al., 2004; Hwang et al., 1995; Hwang et al., 1992; Keese et al., 1999; Ostergaard et al., 2004; Schafer and Buettner, 2001); the more negative redox potential of PDZ5 suggests then that oxidized state would be favored, although it is not clear what the redox potential might be in the context of a full-length InaD protein. In fact, other proteins which utilize disulfide bonds typically have much less negative redox potentials. For instance, potentials for the active site disulfide bond in the ubiquitious thioredoxin protein range from -230mV to -270mV (depending on the organism (Joelson et al., 1990; Krause et al., 1991; Watson et al., 2003)); this range is poised around cytosolic conditions (-230mv to -300mV) and consistent with the idea that disulfide bond formation may be regulated and cycle *in vivo*. In contrast, a potential of -425mV for InaD-PDZ5 actually suggests that InaD should be completely oxidized in the cell. However, two caveats must be taken into account: 1) The redox conditions of the photoreceptor microvilli maybe be significantly different than the "standard" conditions mentioned above; and 2) The redox potential of the Cys606-Cys645 interaction may be quite different in the context of the full protein.

Interestingly, the notion that redox chemistry may play a role in regulating the *Drosophila* visual system is not without precedent; the first PDZ domain of InaD (PDZ1) has been proposed to be involved in an intermolecular disulfide interaction with the C-terminal region of the NorpA PLC-β (Kimple et al., 2001). More specifically, a co-crystal structure of PDZ1 bound to the predicted C-terminal peptide of NorpA (NH_2-GKTEFCA-COOH) indicates a covalent interaction between cysteine 31 on PDZ1 and the cysteine at the penultimate position of the peptide (NorpA PLC-β position 1094), and this interaction has been validated *in vitro* with recombinant protein (Kimple et al., 2001). Thus, any studies of redox chemistry involving the intramolecular disulfide in PDZ5 should be considered in context of this PDZ1 - PLC-β intermolecular interaction.

Figure 3-1 InaD-PDZ5 and NorpA from *Drosophila* and *Calliphora*. (A) Sequence alignments of the 1st and 5th PDZ domains of InaD from the fruitfly *Drosophila melanogaster* (*Dm*) and the blowfly *Calliphora vicinia* (*Cv*). The cysteine (red) implicated in a disulfide bond between the 1st PDZ domain and the NorpA PLC-β of *D.melanogaster* is not conserved in *C.vicinia*, questioning its importance to visual signaling. The cysteines (red) involved in an intramolecular disulfide in the 5th PDZ domain are conserved in both species. (B) Genomic sequencing of the C-terminus of *D. melanogaster* NorpA PLC-β. The arrow indicates Tyr1094 which was previously reported as Cys1094; this concurs with results from the *Drosophila* genome project.

However, while studying this intermolecular interaction, we discovered that the above evidence, though technically accurate, is not physiological. First of all, cysteine 31 is not conserved in the InaD ortholog from the closely related fly *Calliphora vicinia* (Figure 3-1A), suggesting that the interaction is not evolutionarily relevant to the fly. Furthermore, genomic sequencing of the *norpA* gene both by us (Figure 3-1B) and by the *Drosophila* genome project (Celniker et al., 2002) indicates a sequencing error at position 1094 in the original report of the NorpA PLC-β sequence (Bloomquist et al., 1988). The cysteine reported at this site is actually a tyrosine in *Drosophila melanogaster* (and a phenylalanine in *Calliphora vicinia* (A. Huber, personal communication)). The interaction that was previously shown in the literature (Kimple et al., 2001) is therefore a result of using recombinant protein or synthesized peptide with an incorrect NorpA PLC-β sequence. Thus, no intermolecular bond exists between the 1st PDZ domain of InaD (PDZ1) and NorpA PLC-β. Furthermore, previous data indicating an interaction between PDZ1 and NorpA PLC-β concluded that the binding was redox-dependent. In light of the sequence data presented here, we conclude that there exists no evidence for an interaction (covalent or non-covalent) between PDZ1 of InaD and NorpA PLC-β.

The above considerations, particularly the highly negative reducing potential of recombinant PDZ5 and the "artifactual" disulfide bond involving PDZ1, argue that the state of the PDZ5 disulfide needs to be directly measured *in vivo*. To do this, we developed a method modified from earlier work on monitoring disulfide-bonded proteins in bacteria (Leichert and Jakob, 2004). This work used a differential labeling technique whereby free cysteines and disulfide-bonded cysteines were specifically labeled with

distinct chemical groups. Assaying the *in vivo* condition was achieved by homogenizing cells directly into a cold trichloroacetic acid solution, thereby precipitating proteins immediately and quenching them in their native state. Our method utilized similar techniques: In short, dissected retinas from *D.melanogaster* were directly homogenized into a 25% trichloroacetic acid solution and protein pellets were washed with acetone and resolubilized under denaturing conditions. Maleimide chemistry (Figure 3-2) was then used to allow for specific labeling of free thiol groups.

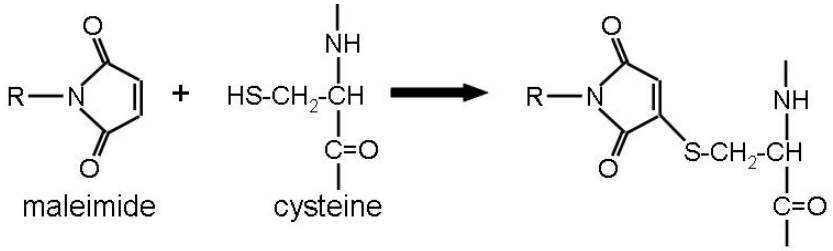

Figure 3-2. Maleimide chemistry. Free thiol groups can be irreversibly modified via reaction with a maleimide adduct.

By utilizing a maleimide compound with fluorescent properties, labeled proteins can be visualized by running the homogenate on a 2-dimensional gel and directly scanning the gel for fluorescent spots. For instance, if protein homogenate is prepared as described above and directly labeled with Cy3-maleimide (Cy3m), all proteins with a free thiol group will be labeled; the resulting Cy3-fluorescent pattern is shown in Figure 3-3A. This gives a rough approximation of the complexity of the total protein population in the retinal homogenate.

In order to specifically label proteins containing disulfide bonds, the following strategy was used: The retinal homogenate was first reacted with an alternative maleimide compound (AMS) in order to "block" all free thiols. After washing away any

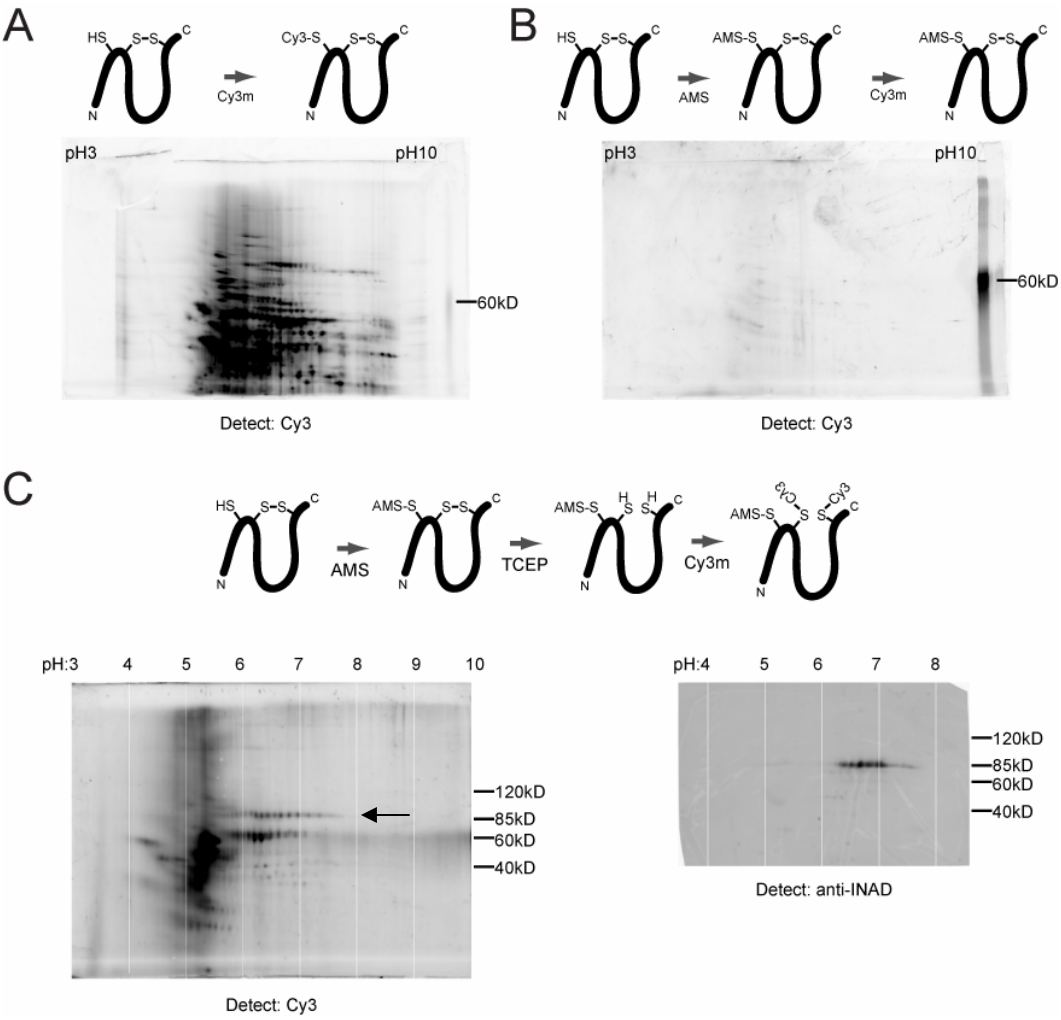

Figure 3-3 An assay to measure disulfide bond formation *in vivo*. (A) Total protein in light-reared wild-type *Drosophila* retinas was visualized by direct labeling with Cy3-maleimide (Cy3m). 2D gel electrophoresis followed by Cy3 detection shows the large number of protein species present in the *Drosophila* retina. (B) Primary reaction with AMS, followed by subsequent reaction with Cy3m precludes any Cy3 labeling. Thus, any labeling in (C) is specific to the disulfide reduction step. (C) (top) The disulfide bond assay consists of sequential reactions with AMS, TCEP and finally Cy3m. (bottom left) Disulfide-bonded proteins in light-reared wild-type flies. A series of Cy3-labeled spots (see arrow) appears in a position consistent with InaD (between pH6 and pH8 and a mobility of approximately 85kD). (bottom right) Western blot (probed against InaD) of a 2D gel from wild-type flies. InaD runs at 85kD, between pH6 and pH8.

residual AMS, subsequent reaction with Cy3m showed no labeling (Figure 3-3B), evidencing that all free cysteines have been "blocked." Cysteines involved in disulfide bonds can then be "freed" by reaction with a reducing agent (Tris(2-carboxyethyl)phosphine hydrochloride, TCEP) and then specifically labeled with the fluorescent maleimide, Cy3m. This differential labeling scheme (Figure 3-3C, top), followed by separation on a 2D gel and Cy3-detection, allows specific visualization of disulfide-bond containing proteins (Figure 3-3C, bottom left).

In light-reared wild-type flies, a series of Cy3-labeled spots appears at a mobility of ~85kD and a pH range between 6 and 8 (Figure 3-3C, bottom left, see arrow); strikingly, these are the predicted parameters for a multiply-phosphorylated InaD species. (The calculated isolectric point (pI) for an unmodified denatured InaD is 8.30; subsequent phosphorylation will cause the pI to drop). A 2D western blot probed against InaD (Figure 3-3C, bottom right) confirms that total InaD does indeed run at this mobility and pH range, suggesting that the labeled spots represent a disulfide-bonded InaD species. As a reminder, InaD is known to be phosphorylated *in vivo* by eye-PKC (Huber et al., 1996; Matsumoto et al., 1999; Matsumoto et al., 1982; Matsumoto and Pak, 1984).

To further characterize the disulfide bond *in vivo*, we constructed transgenic flies expressing either a wild-type copy of InaD or the C645S mutant (under the control of a photoreceptor-specific promoter) in an InaD-null ($inaD^{1}$) genetic background. These transgenic lines ($yw;inaD^{1};P[inaD^{wt}]$ and $yw;inaD^{1}P[inaD^{C645S}]$, hereafter called $inaD^{wt}$ and $inaD^{C645S}$, respectively) showed normal expression levels of both wild-type and mutant InaD *in vivo* (Figure 3-4F). InaD-null (Figure 3-4C) and $inaD^{C645S}$ flies (Figure 3-4D) showed no Cy3-labeling at the expected position for InaD, while $inaD^{wt}$ flies (Figure

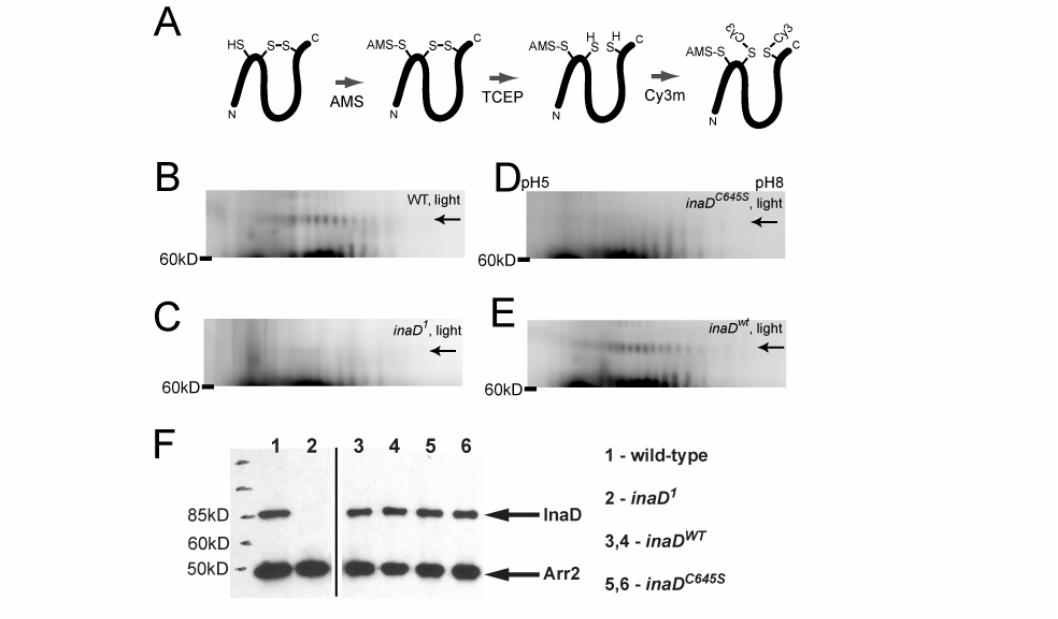

Figure 3-4 InaD-PDZ5 is oxidized *in vivo*. (A) Schematic for specific labeling of disulfide-bond containing proteins *in vivo*. (B-E) Spots corresponding to oxidized InaD are visible in light-exposed wild-type (B) and $inaD^{wt}$ (E) flies, but not InaD-null ($inaD^{1}$, (C)) or $inaD^{C645S}$ (D) flies. (F) Western blots of retinal extracts. Retinal homogenate was separated by 10% SDS-PAGE, transferred to PVDF membrane and probed with antibodies against the 1st PDZ domain of InaD and βarrestin-2 (Arr2; loading control). All transgenic flies (lanes 3-6) express levels of InaD comparable with wild-type.

3-4E) retained the pattern of spots seen in wild-type flies (Figure 3-4B), strongly suggesting (1) that the spots are indeed InaD, and (2) that the disulfide-detected is the Cys606-Cys645 interaction.

Dynamic behavior in vivo

We compared the pattern of disulfide-bond containing proteins in dark-reared and light-exposed flies. Interestingly, spots corresponding to oxidized InaD were not present in dark-reared flies (Figure 3-5A); however, brief exposure to light (approximately 5 minutes) was sufficient for reformation of the oxidized species,

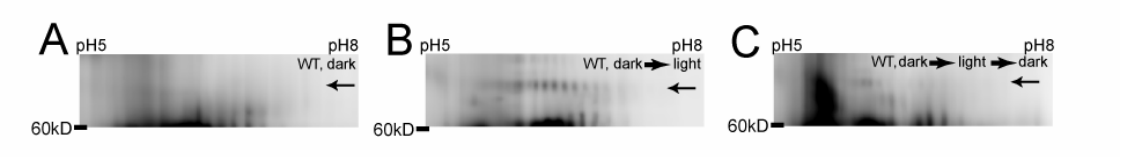

Figure 3-5 Dynamic behavior of InaD. 2D gels of disulfide containing proteins from dark-reared wild-type flies (A), light-exposed wild-type flies (B), and light-exposed wild-type flies returned to the dark for 10 minutes (C). The data indicate light-dependent reversible formation of the disulfide bond in InaD-PDZ5 *in vivo*.

indicated by the appearance of the Cy3-labeled InaD spots (Figure 3-5B). Dark-adaptation (for approximately 10 minutes) of light-exposed flies caused to spots to disappear (Figure 3-5C), indicating that the PDZ5 disulfide is transient - forming upon light exposure and relaxing back to the reduced state when the cell is returned to the dark. To independently confirm these results, we directly monitored InaD's mobility on a non-reducing 1D gel (Figure 3-6). In this assay, we replaced the fluorescent Cy3-maleimide with a pegylated-maleimide (pegM) with a molecular weight of approximately 5kD. Thus, the presence of a disulfide bond will cause a molecular weight shift of ~10kD in InaD's position on a 1D western blot (Figure 3-6B, right). This assay provided similar results as those in Figures 3-4 and 3-5, and also confirms that the disulfide bond is not intermolecular (Figure 3-6B, left). Thus, InaD cycles between an oxidized and reduced state *in vivo* in response to light stimuli.

Additional results indicate that transition of the PDZ5 disulfide bond is not only dependent on light-exposure but, more specifically, dependent on activation of the phototransduction cascade. Mutant flies which lack the major rhodopsin (*ninaE*^{I17}) show greatly reduced Cy3m labeling of InaD (Figure 3-7C) though total levels of InaD are unaffected (Figure 3-7E); this suggests that PDZ5 disulfide formation is dependent on activation of visual signaling. (Residual labeling is expected due to expression of minor

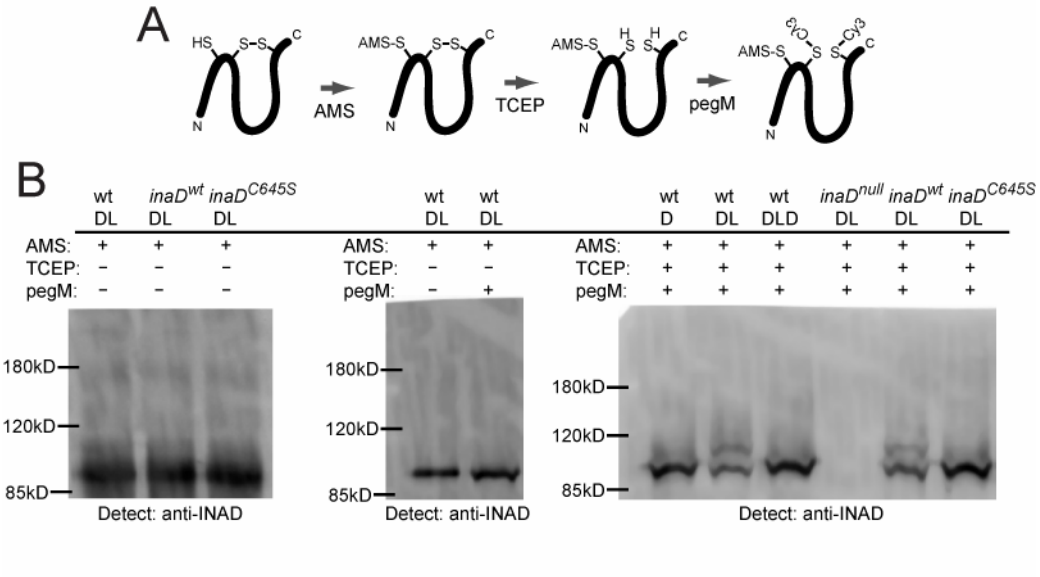

Figure 3-6 Dynamic behavior of InaD *in vivo*. (A) Schematic for specific labeling of disulfide-bond containing proteins *in vivo*. A similar assay as in Figures 3-2, 3-3 and 3-4, except a 5kD pegylated- maleimide (pegM, Sigma) is used in place of Cy3-maleimide. (B) Western blots (probed against InaD) are shown. (Left) TCEP and pegM are omitted. In this condition, we can examine InaD's participation in intermolecular disulfide bonds. The lack of higher molecular weight species (>85kD) indicate that InaD is not involved in an intermolecular disulfide bond, in either its wild-type or mutant (C645S) form. (Middle) Omission of TCEP precludes any labeling by pegM. Thus, any pegM labeling (see below) is specific to the disulfide-reduction step. (Right) With inclusion of TCEP, pegM will cause mobility shifts in disulfide-bond containing proteins. Dark-reared wild-type flies (D) show no shift, unless exposed to light (DL). When returned to the dark conditions (DLD), wild-type flies again relax to a reduced state with no mobility shift. Light-exposed $inaD^{wt}$ flies show a mobility shift, while light-exposed $inaD^{C645S}$ flies do not. These results confirm those from the 2D gels shown in Figures 3-3, 3-4 and 3-5.

rhodopsin isoforms (Iakhine et al., 2004)). The mechanism downstream of rhodopsin that triggers this transition is yet unknown, but one obvious hypothesis implicates eye-PKC, the component of the InaD complex that mediates light-dependent feedback regulation. Known substrates of eye-PKC include the TRP channel and InaD itself (Huber et al., 1996; Matsumoto et al., 1999; Matsumoto et al., 1982; Matsumoto and Pak, 1984; Popescu et al., 2006); thus, phosphorylation of InaD could represent the signal by

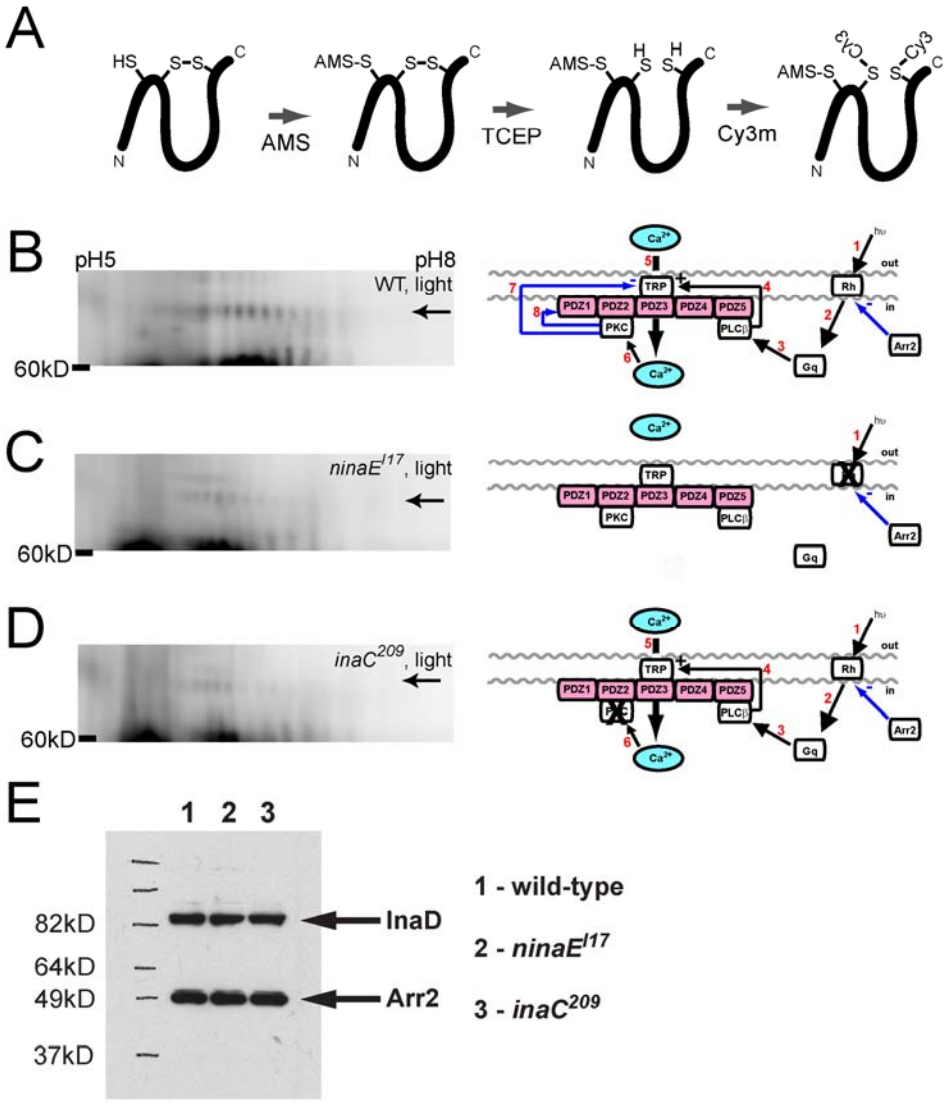

Figure 3-7 Redox state of InaD in *ninaE*^{I17} and *inaC*^{209} flies. (A) Schematic for specific labeling of disulfide-bond containing proteins *in vivo*. (B-D) 2D gels of disulfide containing proteins from light-exposed wild-type flies (B), *ninaE*^{I17} flies (which are null for the major rhodopsin, (C)), and *inaC*^{209} flies (which are null for eye-PKC, (D)). The data indicate that light-induced formation of the disulfide bond in InaD-PDZ5 depends at least in part on phototransduction through eye-PKC. (E) Western blots of retinal extracts. Retinal homogenate was separated by 10% SDS-PAGE, transferred to PVDF membrane and probed with antibodies against the 1st PDZ domain of InaD and βarrestin-2 (Arr2; loading control). *ninaE*^{I17} and *inaC*^{209} flies express wild-type levels of InaD.

which light shifts the equilibrium of the Cys606-Cys645 disulfide. Light exposure fails to trigger proper formation of the InaD disulfide bond in *inaC*^{209} mutant (null for eye-PKC, Figure 3-7D) despite wild-type levels of InaD (Figure 3-7E), providing an initial clue that eye-PKC activity may control InaD conformational dynamics. This result motivates a thorough mapping and characterization of the multiple eye-PKC phosphorylation sites on InaD.

Lastly, we examined InaD-PDZ5 disulfide formation in two other InaD mutants, *inaD*^{2} and *inaD*^{215}. The *inaD*^{2} mutation (G605E) is adjacent to position 606 (the cysteine involved in the disulfide bond with position 645), and causes destabilization of the 5th domain (Mishra, unpublished data) and a specific mislocalization of PLC-β (Tsunoda et al., 1997). Given that the domain is likely unfolded *in vivo*, it is not surprising that we do not observe disulfide bond formation *in vivo* (Figure 3-8C). The *inaD*^{215} mutation (M442K) is located in the 3rd PDZ domain of InaD, making it unable to bind and localize the TRP channel (Tsunoda et al., 1997). Functionally, this mutation results in defective channel inactivation (Henderson et al., 2000), most likely due to inefficient phosphorylation of TRP by eye-PKC. Despite this, the data indicate that disulfide-bond formation in InaD is not hindered (Figure 3-8D), although phosphorylation seems to be somewhat affected as evidenced by a shift in the isoelectric point of the InaD species towards the more basic region. Since eye-PKC and InaD are still colocalized in the *inaD*^{215} mutant (Tsunoda et al., 1997), we hypothesize that the phosphorylation events necessary for disulfide bond transition still occur efficiently, while other phosphorylation events occur less efficiently. A detailed characterization of these eye-PKC-mediated phosphorylation events, how they control disulfide bond formation, and how they are

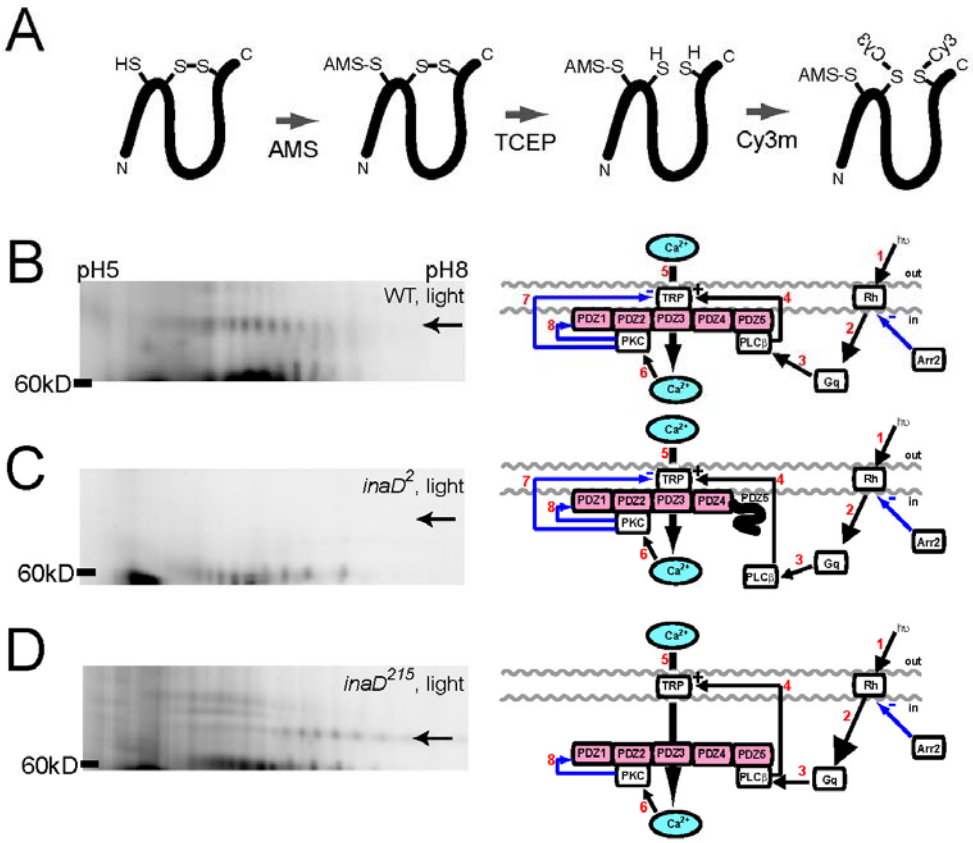

Figure 3-8 Redox state of InaD in *inaD*^{2} and *inaD*^{215} flies. (A) Schematic for specific labeling of disulfide-bond containing proteins *in vivo*. (B-D) 2D gels of disulfide containing proteins from light-exposed wild-type flies (B), *inaD*^{2} flies (in which the 5th PDZ domain is destabilized, (C)), and *inaD*^{215} flies (in which the TRP channel is mislocalized from the remainder of the InaD complex, (D)). The data indicate that light-induced formation of the disulfide bond does not occur when PDZ5 is unfolded, but is not dependent on proper localization to the TRP channel.

regulated in an "*inaD*^{215}" state will be an important avenue of future study.

In summary, we have shown that the 5th PDZ domain of InaD exhibits dynamic behavior *in vivo*, shifting between an oxidized and reduced state in a light-regulated manner. The crystallographic studies from chapter two define this conformational switch at atomic resolution, and suggest that such behavior will have subsequent effects on the

localization of PDZ5's binding partner. To our knowledge, this work provides the first example of such large-scale conformational switching in the PDZ domain, and opens the possibility that other members of this large family of scaffolding modules may also be engaged in dynamic conformational changes. In addition, our data indicate that the redox state of PDZ5 is controlled by the phosphorylation state of InaD. Many other scaffolds are known to be phosphorylated (Bhattacharyya et al., 2006; Lonart et al., 2003), though the results of such events are not understood at a structural level. Future work on InaD phosphorylation and its role in controlling PDZ5 structure and function may contribute a valuable model for understanding the mechanistic basis for regulation of scaffolding proteins in general.

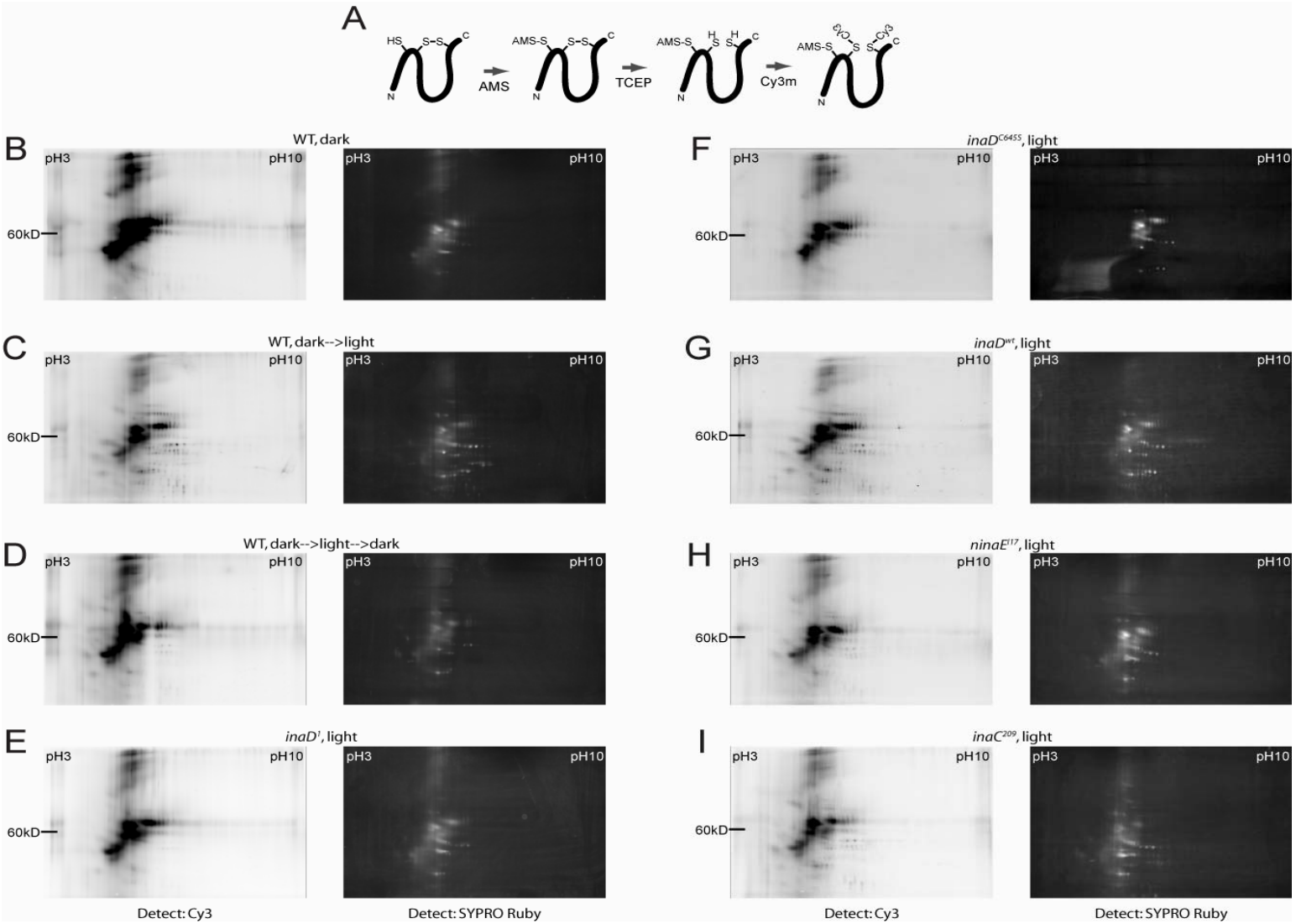
A
HS
S-S
C
N
AMS
AMS-S
TCEP
H
Cy3m
Cy3
B
WT, dark
C
WT, dark-->light
D
WT, dark-->light-->dark
E
inaD1, light
F
inaDC6455, light
G
inaDwt, light
H
ninaE117, light
I
inaC209, light
pH3
pH10
60kD
Detect: Cy3
Detect: SYPRO Ruby

Methods

Fly Stocks

The following fly stocks were used: wild-type (y^2w^1), InaD-null (y^2w^1; $inaD^1$), $inaD^2$, $inaD^{wt}$ (y^2w^1; $inaD^1$;$P[y^+,inaD^{wt}]$), $inaD^{C645S}$ (y^2w^1;$inaD^1$ $P[y^+,inaD^{C645S}]$), $ninaE^{I17}$, $inaC^{209}$, $arr2^3$, and $inaD^{C645S}$,$arr2^3$ (y^2w^1;$inaD^1$ $P[y^+,inaD^{C645S}]$;$arr2^3$). $inaD^{wt}$ and $inaD^{C645S}$ were constructed via standard P-element transformation using the YC4 vector (gift from Steve Britt; derived from the Y.E.S. vector (Patton et al., 1992)). The coding sequence of InaD, flanked by the 5' and 3' UTRs of the Rh1 gene, was subcloned into YC4 and injected into *yw;* $inaD^1$ embryos. Transformants were homozygosed in an $inaD^1$ background using standard genetic crosses.

Cysteine-labeling assays

For *in vivo* assays, 1-day old flies were frozen in liquid nitrogen and dehydrated in acetone at -80°C. Retinas were dissected and homogenized into PBS supplemented with 25% TCA (trichloroacetic acid). Protein was precipitated on ice for >1 hour and collected by centrifugation at 13,000g for 10 minutes. After washing 3x with acetone, the pellet was resolubilized in denaturing buffer (8M urea, 100mM HEPES, 2% CHAPS,

Figure 3-9 Disulfide bond-containing proteins *in vivo*. (A) Schematic for specific labeling of disulfide bond-containing proteins *in vivo*. (B-I) Full gels for images in Figures 3-4, 3-5 and 3-7. Shown on the left are 2D gels of disulfide containing proteins (visualized by Cy3 detection) from dark-reared wild-type flies (B), light-exposed wild-type flies (C), light-exposed wild-type flies returned to the dark for 10 minutes (D), light-exposed InaD-null flies ($inaD^1$) (E), light-exposed $inaD^{C645S}$ flies (F), light-exposed $inaD^{wt}$ flies (G), light-exposed $ninaE^{I17}$ flies which are null for the major rhodopsin (H), light-exposed $inaC^{209}$ flies which are null for eye-PKC (I). The same gels were then fixed, stained for total protein using SYPRO Ruby stain, and imaged (on right). Cy3 image intensities are normalized for total protein levels.

pH7.0) + 20mM AMS (4-acetamido-4'-maleimidylstilbene-2,2'-disulfonic acid, MW = 536.44Da, Molecular Probes). The reaction was allowed to proceed for 10 minutes at room temperature and was quenched by addition of cold TCA to 25%. After precipitation on ice for >1 hour, the pellet was collected and washed as before. The pellet was resolubilized in denaturing buffer + 10mM TCEP (Tris(2-carboxyethyl)phosphine) and incubated at room temperature for 1 hour to reduce disulfide bonds. After 1 hour, Cy3-maleimide (GE) was added to 10mM and the reaction was allowed to proceed for 10 minutes at room temperature. The reaction was stopped by addition of TCA to 25%, and the protein was precipitated and collected as before. The pellet was resolubilized in 8M urea, 2% CHAPS, 2% IPG buffer pH3-10L (GE) and loaded onto a Immobiline DryStrip pH3-10 linear gel (GE) for electrofocusing, followed by SDS-PAGE on a 10% Tris-HCl gel (BioRad). The gel was directly imaged on a Typhoon 9210 (GE) with excitation at 532nM and detection at 580nm. Gels were then fixed and stained for total protein using SYPRO Ruby stain (Molecular Probes), and imaged on an AlphaImager HP (AlphaInnotech). Full gels are shown in Figure 3-9.

Genomic sequencing

A genomic fragment of the *norpA* gene was amplified from a wild-type (y^2w^1) fly using the Polymerase Chain Reaction (PCR) and the following oligonucleotides (5'-TGTTGAGATAATTTCGAGCACGGTTTCGCG-3' and 5'-GGTATTAAGAATATAAGCTTATGCTTCCGGC-3'); the fragment was sequenced using the following oligonucleotide (5'-TCACCCCAAATCGCTAATGGC-3').

Sequencing was performed by the McDermott Center for Human Genetics (The University of Texas Southwestern Medical Center at Dallas).

References

Bhattacharyya, R. P., Remenyi, A., Good, M. C., Bashor, C. J., Falick, A. M., and Lim, W. A. (2006). The Ste5 scaffold allosterically modulates signaling output of the yeast mating pathway. Science *311*, 822-826.

Bloomquist, B. T., Shortridge, R. D., Schneuwly, S., Perdew, M., Montell, C., Steller, H., Rubin, G., and Pak, W. L. (1988). Isolation of a putative phospholipase C gene of Drosophila, norpA, and its role in phototransduction. Cell *54*, 723-733.

Celniker, S. E., Wheeler, D. A., Kronmiller, B., Carlson, J. W., Halpern, A., Patel, S., Adams, M., Champe, M., Dugan, S. P., Frise, E., *et al.* (2002). Finishing a whole-genome shotgun: release 3 of the Drosophila melanogaster euchromatic genome sequence. Genome Biol *3*, RESEARCH0079.

Hanson, G. T., Aggeler, R., Oglesbee, D., Cannon, M., Capaldi, R. A., Tsien, R. Y., and Remington, S. J. (2004). Investigating mitochondrial redox potential with redox-sensitive green fluorescent protein indicators. J Biol Chem *279*, 13044-13053.

Henderson, S. R., Reuss, H., and Hardie, R. C. (2000). Single photon responses in Drosophila photoreceptors and their regulation by Ca2+. J Physiol *524 Pt 1*, 179-194.

Huber, A., Sander, P., and Paulsen, R. (1996). Phosphorylation of the InaD gene product, a photoreceptor membrane protein required for recovery of visual excitation. J Biol Chem *271*, 11710-11717.

Hwang, C., Lodish, H. F., and Sinskey, A. J. (1995). Measurement of glutathione redox state in cytosol and secretory pathway of cultured cells. Methods Enzymol *251*, 212-221.

Hwang, C., Sinskey, A. J., and Lodish, H. F. (1992). Oxidized redox state of glutathione in the endoplasmic reticulum. Science *257*, 1496-1502.

Iakhine, R., Chorna-Ornan, I., Zars, T., Elia, N., Cheng, Y., Selinger, Z., Minke, B., and Hyde, D. R. (2004). Novel dominant rhodopsin mutation triggers two mechanisms of retinal degeneration and photoreceptor desensitization. J Neurosci *24*, 2516-2526.

Joelson, T., Sjoberg, B. M., and Eklund, H. (1990). Modifications of the active center of T4 thioredoxin by site-directed mutagenesis. J Biol Chem *265*, 3183-3188.

Keese, M. A., Saffrich, R., Dandekar, T., Becker, K., and Schirmer, R. H. (1999). Microinjected glutathione reductase crystals as indicators of the redox status in living cells. FEBS Lett *447*, 135-138.

Kimple, M. E., Siderovski, D. P., and Sondek, J. (2001). Functional relevance of the disulfide-linked complex of the N-terminal PDZ domain of InaD with NorpA. Embo J *20*, 4414-4422.

Krause, G., Lundstrom, J., Barea, J. L., Pueyo de la Cuesta, C., and Holmgren, A. (1991). Mimicking the active site of protein disulfide-isomerase by substitution of proline 34 in Escherichia coli thioredoxin. J Biol Chem *266*, 9494-9500.

Leichert, L. I., and Jakob, U. (2004). Protein thiol modifications visualized in vivo. PLoS Biol *2*, e333.

Lonart, G., Schoch, S., Kaeser, P. S., Larkin, C. J., Sudhof, T. C., and Linden, D. J. (2003). Phosphorylation of RIM1alpha by PKA triggers presynaptic long-term potentiation at cerebellar parallel fiber synapses. Cell *115*, 49-60.

Matsumoto, H., Kahn, E. S., and Komori, N. (1999). The emerging role of mass spectrometry in molecular biosciences: studies of protein phosphorylation in fly eyes as an example. Novartis Found Symp *224*, 225-244; discussion 244-228.

Matsumoto, H., O'Tousa, J. E., and Pak, W. L. (1982). Light-induced modification of Drosophila retinal polypeptides in vivo. Science *217*, 839-841.

Matsumoto, H., and Pak, W. L. (1984). Light-induced phosphorylation of retina-specific polypeptides of Drosophila in vivo. Science *223*, 184-186.

Ostergaard, H., Tachibana, C., and Winther, J. R. (2004). Monitoring disulfide bond formation in the eukaryotic cytosol. J Cell Biol *166*, 337-345.

Patton, J. S., Gomes, X. V., and Geyer, P. K. (1992). Position-independent germline transformation in Drosophila using a cuticle pigmentation gene as a selectable marker. Nucleic Acids Res *20*, 5859-5860.

Popescu, D. C., Ham, A. J., and Shieh, B. H. (2006). Scaffolding protein INAD regulates deactivation of vision by promoting phosphorylation of transient receptor potential by eye protein kinase C in Drosophila. J Neurosci *26*, 8570-8577.

Schafer, F. Q., and Buettner, G. R. (2001). Redox environment of the cell as viewed through the redox state of the glutathione disulfide/glutathione couple. Free Radic Biol Med *30*, 1191-1212.

Tsunoda, S., Sierralta, J., Sun, Y., Bodner, R., Suzuki, E., Becker, A., Socolich, M., and Zuker, C. S. (1997). A multivalent PDZ-domain protein assembles signalling complexes in a G-protein-coupled cascade. Nature *388*, 243-249.

Watson, W. H., Pohl, J., Montfort, W. R., Stuchlik, O., Reed, M. S., Powis, G., and Jones, D. P. (2003). Redox potential of human thioredoxin 1 and identification of a second dithiol/disulfide motif. J Biol Chem *278*, 33408-33415.

Chapter Four
Functional characterization of the PDZ5 disulfide (I).

The quantum bump

Data from chapter three indicate that the redox state of InaD-PDZ5 is regulated by activation of the phototransduction cascade, most likely via eye-PKC mediated phosphorylation of the InaD scaffold itself. To understand what functional role this transition might play in visual signaling, we compared light responses from wild-type (or $inaD^{wt}$ flies) with those from the mutant $inaD^{C645S}$ flies. These mutant flies cannot form an oxidized state (due to lack of a cysteine at position 645) and are thus "locked" in the reduced state (see more below).

We used whole-cell voltage clamp recordings in isolated photoreceptor cells to measure their electrical responses to light (Figure 4-1). The electrical response is a direct result of the opening of TRP channels in the microvillar membrane; performing the measurement in voltage-clamp mode allows one to avoid contamination from voltage-gated K^+ and Na^+ channels present in the cell body and axon (Hardie, 1991; Ranganathan et al., 1991). Cells were stimulated with brief (~3nsec) flashes of light allowing us monitor activation and deactivation of the phototransduction cascade in the same experiment (Figure 4-1). Quantum bumps (single photon responses) and macroscopic (multi-photon) responses were measured from wild-type and mutant cells. In both types of experiments, activation refers to the opening of TRP channels, while inactivation refers to their closing (see Figure 4-1).

In a dark-adapted state (i.e., no light for >4hr), wild-type photoreceptors respond to single photons by producing transient all-or-nothing responses known as quantum

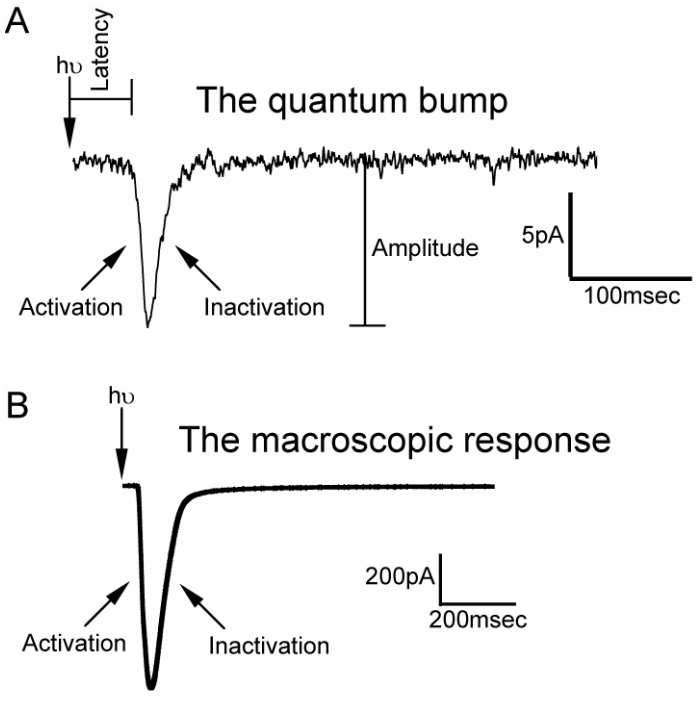

Figure 4-1 Typical light responses from wild-type cells. (A) Whole-cell voltage-clamp recording of a single photon response (also known as a quantum bump). A single photon was delivered at time indicated by the arrow. After a brief delay (latency), an activation phase occurs as a result of the opening of TRP channels and an inward current of Na^+ and Ca^{2+} ions. As mechanisms to shut down signaling kick in, TRP channels close, resulting in the inactivation phase of the response. (B) A typical multi-photon response (also known as a macroscopic response). Numerous photons were delivered in a ~3nsec flash at the time indicated by the arrow, resulting in an electrical response with an activation and inactivation phase (akin to those of the quantum bump). Note that the macroscopic response is much larger in amplitude than the quantum bump as it is the linear sum of numerous bumps.

bumps; these are thought to represent the coordinated opening (and subsequent closing) of TRP channels in an individual microvillus (Figure 4-1A) (Henderson et al., 2000). Wild type quantum bumps are ~10pA in amplitude, have a stereotypical shape, and occur with a variable time delay (or "latency") after photon delivery (Figure 4-1A, 4-2A). These parameters represent various kinetic aspects of signaling – for instance, the latency represents the time from rhodpsin activation to opening of the first TRP channel, while

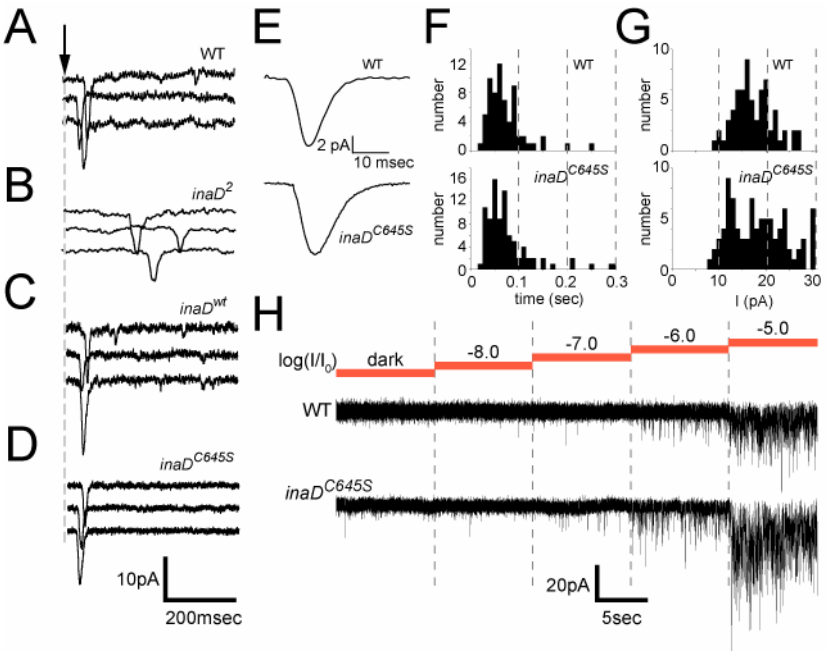

Figure 4-2 Single photon responses (quantum bumps) from wild-type and mutant cells in a dark-adapted state. (A-D) Representative quantum bumps from wild-type photoreceptors (A), *inaD*^{2} photoreceptors (B), *inaD*^{wt} photoreceptors (C), and *inaD*^{C645S} photoreceptors (D). Time of photon delivery is indicated by the arrow. (E-G) Quantitative analysis of the average quantum bump shape (E), latency distribution (F), and amplitude distribution (G) from wild-type and *inaD*^{C645S} photoreceptors shows no significant differences in any of these properties. (H) Stimulus thresholds (sensitivity) for quantum bump production in wild-type and *inaD*^{C645S} photoreceptors are similar. Dark-adapted cells are challenged with consecutively increasing amounts of light at a 30Hz frequency. Both genotypes consistently produce quantum bumps at the same stimulus intensity (log (I/I_0) = -6.0; I is the stimulus intensity; I_0 is the (reference) intensity of the unattenuated laser).

the shape parameters represent the kinetics of channel activation and inactivation. Overall, the quantum bump provides a sensitive measure of InaD function; mutants that impair its ability to bind TRP, eye-PKC or PLC-β display severe defects in various bump properties (Henderson et al., 2000; Scott and Zuker, 1998).

In the recording conditions used here, wild-type cells show a mean latency of about 50 milliseconds (Figure 4-2A). PDZ5 function is critical for this fast average

response time; a point mutation in PDZ5 which specifically abrogates the interaction of InaD with NorpA PLC-β (the *inaD*^{2} allele (Tsunoda et al., 1997)) shows normal quantum bump shape and amplitude, but a dramatically lengthened latency (Figure 4-2B) (Scott and Zuker, 1998). These mutants are capable of producing quantum bumps, but unable to organize them in time.

As expected, *inaD*^{wt} photoreceptors show normal quantum bumps (Figure 4-2C), consistent with full rescue of InaD function. Interestingly, we find that *inaD*^{C645S} mutants also show entirely wild-type quantum bump shape, latency, and amplitude (Figure 4-2D, E, F, and G). In addition, *inaD*^{C645S} mutants also show the same stimulus threshold for quantum bump production as wild-type cells (Figure 4-2H), indicating normal sensitivity to light. In short, *inaD*^{C645S} photoreceptors are completely normal in their ability to produce and time quantum bumps.

In wild-type cells, InaD-PDZ5 occupies the reduced state in the absence of light (see chapter three). The finding that *inaD*^{C645S} photoreceptors have entirely normal quantum bumps is thus consistent with the interpretation that the Cys645Ser form simply mimics the reduced state of the domain. In fact, the normal quantum bump properties imply that the mutant protein is not impaired in its ability to bind any of its core binding partners (TRP, PLC-β, and eye-PKC). In addition, the PDZ5^{Cys645Ser} mutant shows identical thermal stability to the reduced form of the wild-type domain (Figure 4-3) as well as an identical crystal structure (all atom RMSD = 0.96Å, see chapter two), suggesting that the mutation simply locks the domain in the reduced conformation without the introduction of any neomorphic or non-specific effects.

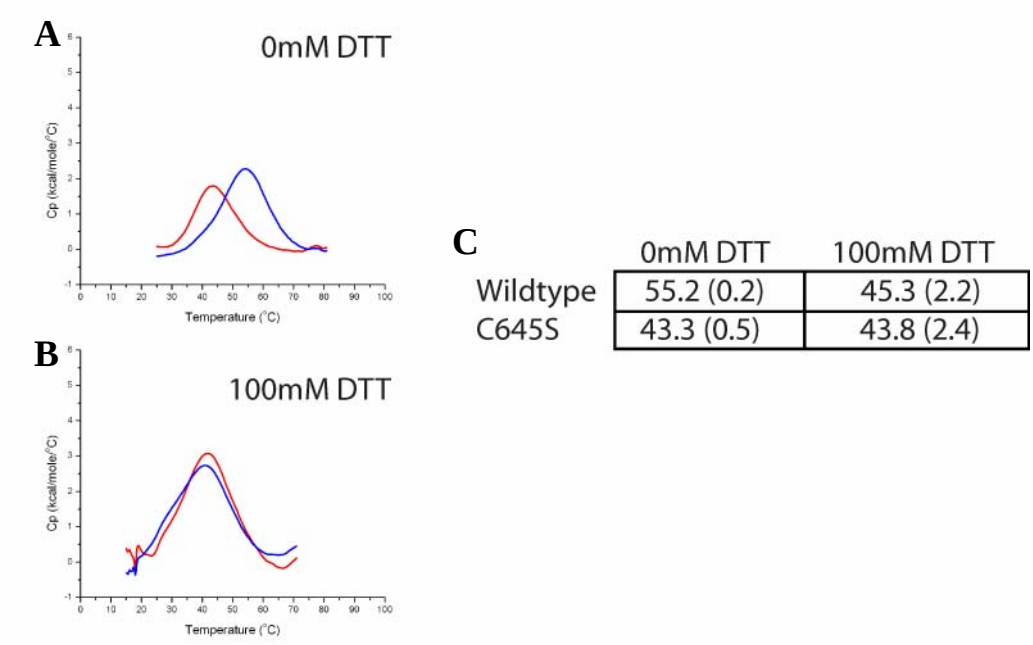

Figure 4-3 Thermal stability of InaD-PDZ5. (A) Wild-type (blue) or Cys645Ser (red) recombinant PDZ5 was assayed for thermal stability in the absence of reducing agent via differential scanning calorimetry. Normalized, baseline subtracted curves show a clear transition, indicating that oxidized wild-type PDZ5 has a higher melting temperature (T_m) and enthalpy of unfolding (likely due to the presence of a disulfide bond. (B) Same as top panel, except 100mM DTT was included in buffer solutions, thereby reducing wild-type PDZ5 (see Figure 2-6A). Similar T_ms are observed for wild-type and mutant (Cys645Ser) PDZ5. (C) Summary of thermal stability experiments. Assays were performed in triplicate; mean T_m (°C) and standard deviations are reported. Oxidized PDZ5 is significantly more stable than reduced or mutant (Cys645Ser) PDZ5; however, no differences in stability are observed between mutant and reduced wild-type PDZ5.

A light intensity-dependent inactivation defect

The quantum bump results (detailed above) were in response to single photons of light (i.e., very low levels). What happens at higher levels of light? Previous data indicate that in response to a multi-photon flash, the macroscopic photoreceptor response results from a linear summation of quantum bumps produced among different microvilli

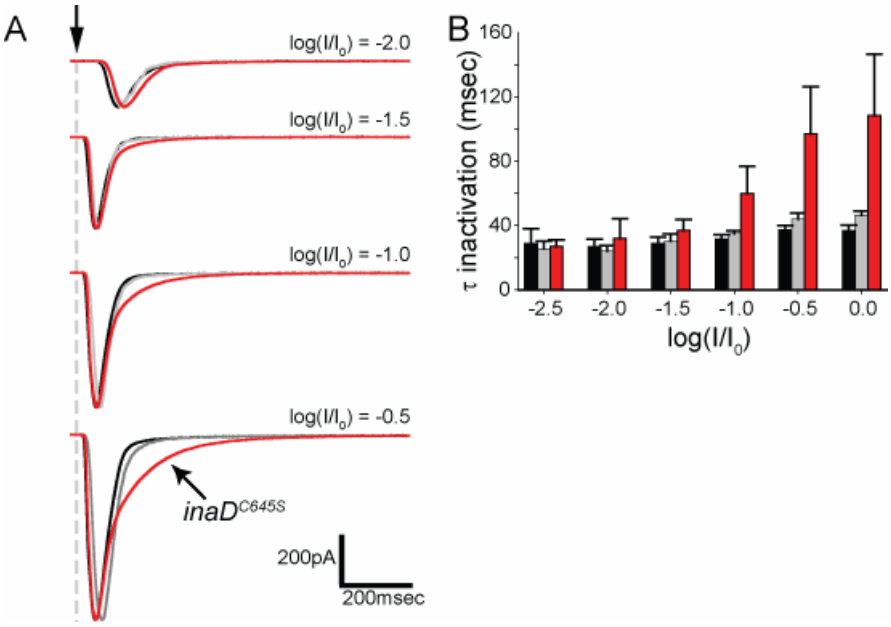

Figure 4-4 Light-dependent inactivation defects in *inaD*^{C645S} cells. (A) Average macroscopic responses from wild-type (black), *inaD*^{wt} (gray) or *inaD*^{C645S} (red) to 3 nsec flashes of 580nm laser light at the indicated intensities. Responses are normalized to peak at each light intensity, and I_0 is the (reference) intensity of the unattenuated laser (corresponding to ~10^4 absorbed photons). (B) Time constants obtained from fitting the inactivation segments of macroscopic responses to a single exponential. Error bars indicade standard deviations and the color scheme is the same as that used in (A).

(Henderson et al., 2000). Thus, knowledge of quantum bump parameters allows one to accurately predict the shape of the macroscopic response. Given the above results, one would predict that *inaD*^{C645S} macroscopic responses should be identical to the wild-type responses, at least in the regime where the quantum bumps have not changed in their parameters. This does appear to be the case, at least at low light levels where the quantum bumps parameters are expected to be similar to those measured in the dark-adapted state (Figure 4-4A, top; $\log(I/I_0) = -2.0$ or approximately 100 absorbed photons per flash).

In contrast, severe defects appear in *inaD*^{C645S} mutants upon stimulation with brighter light flashes. At lower light levels (Figure 4-4A, top panel), the response from *inaD*^{C645S} photoreceptors is indistinguishable from wild-type and *inaD*^{wt} responses. However, as the flash intensity is increased, an inactivation defect appears and becomes more pronounced in *inaD*^{C645S}, but not *inaD*^{wt} cells (Figure 4-4A, bottom panels). No defects appear in the kinetics of activation. We conclude, then, that the reduced state of PDZ5 supports normal visual function at low-light levels, but transition to the oxidized state is necessary (within milliseconds of rhodopsin activation) in order to maintain fast shutoff during responses to brighter, more physiologic stimuli.

The inactivation defect in *inaD*^{C645S} mutants (Figure 4-4A) has (at least) two interesting properties. First, the current decay appears to be biphasic in nature. Although the inactivation time constants reported in Figure 4-4B were obtained from fitting the curves to a single exponential, fits to a double exponential provided significantly better results (Figure 4-5), especially at higher light intensities. At lower light intensities (Figure 4-5A, B, C), single and double exponential fits (red and green, respectively) performed approximately the same; histograms of residuals from the single exponential fit (Figure 4-5F, G, H) and the double exponential fit (Figure 4-5K, L, M) were approximately gaussian in shape. At higher light intensities (Figure 4-5D, E), fits to a double exponential performed significantly better. Histograms of residuals from the single exponential fit (Figure 4-5I, J) had significant shoulders, suggesting the presence of an additional signal. Histograms of residuals from the double exponential fit (Figure 4-5N, O) were still gaussian in shape.

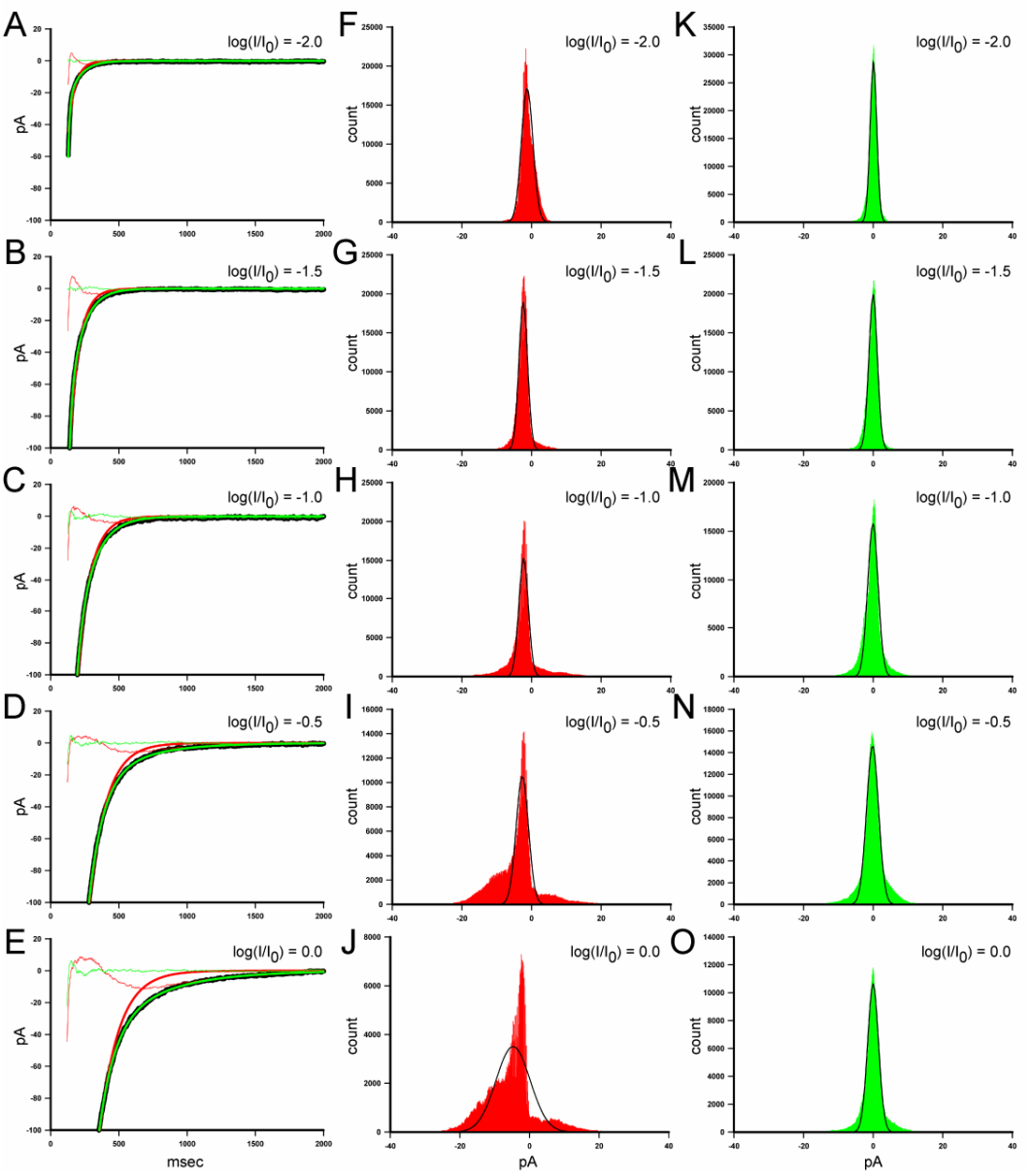

Figure 4-5 Biphasic inactivation kinetics in *inaD*^{C645S} cells. (A-E) The inactivation segements of macroscopic responses from *inaD*^{C645S} (black) at the indicated light intensity were fit to either single (thick red) or double (thick green) exponential decays. The respective residuals are plotted as thin lines (same color scheme). At lower light intensities (A-C), the single and double exponentials perform similarly; at higher light intensities (D, E), the double exponential performs significantly better. (F-J) Histograms of residuals from fits to a single exponential at the indicated light

These data suggest that there are at least two phases of inactivation of the light response: an initial "fast" phase and a second "slow" phase. Mutants such as *inaC*^{209} (which are null for eye-PKC) and *inaD*^{215} (a point mutant in the 3rd PDZ domain of InaD causing mislocalization of the TRP channel (Tsunoda et al., 1997)) also show significant inactivation defects; however, these defects are in the first "fast" phase (Henderson et al., 2000; Ranganathan et al., 1991; Smith et al., 1991), suggesting that eye-PKC mediated phosphorylation of the TRP channel is necessary for fast channel closure and inactivation. The deactivation kinetics of these mutants (*inaC*^{209}, *inaD*^{215}) do not appear biphasic in nature.

In contrast, *arr2*^{3} mutants (hypomorphs for βarrestin-2, the inactivator of activated rhodopsin) also have significant inactivation defects; however, the kinetics are biphasic in nature (Dolph et al., 1993; Ranganathan and Stevens, 1995) and there is no defect in the first "fast" phase. The *arr2*^{3} phenotype therefore suggests that this second phase is dependent on proper inactivation of rhodopsin. In consideration of this, the phenotype of *inaD*^{C645S} mutants (at high light intensity (Figure 4-4A)) seems to be quite reminiscent of the *arr2*^{3} phenotype, with the inactivation defect restricted to a second "slow" phase, thereby suggesting a problem with rhodopsin inactivation. This is surprising since no functional link between InaD and rhodopsin has been previously

---

intensity. The black line is the best fit to a gaussian curve. At higher light intensities (I, J), the histograms deviate significantly from a gaussian shape. (K-O) Histograms of residuals from fits to a double exponential at the indicated light intensity are approximately gaussian in shape at all light intensities. Black lines indicate the best fits to a gaussian curve.

demonstrated and thus merits further study. A more detailed characterization of the *inaD*^{C645S} phenotype will be undertaken in chapter five.

A second interesting property is that the *inaD*^{C645S} phenotype has a clear dependence on the intensity of light used. Quantum bumps and low light level macroscopics appear completely normal; only at high light levels does the phenotype emerge. In other mutants which cause inactivation defects (i.e., *inaC*^{209}, *inaD*^{215}, *arr2*^{3}), phenotypes are present at all light levels, including the single photon limit. There are some phototransduction mutants whose phenotype is only present at higher light levels; these usually involve defects in the PIP2 (phosphatidylinositol-4,5-bisphosphate) recycling pathway. For instance, the *rdgB* mutant (which is hypomorphic for the phosphatidylinositol transfer protein (PITP)) only shows a phenotype after exposure to bright light. This is presumably due to depletion of PIP2 at bright lights; without the PITP, adequate supplies of PIP2 cannot be resynthesized for further signaling (Hardie et al., 2001). However, InaD is not known to have any role in controlling PIP2 levels, suggesting that the phenotype in *inaD*^{C645S} cells is due to an alternative mechanism. We will return to this issue in chapter five.

Cellular consequences of an inactivation defect

Deactivation of the light response is perhaps the most tightly regulated property of visual signaling in photoreceptor cells; feedback control mechanisms are known to exist at several stages including arrestin-dependent inactivation of rhodopsin (Dolph et al., 1993; Ranganathan and Stevens, 1995) and PKC-mediated feedback control of TRP channels (Henderson et al., 2000; Ranganathan et al., 1991; Smith et al., 1991). One

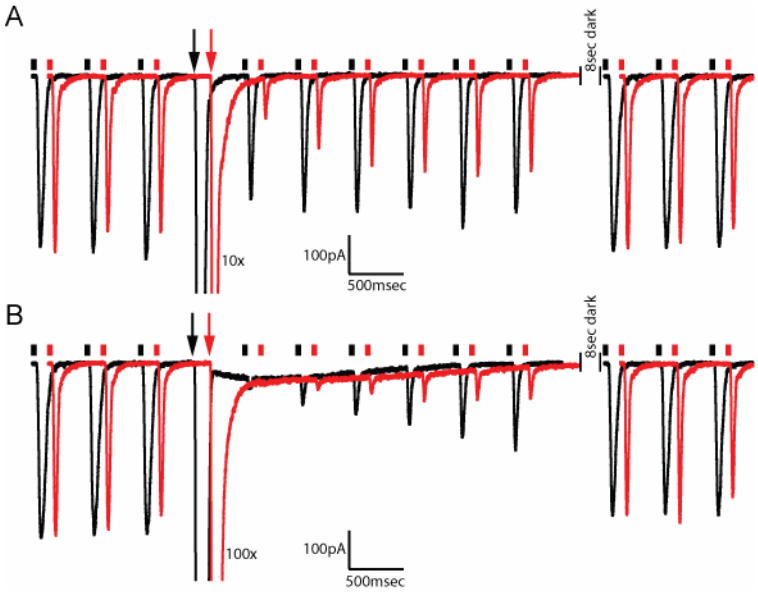

Figure 4-6 Response compression in *inaD*^{C645S} flies. (A) Light responses from wild-type (black) and *inaD*^{C645S} (red) cells in response to weak test flashes (rectangles) before and after an adapting flash (arrow) of 10x higher intensity. *inaD*^{C645S} responses are shifted relative to wild-type for clarity. The data show that mutant cells are unable to maintain sensitivity following changes in light levels. (B) Same as in (A) except that the adapting flash (arrow) is 100x higher in intensity than the test flashes.

known consequence of defective termination is the inability to rapidly reset photoreceptor sensitivity following a bright (but physiological) stimulus (Smith et al., 1991) - excess signaling activity due to slow response shutoff either overdrives adaptation mechanisms (due to excess Ca^{2+} entry into the cell) or depletes excitatory intermediates (e.g., PIP2 (Hardie et al., 2004; Hardie et al., 2001)).

To test this (see Figure 4-6), photoreceptors were challenged with weak test flashes of light (every 500msec) before and after a much brighter adapting flash. After an adapting flash of 10x brighter intensity than the test flashes (Figure 4-6A), wild-type cells (black trace) reduce the response amplitude, but slowly recover to the original response

amplitude after approximately 10 seconds. In comparison, *inaD*^{C645S} photoreceptors (red trace) show a greater reduction in response amplitude, though their overall ability to recover to the original response amplitude is unaffected. This phenotype is even more apparent after an adapting flash 100x brighter in intensity than the test flashes (Figure 4-6B). Thus, *inaD*^{C645S} mutant photoreceptors are unable to maintain sensitivity following sudden changes in light levels, indicating that transient formation of the PDZ5 disulfide is critical to maintaining responsiveness in the face of sudden bright stimuli. However, the mutants do not appear defective in their ability to recover sensitivity, suggesting that there are no defects in PIP2 resynthesis or Ca^{2+} efflux.

Behavioral consequences of an inactivation defect

Why is inactivation so tightly controlled in the *Drosophila* photoreceptor? As mentioned in chapter one, photoreceptors (the 1st order sensory neurons) signal to large monopolar cells (LMCs, the 2nd order neurons) in the lamina. Interestingly, histamine is the primary neurotransmitter at the photoreceptor-LMC synapse (Hardie, 1987; Hardie, 1989; Nassel et al., 1988). Histamine-activated chloride channels present on the LMC post-synaptic membrane open in response to neurotransmitter, allowing chloride ions to flow in, thereby hyperpolarizing the cell. Since depolarization is the actual signal that triggers synaptic vesicle release in neurons, the photoreceptor-LMC synapse thus serves as a "sign-reversing" synapse (Stuart et al., 2007) (Figure 4-7). Light (through activation of TRP channels) causes a depolarization in the photoreceptor, thereby activating synaptic-vesicle mediated histamine release; the increased levels in histamine then cause a hyperpolarization in the LMC; however hyperpolarization does not activate, but inhibits

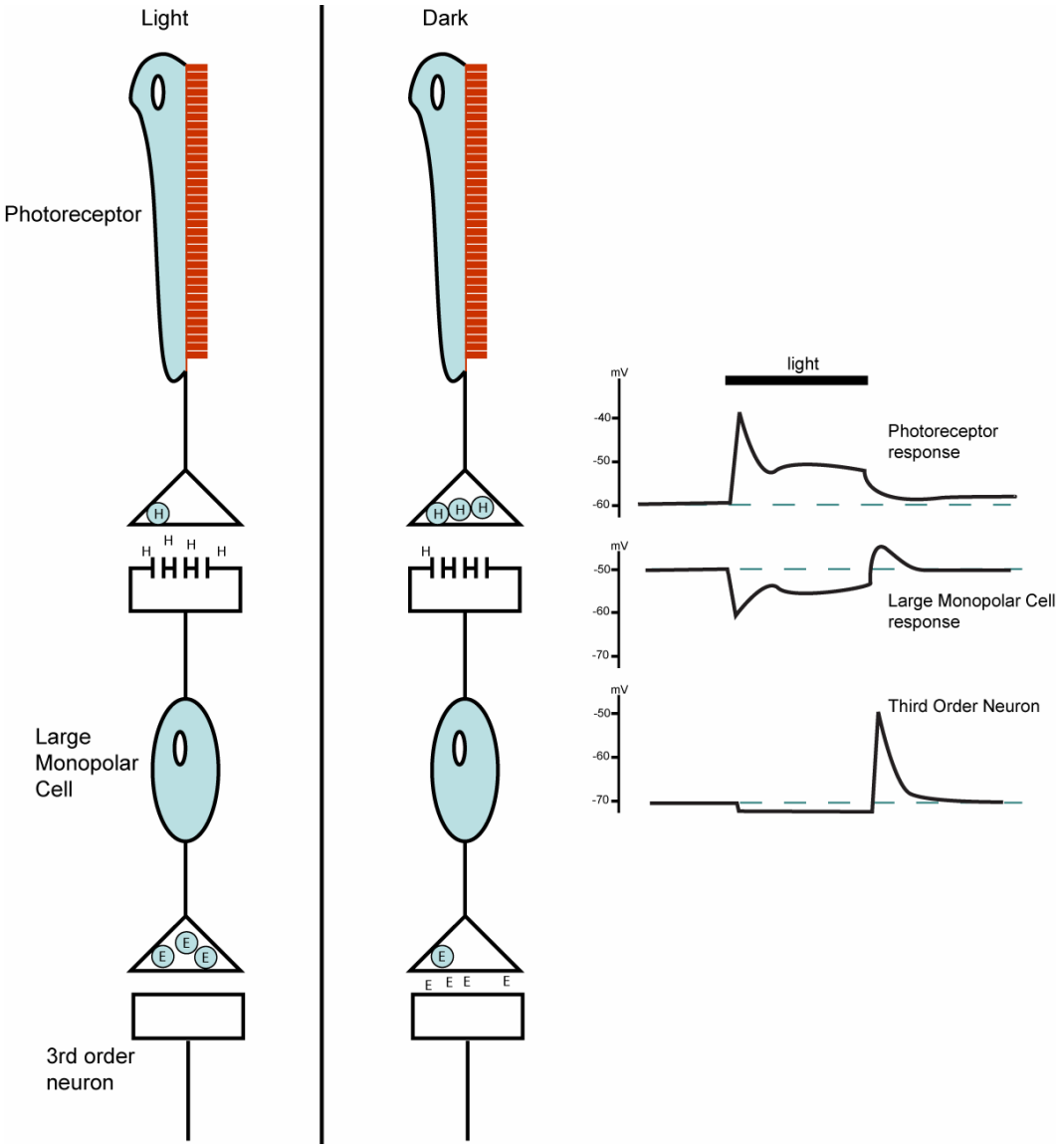

Figure 4-7 Sign reversal at the photoreceptor-LMC synapse. Light activates the phototransduction cascade, thereby depolarizing the 1st order photoreceptor neuron. Depolarization leads to release of the neurotransmitter histamine (H) into the synaptic cleft. Histamine-activated chloride channels then hyperpolarize the large monopolar cell (LMC), preventing further signal transmission. Conversely, a decrease in light levels leads to hyperpolarization of the photoreceptor, a decrease in synaptic histamine concentration, depolarization of the LMC, and release of excitatory neurotransmitter (E) onto a third order neuron. Adapted from (Stuart et al., 2007).

synaptic transmission at the synapse between the LMC and the 3rd order neuron. Conversely though, a decline in light level will hyperpolarize the photoreceptor, leading to a drop in histamine synaptic cleft concentration and activation (depolarization) of the LMC and other downstream neurons (Figure 4-7). Given this, it is not surprising that the deactivation kinetics of phototransduction might be tightly controlled; they are responsible for the activation kinetics of 2nd order and downstream neurons. Furthermore, insects (and invertebrates) have been long known to be exquisitely sensitive to declines in light levels (Darwin, 1854).

Interestingly, *Drosophila* (and other insects) have evolved specialized reflex circuits which trigger escape behavior in response to specific visual cues such as a decline in light levels. For instance, an approaching predator produces an expanding shadow (by blocking light) over the retina of a fly, thereby causing a sudden decline in light levels. The giant fiber neuron (receiving input from visual fibers) then activates the tergotrochanteral and dorsal lateral muscles in the legs and thorax respectively, producing an escape jump and flight behavior (Holmqvist and Srinivasan, 1991; Trimarchi and Schneiderman, 1995; Wyman et al., 1984).

This evolutionarily conserved behavior can be reliably evoked in white-eyed flies in a laboratory setting by rapid shutoff of ambient light (Movie S1); in response to a 20msec "lights-off" stimulus, wild-type and $inaD^{wt}$ flies jump approximately 70% of the time (Figure 4-8A). In contrast, $inaD^{C645S}$ flies have a dramatic defect in this escape reflex (jumping only 10% of the time, Movie S2, Figure 4-8A), indicating that they are unable to sense sudden decreases in light intensity. The phenotype is specific to the ability to rapidly deactivate the light response as mutant animals show no defects in

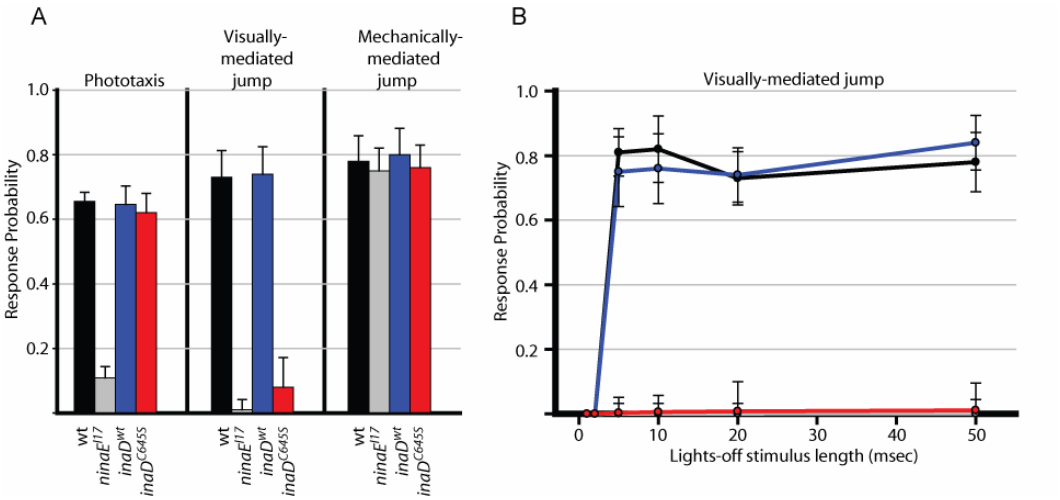

Figure 4-8 Escape behavior in *Drosophila*. (A) Response probabilities of individual flies in three kinds of behavioral taks: (left) phototaxis, which measures the ability of flies to walk toward a light source; (middle) visually-mediated jumps, which measures the ability of flies to execute an escape jump in response to a sudden transient (20 msec) of darkness; (right) mechanically-mediated jumps, which measures the ability of flies to execute an escape jump in response to a brief mechanical shock. The data show that wild-type and $inaD^{wt}$ flies perform well on all tasks, while $ninaE^{I17}$ flies (null for the major rhodopsin and effectively blind) show defects in both slow and fast time scale visual tasks. $inaD^{C645S}$ flies show specific and dramatic loss of the visually-mediated escape jump (see Movies S1 and S2). Error bars indicate the standard deviations from >10 individual flies per genotype per task. (B) Response probability for the visually-mediated escape jump assay as a function of lights-off stimulus length. Same color scheme and error bars as in (A). Wild-type and $inaD^{wt}$ flies are not able to respond to flickers <5 msec; $ninaE^{I17}$ and $inaD^{C645S}$ do not respond at any stimulus length.

phototaxis behavior, or escape behavior due to a brief mechanical stimulus (also mediated by the giant fiber system) (Figure 4-8A). In contrast, $ninaE^{I17}$ flies (null for the major rhodopsin and effectively blind) perform poorly on all visual tasks, while $inaD^{wt}$ flies are indistinguishable from wild-type flies.

In addition, the $inaD^{C645S}$ phenotype is independent of the length of the lights-off stimulus (Figure 4-8B), although, interestingly, wild-type (and $inaD^{wt}$) flies do not respond at flickers less than 5msec in length. Lastly, given the light-dependence of the

inactivation defect (Figure 4-4), one might expect that *inaD*^{C645S} animals would execute escape jumps at lower light levels. However, even wild-type animals do not execute escape jumps at low intensity, suggesting that this behavior has evolved in specific response to large changes in light levels. Indeed, the low light levels at which *inaD*^{C645S} responses are indistinguishable from wild-type responses may not be physiologically relevant in the daily life of a fly.

In summary, conformational dynamics in the InaD scaffold play no role in shaping the light response at low intensity, but are intricately involved in maintaining rapid deactivation of the light response at high intensities. Furthermore, these rapid signaling kinetics are important for preventing excess signaling, thereby maintaining response sensitivity in the face of sudden changes in light contrast. Lastly, rapid deactivation appears important for an evolutionarily conserved escape behavior that likely provides a competitive advantage to the fly. Given that there are numerous mechanisms involved in deactivation, it is unclear though how this disulfide transition fits into the G-protein signaling mechanism. Work in chapter five will address this issue.

Movies

Movie S1: The visually-mediated jump assay performed on an *inaD*^{wt} fly (see Methods). The 20msec "lights-off" stimulus is provided every 5-10 seconds. The *inaD*^{wt} fly executes an escape jump in response to the majority of stimuli. In most cases, the actual jump is not visible but is evidenced by a sudden change in the fly's position after the stimulus. In a few cases when the fly jumps, she hits the side of the container and falls to the ground writhing. For quantitation, see Figure 4-8A.

Movie S2: The visually-mediated jump assay performed on an *inaD*^{C645S} fly (see Methods). The 20msec "lights-off" stimulus is provided every 5-10 seconds. The *inaD*^{C645S} fly rarely executes an escape jump in response to the stimuli as evidenced by the fact that she is often in the same position before and after the stimulus (compare with Movie S1). For quantitation, see Figure 4-8A.

Methods

Electrophysiology

Whole-cell patch clamp on isolated photoreceptors was performed as described previously (Ranganathan et al., 1991). Briefly, flies were dark-reared for >12 hour and their retinas were dissected under dim red light in 125mM $CsCl_2$, 10mM HEPES, 30mM sucrose, pH7.1. The retinas were gently triturated into bath solution (120mM NaCl, 5mM KCl, 10mM HEPES, 4mM $MgCl_2$, 24mM proline, 5mM alanine, 1.5mM $CaCl_2$, pH7.1) and were imaged via Hoffman interference contrast on an inverted light microscope (Olympus IX70). Recordings were performed using fiber-filled borosilicate pipettes pulled using a Sutter P-97 (Sutter Instruments) and fire polished to a final resistance of 4-6 MΩ. Electrode solution was 140mM K-gluconate, 10mM HEPES, 2mM $MgSO_4$, 1mM NAD, 4mM MgATP, 0.5mM NaGTP, 0.5mM EGTA, pH7.1. Reversal potentials were between -40 and -70mV; series resistance was typically 10-20 MΩ and was routinely compensated to 75%. No series compensation was used during quantum bump recordings.

Light responses were elicited by a 3nsec flash of 580nm light from a dye-stirred VSL-337-ND-S nitrogen laser (Laser Science, Inc.) controlled by a PCI-DIO32HS board (National Instruments). Unattenuated intensity corresponds to ~10^4 effective photons per flash; light was filtered using neutral density filters (Oriel). To measure the sensitivity threshold (Fig. 4-2H), laser flashes of the appropriate intensity were given at 30 Hz for consecutive ten second intervals. Currents were amplified using an Axopatch 200B (Axon Instruments) and low-pass filtered at 100 or 200Hz (LPF-8, Warner Instrument). Data were collected and digitized via a PCI-6052E DAQ board (National Instruments) using custom software.

Quantum bumps were collected using laser flashes at intensities which generated responses at less than 30% success rate; typically $\log(I/I_0) < -5.0$. Latencies were calculated by hand and used to align bumps. Average bump shapes were calculated by averaging >50 aligned and normalized bumps per genotype. For macroscopic recordings, numerous responses (n=10) were collected at each light intensity from multiple cells (n>3). For a given light intensity, responses were normalized to a common scale and averaged. Analysis was done in MatLab.

Behavioral Assays

All assays were performed on flies less than 1 day old. Phototaxis was tested using the countercurrent apparatus (Benzer, 1967); groups of 25 flies were given a choice between a vial facing a light source (provided by a green light-emittind diode (LED)) and a vial facing away from the light source. Each fly was given the choice 8 times.

For the visual mediated escape jump, individual flies were tested in a small (3.5cm) Petri dish illuminated with four green LEDs placed at 90° to one another. A "lights-off" stimulus was provided by turning the LEDs off for the indicated number of milliseconds using a TTL signal; escape jumps were monitored visually and recorded. For a mechanical stimulus, the Petri dish was dropped onto a table from a height of 1cm; escape jumps were monitored visually and recorded. Each fly received 10 trials of each stimulus.

References

Benzer, S. (1967). Behavioral mutants of Drosophila isolated by countercurrent distribution. Proc Natl Acad Sci U S A *58*, 1112-1119.

Darwin, C. (1854). The Balanidae, In A monograph on the subclass Cirripedia (London: The Ray Society), pp. 54.

Dolph, P. J., Ranganathan, R., Colley, N. J., Hardy, R. W., Socolich, M., and Zuker, C. S. (1993). Arrestin function in inactivation of G protein-coupled receptor rhodopsin in vivo. Science *260*, 1910-1916.

Hardie, R. C. (1987). Is histamine a neurotransmitter in insect photoreceptors? J Comp Physiol [A] *161*, 201-213.

Hardie, R. C. (1989). A histamine-activated chloride channel involved in neurotransmission at a photoreceptor synapse. Nature *339*, 704-706.

Hardie, R. C. (1991). Voltage-sensitive potassium channels in Drosophila photoreceptors. J Neurosci *11*, 3079-3095.

Hardie, R. C., Gu, Y., Martin, F., Sweeney, S. T., and Raghu, P. (2004). In vivo light-induced and basal phospholipase C activity in Drosophila photoreceptors measured with genetically targeted phosphatidylinositol 4,5-bisphosphate-sensitive ion channels (Kir2.1). J Biol Chem *279*, 47773-47782.

Hardie, R. C., Raghu, P., Moore, S., Juusola, M., Baines, R. A., and Sweeney, S. T. (2001). Calcium influx via TRP channels is required to maintain PIP2 levels in Drosophila photoreceptors. Neuron *30*, 149-159.

Henderson, S. R., Reuss, H., and Hardie, R. C. (2000). Single photon responses in Drosophila photoreceptors and their regulation by Ca2+. J Physiol *524 Pt 1*, 179-194.

Holmqvist, M. H., and Srinivasan, M. V. (1991). A visually evoked escape response of the housefly. J Comp Physiol [A] *169*, 451-459.

Nassel, D. R., Holmqvist, M. H., Hardie, R. C., Hakanson, R., and Sundler, F. (1988). Histamine-like immunoreactivity in photoreceptors of the compound eyes and ocelli of the flies Calliphora erythrocephala and Musca domestica. Cell Tissue Res *253*, 639-646.

Ranganathan, R., Harris, G. L., Stevens, C. F., and Zuker, C. S. (1991). A Drosophila mutant defective in extracellular calcium-dependent photoreceptor deactivation and rapid desensitization. Nature *354*, 230-232.

Ranganathan, R., and Stevens, C. F. (1995). Arrestin binding determines the rate of inactivation of the G protein-coupled receptor rhodopsin in vivo. Cell *81*, 841-848.

Scott, K., and Zuker, C. S. (1998). Assembly of the Drosophila phototransduction cascade into a signalling complex shapes elementary responses. Nature *395*, 805-808.

Smith, D. P., Ranganathan, R., Hardy, R. W., Marx, J., Tsuchida, T., and Zuker, C. S. (1991). Photoreceptor deactivation and retinal degeneration mediated by a photoreceptor-specific protein kinase C. Science *254*, 1478-1484.

Stuart, A. E., Borycz, J., and Meinertzhagen, I. A. (2007). The dynamics of signaling at the histaminergic photoreceptor synapse of arthropods. Prog Neurobiol.

Trimarchi, J. R., and Schneiderman, A. M. (1995). Initiation of flight in the unrestrained fly, Drosophila melanogaster. J Zool,
Lond *235*, 211-222.

Tsunoda, S., Sierralta, J., Sun, Y., Bodner, R., Suzuki, E., Becker, A., Socolich, M., and Zuker, C. S. (1997). A multivalent PDZ-domain protein assembles signalling complexes in a G-protein-coupled cascade. Nature *388*, 243-249.

Wyman, R. J., Thomas, J. B., Salkoff, L., and King, D. G. (1984). The Drosophila giant fiber system, In Neural mechanisms of startle behavior, E. R.C., ed. (New York: Plenum Press), pp. 133-161.

Chapter Five
Functional characterization of the PDZ5 disulfide (II).

An intensity-dependent effect

As mentioned previously, there are many potential explanations for an inactivation defect in *Drosophila* visual signaling. For instance, loss-of-function mutations in arrestin (*arr2*^{3}), the inhibitor of activated rhodopsin, or eye-PKC (*inaC*^{209}) or Gβ all show slow termination of macroscopic light responses (Dolph et al., 1994; Dolph et al., 1993; Henderson et al., 2000; Ranganathan et al., 1991; Ranganathan and Stevens, 1995; Smith et al., 1991; Tsunoda et al., 1997). Defects in these mutants are evident at all light intensities, including at the single photon limit. Unique to the *inaD*^{C645S} phenotype described in chapter four is an intensity-dependent effect: No defects are seen in the responses to single photons, or even very low fluxes. An inactivation defect does appear, and becomes more and more pronounced, as light intensities are raised. Thus, the mechanism underlying the *inaD*^{C645S} phenotype is likely novel and merits further consideration.

In addressing this issue, we must first consider how photoreceptor cells respond to increasing light levels. As mentioned previously, the multi-photon (macroscopic) response can be considered as a sum of multiple single photon responses (quantum bumps) (Figure 1-3); therefore, knowledge of the characteristics of the single photon response (i.e., amplitude, shape, etc.) allows one to accurately predict characteristics of the macroscopic response (Henderson et al., 2000). In chapter four, we showed that *inaD*^{C645S} cells are no different from wild-type cells in these quantum bump parameters; these measurements were taken in dark-adapted cells and are therefore consistent with the

fact that the low-intensity macroscopic responses are also similar. At higher intensities, macroscopic responses differ between *inaD*^{C645S} and wild-type cells; **thus, the quantum bumps must also be different at higher light intensities.** Put another way, if the quantum bump parameters were identical between *inaD*^{C645S} and wild-type cells at high light intensities, then the macroscopic responses should also be identical – and this is clearly not the case (Figure 4-4).

Why might the quantum bump properties of *inaD*^{C645S} cells be different at higher light intensities? In wild-type cells, it is known that quantum bumps change their properties as a function of light intensity; as light intensity increases, bumps typically drop in size and duration in a process commonly known as classical adaptation or the classical bump adapting model (Wong and Knight, 1980). One might hypothesize then that *inaD*^{C645S} cells are deficient in some characteristic of classical adaptation such that their bump properties no longer match those of wild-type at higher light intensities. Unfortunately, the molecular details underlying classical adaptation are poorly understood in invertebrates.

If *inaD*^{C645S} photoreceptors were deficient in classical adaptation, what sorts of differences in the quantum bump properties might account for the inactivation defect described earlier? One can imagine many possibilities; for instance, bumps in *inaD*^{C645S} cells might be too wide (i.e, duration too long) or there may be too many bumps later in time (i.e., an altered latency distribution). Distinguishing between these possibilities may provide insight into the precise defect present in *inaD*^{C645S} mutants and thus, the role that redox-mediated transitions in InaD play in visual signaling.

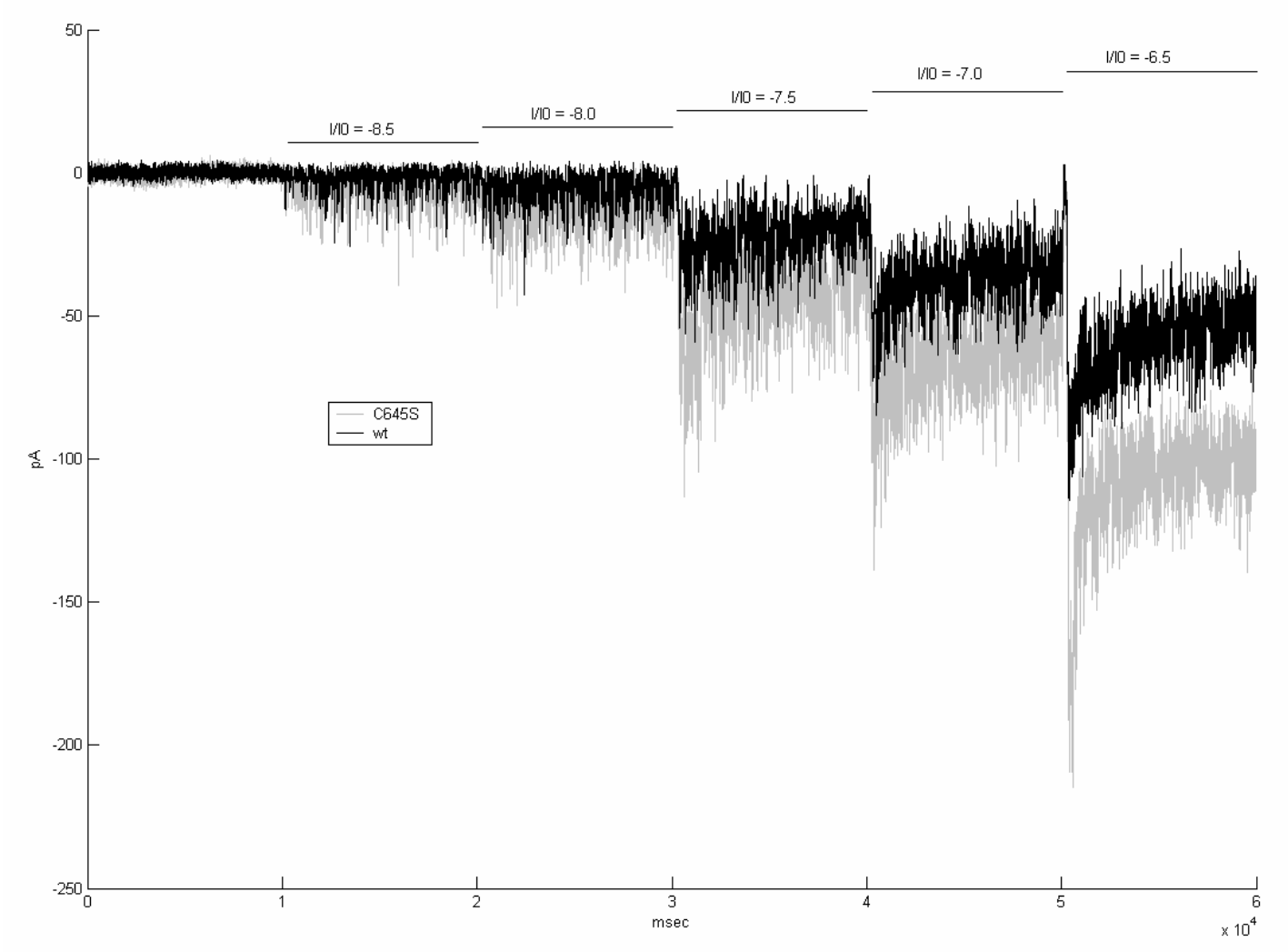
I/I0 = -8.5
I/I0 = -8.0
I/I0 = -7.5
I/I0 = -7.0
I/I0 = -6.5
C645S
wt
pA
msec
x 10^4
50
0
-50
-100
-150
-200
-250
0
1
2
3
4
5
6

Stationary Fluctuation Analysis

Thus, to understand the defect in *inaD*^{C645S} cells, we examined the average size, shape and rate of production of quantum bumps as function of increasing stimulus intensity. Unfortunately, individual bumps cannot be resolved during multi-photon stimuli since they are not well-separated in time. However, average properties of the quantum bumps can be extracted from steady-state macroscopic responses using stationary fluctuation analysis (Juusola and Hardie, 2001; Wong and Knight, 1980; Wu and Pak, 1978). In essence, bump properties can be extracted by a careful examination of the noise (variance) in a steady-state recording; for instance, larger bumps produce larger noise and the temporal properties of the noise are related to the duration of the bump. For details, see the methods section.

We collected whole-cell voltage-clamped current recordings from wild-type and *inaD*^{C645S} cells stimulated with constant white light of various intensities (Figure 5-1). Cells were started in the dark and challenged with consecutive 10 second intervals of light starting at the lowest intensity and stepping up in 0.5 log units. Data were taken from the last two seconds of each interval (when the recording had reached steady-state) and

Figure 5-1 Photoreceptor responses to constant light. Shown are representative current recordings from a wild-type (black) and an *inaD*^{C645S} (gray) cell. Cells were dark-adapted and then challenged with consecutive 10-second intervals of constant white light from a Xenon arc lamp. Light started at the lowest intensity ($\log(I/I_0) = -8.5$) and increased in 0.5 log unit steps. Here, I refers to the provided intensity and I_0 refers to the reference intensity of the unattenuated lamp (~60 lux). At higher light intensities, $\log(I/I_0)>-7.5$, *inaD*^{C645S} cells typically had larger current levels. Data from the last two seconds of each 10-second interval were used for stationary fluctuation analysis.

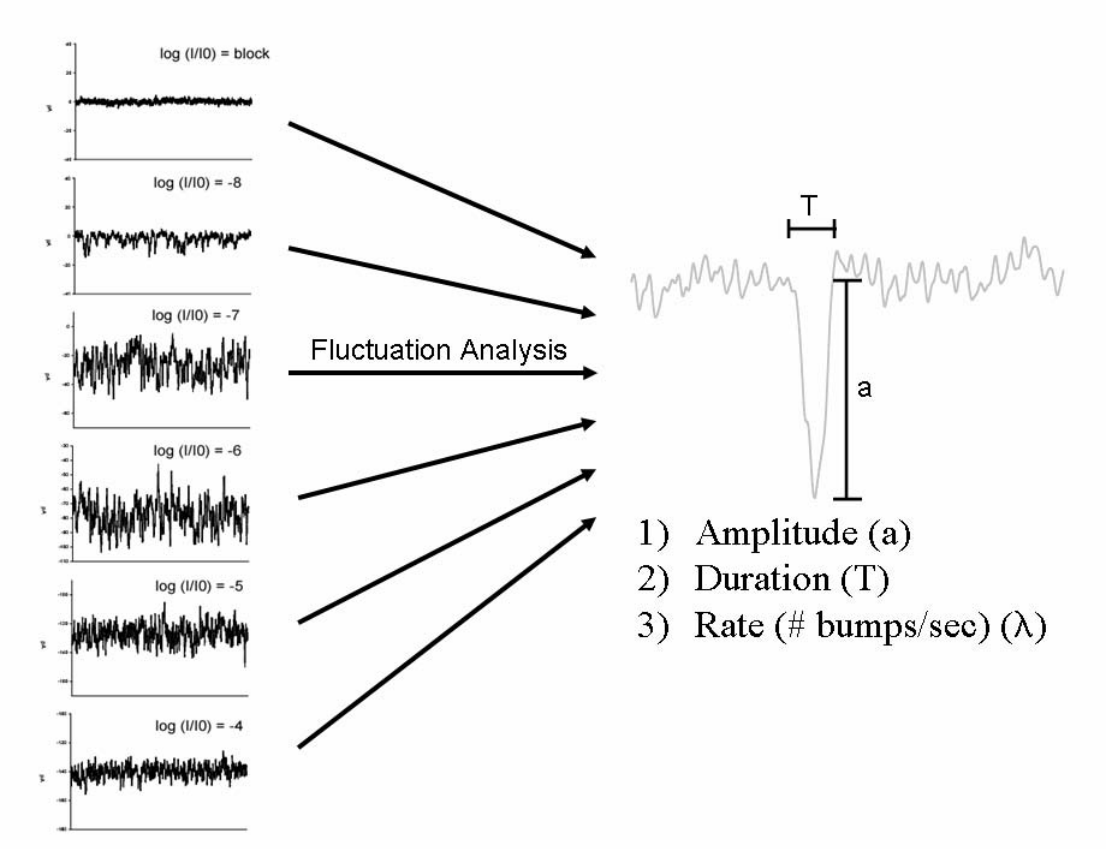

Figure 5-2 Stationary fluctuation analysis performed on current recordings from *Drosophila* photoreceptor cells. On the left are representative steady-state data from a wild-type cell stimulated at different light intensities. Note the large differences in the size and temporal properties of the noise. Fluctuation analysis can then be performed (as described in Methods) to extract an average amplitude, duration and rate for the underlying bumps in these multi-photon responses.

subjected to stationary fluctuation analysis (Figure 5-2). As previously done (Juusola and Hardie, 2001; Wong and Knight, 1980; Wu and Pak, 1978), we utilized Campbell's theorem which parameterizes the data into three properties: 1) The average amplitude of bumps (a); 2) The average duration of bumps (T); and 3) The rate at which bumps are being produced (λ).

It is possible, of course, that our inactivation defect (a kinetic property of a flash response) is slight enough to not produce systematic differences in our steady-state recordings. However, we do note (in Figure 5-1) that at higher light intensities, recordings from *inaD*^{C645S} cells exhibit larger current levels. This is likely a manifestation of the inactivation defect, which cannot be directly demonstrated in these steady-state responses (as opposed to the flash responses measured in chapter four). Integration of the excess current from delayed channel deactivation is likely producing higher current levels; thus, the inactivation defect is significant enough to produce systematic differences in these steady-state recordings. This gives us hope that our fluctuation analysis will reveal the quantum bump defect in *inaD*^{C645S} cells. We should keep in mind, though, that fluctuation analysis only approximates the properties of the underlying bumps since it assumes a characteristic shape for the quantum bump and that bumps occur randomly and independently in time.

A quantum bump rate defect

Results from the stationary fluctuation analysis are presented in Figure 5-3. As expected, wild-type photoreceptor cells show a classical adaptation response in which both the quantum bump amplitude and duration decrease steadily as the stimulus intensity increases (Figure 5-3A and B, black traces) (Johnson and Pak, 1986; Juusola and Hardie, 2001). These adjustments allow photoreceptors to extend the dynamic range of vision over several log orders of stimulation without saturation. *inaD*^{C645S} mutants are indistinguishable from wild-type in these parameters (Figure 5-3A and B, red traces),

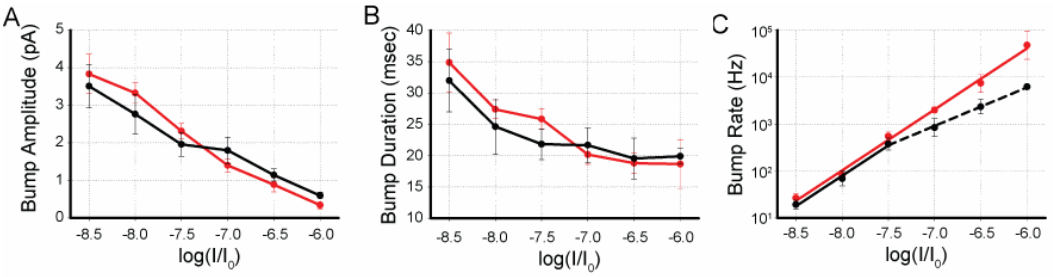

Figure 5-3 Results from fluctuation analysis. Stationary fluctuation analysis was used to measure average bump amplitude (A), duration (B), and rate (C) as a function of light intensity in wild-type (black) and *inaD*^{C645S} (red) photoreceptors. Bars indicate standard errors. Here I_0 is the reference intensity of the unattenuated Xe arc lamp, corresponding to ~60 lux. The data show that *inaD*^{C645S} photoreceptors have a specific intensity-dependent defect in the rate of quantum bump production.

indicating that the inactivation defect (and conformational switching in PDZ5) is unrelated to classical light adaptation.

In contrast, a clear defect emerges in the rate of production of quantum bumps (Figure 5-3C). At low stimulus intensity, the bump rate rises linearly with a slope close to unity in both wild-type and *inaD*^{C645S} photoreceptors (Figure 5-3C, solid black and red lines). This is the expected outcome when each photon stimulates a distinct microvillus and quantum bumps are produced independently. However, at higher light intensities, the bump rate in wild-type cells rises with a shallower slope (Figure 5-3C, dashed black line), indicating that some mechanism limits the rate of bump production to less than the rate of incoming photons. Strikingly, bump rates in *inaD*^{C645S} mutants continue to rise unattenuated for the entire range tested (Figure 5-3C, red line). Interestingly, this difference between rate parameters (wild-type versus *inaD*^{C645S}) is also intensity dependent; no difference occurs at low light levels, but the divergence emerges and becomes more profound as the light intensity rises. Thus, our analysis suggests, within

the limits of its assumptions, that *inaD*^{C645S} photoreceptors have a specific, intensity-dependent defect in the rate of quantum bump production.

Light adaptation in invertebrate photoreceptors has been classically defined according to the "adapting bump model" (Wong and Knight, 1980): As stimulus intensity increases, quantum bump size and duration decrease. The data in Figure 5-3C suggest that an addition role is played by adaptation in the rate of quantum bump production. The mechanism causing the attenuation in bump rate is unknown, but, interestingly, appears to be disturbed in the *inaD*^{C645S} mutant.

A specific defect in the refractory period following a quantum bump

These data indicate that defining the *inaD*^{C645S} phenotype begins with understanding why the bump rate levels off in wild-type cells (Figure 5-3C, dashed black line). At low intensities, bump rates rise linearly with a slope of ~1, consistent with the fact that each absorbed photon produces a single quantum bump. This should happen when activated rhodopsins are well separated in space from one another (i.e., in separate microvilli); in this case, they do not need to compete for downstream signaling molecules and can produce quantum bumps independent of other activated rhodopsins. However, as light intensities are raised, the incoming photon flux will eventually be high enough that multiple rhodopsins within the same microvillus will be activated.

What happens when multiple rhodopsins are activated in an individual microvillus? An ideal experiment would be to measure this response directly; in other words, one would directly activate multiple rhodopsin in one microvillus, without disturbing other microvilli, and measure the resulting current. Unfortunately, the size of

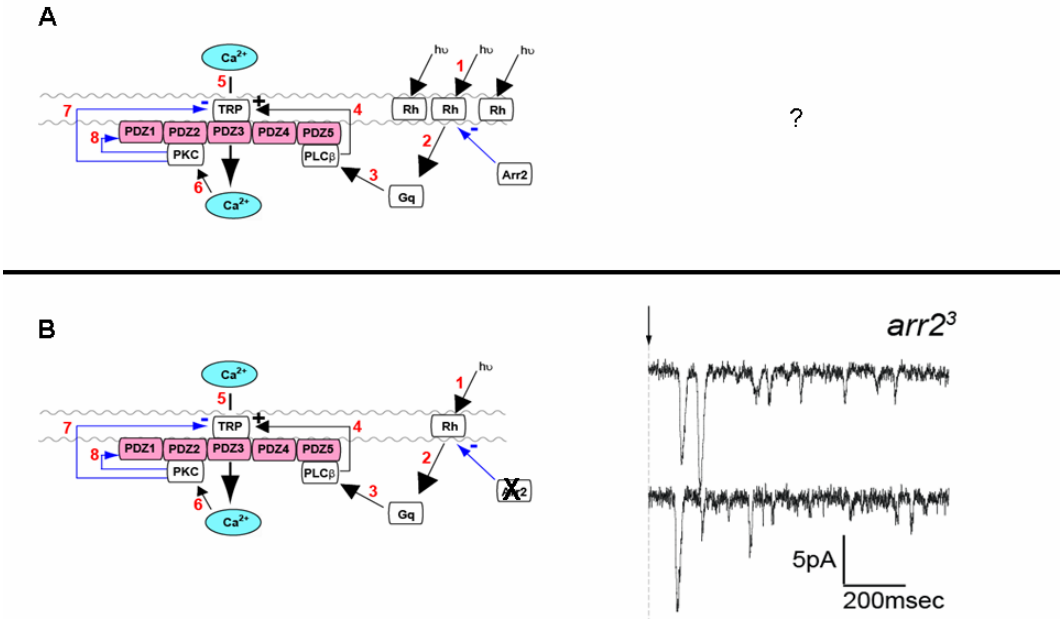

Figure 5-4 The single microvillus response to constant light. (A) Technical difficulties (due to the small size of the microvillus) prevent us from measuring the response to simultaneous activation of multiple rhodopsins in a single microvillus. To circumvent this (B), single photon responses can be measured in the *arr2*^{3} mutant (hypomorphic for βarrestin-2, the inactivator of active rhodopsin). The *arr2*^{3} quantum bump consists of a train of electrical responses, separated by periods of channel closure termed "refractory periods." A similar phenotype occurs in the calmodulin (*cam*) hypomorph (Scott et al., 1997).

a single microvillus (diameter ~50nm) is beyond the diffraction limit of light and precludes this experiment. However, an alternative experimental approach for addressing this question has been suggested by previous work on hypomorphic mutants of arrestin (*arr2*^{3}) and calmodulin (*cam*) (Scott et al., 1997). Both these mutants are severely defective in the shutoff of activated rhodopsin. Thus, single photon stimulation leads to an activated rhodopsin with an elongated lifetime, therefore providing persistent signaling activity that approximates a continual stream of incoming photons into one microvillus. As previously demonstrated (Scott et al., 1997), the quantum bump response in these mutants is not merely a single bump with broad kinetics. Instead, it

consists of a normal shaped initial bump followed by a series of irregularly timed subsequent responses that have been referred to as a "bump train" (Figure 5-4B) (Hardie, 2001; Hardie and Raghu, 2001; Scott et al., 1997). The key feature of this phenotype is the existence of a refractory period following an individual quantum bump during which channel activity is silenced in the activated microvillus (Hardie, 2001; Hardie and Raghu, 2001; Scott et al., 1997). Unfortunately, the mechanistic basis for this refractory period is still unknown.

These findings suggest a straightforward hypothesis for the $inaD^{C645S}$ phenotype. By definition, the maximum bump rate for any wild-type microvillus is limited to once per refractory period. Thus, at low stimulus levels where microvilli rarely receive multiple photons, the refractory period is of no consequence and bump rates rise linearly with photon flux. However, at stimulus levels that are high enough to yield a reasonable probability that microvilli receive multiple photons within a refractory period, we expect the leveling off of bump rates observed in wild-type cells (Figure 5-3C, dashed black line). Given this, the unattenuated production of quantum bumps observed in $inaD^{C645S}$ cells (Figure 5-3C, red line) suggests a dramatically shortened (or even absent) refractory period.

To test this, we recorded from $inaD^{C645S}$, $arr2^{3}$ double mutant animals. If the refractory period is absent, then the combination of these mutations should transform the $arr2^{3}$ bump train into just a continuously decaying quantum bump. Figure 5-5B confirms this prediction, supporting the model that the fundamental physiological defect in $inaD^{C645S}$ mutants is selective abrogation of the refractory period following a quantum bump.

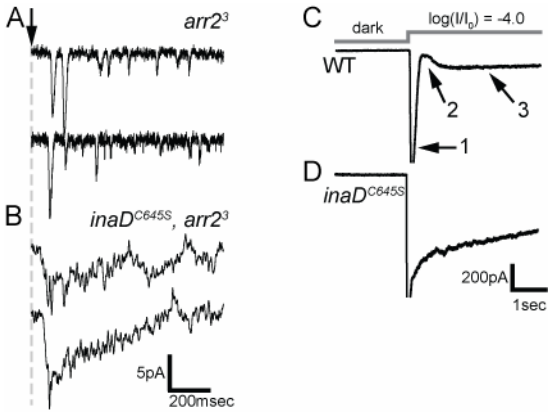

Figure 5-5 The refractory period in *inaD*^{C645S} cells. (A-B) Representative single photon responses from *arr2*^{3} (A) and *inaD*^{C645S}, *arr2*^{3} photoreceptors (B) confirm that *inaD*^{C645S} has a near complete loss of the refractory period between sequential quantum bump events. (C-D) Electrical responses from dark-adapted wild-type (C) and *inaD*^{C645S} (D) photoreceptors suddenly stimulated with constant light at the indicated time and intensity reinforce this conclusions (see text).

Of course, observation of the refractory period in an *arr2*^{3} mutant at low light levels (i.e., single photon responses) does not necessarily imply that wild-type cells utilize a refractory period under brighter, more physiological, light levels. The *arr2*^{3} mutant may have unknown effects besides a prolonged activated rhodopsin lifetime, and adaptation processes may cause significant differences between signaling at low and high light levels. Direct observation of the refractory period in wild-type cells under conditions of brighter, constant light stimulation is difficult as the electrical responses from different microvilli are not matched in time. Thus, the steady state macroscopic response will represent the sum of many unsynchronized quantum bump trains from different microvilli. However, synchronization can be transiently achieved by instantly shifting cells from darkness to bright light (Figure 5-5C). By using a shutter with an

opening time (~8 msec) that is significantly faster than the average latency for bumps (~50 msec, Figure 4-2F), we expect that the initial responses and refractory periods from an ensemble of microvilli will occur approximately simultaneously. This synchronization is not expected to last for long; the random nature of the refractory periods between quantum bumps (Figure 5-5A) will cause rapid decorrelation of the responses from different microvilli as time progresses. Accordingly, wild-type cells show an initial transient of channel opening (Figure 5-5C, arrow 1), followed by a dip in activity (arrow 2) that then progresses to a constant steady state current (arrow 3). *inaD*^{C645S} animals show no dip in channel activity (Figure 5-5D). These data strongly suggest (1) the existence of a refractory period in wild-type photoreceptor cells under physiologic conditions and (2) that *inaD*^{C645S} mutants have specifically lost the refractory period between quantal responses.

A model for PDZ5 function

Taken together with the structural and biochemical data in chapters two, three and four, these findings allow us to propose a simple mechanistic model: The reduced conformation of PDZ5 defines a permissive condition for signaling and the oxidized conformation defines the refractory period. From a dynamic perspective, this model suggests that InaD-PDZ5 cycles between these two states on the hundreds of milliseconds time scale during a bump train, thereby producing electrical responses while in the reduced state, and refractory periods while in the oxidized state. Thus, InaD acts more like a dynamic machine than a passive scaffold, controlling reactions that shape the visual response through stimulus-dependent conformational change.

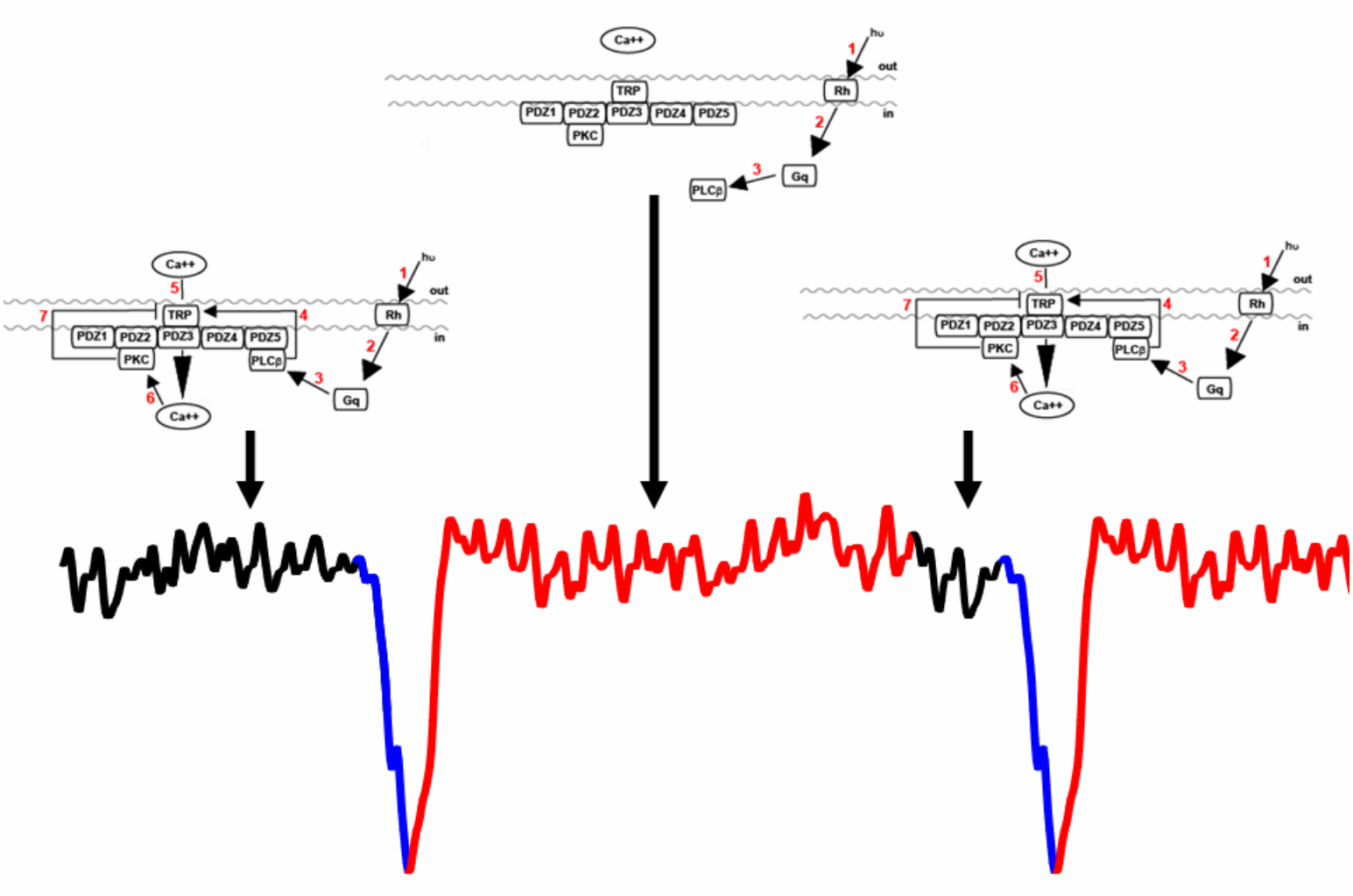
Ca++
hυ
1
out
TRP
Rh
PDZ1
PDZ2
PDZ3
PDZ4
PDZ5
in
PKC
2
3
Gq
PLCβ
Ca++
5
hυ
1
out
7
TRP
4
Rh
PDZ1
PDZ2
PDZ3
PDZ4
PDZ5
in
PKC
PLCβ
2
3
6
Gq
Ca++
Ca++
5
hυ
1
out
7
TRP
4
Rh
PDZ1
PDZ2
PDZ3
PDZ4
PDZ5
in
PKC
PLCβ
2
3
6
Gq
Ca++

How might transient formation of the PDZ5 disulfide mechanistically lead to a refractory period? Genetic studies have demonstrated a role for PDZ5 in controlling the rhabdomeric localization of PLC-β, the main effector molecule for visual transduction and a component of the InaD complex (Tsunoda et al., 1997). This leads to the obvious hypothesis that light-dependent transient formation of the oxidized state causes transient unbinding (and mislocalization) of PLC-β from the InaD complex. Since PLC-β localization is known to be required for efficient visual signaling (Scott and Zuker, 1998), it follows that this brief unbinding event might represent the physical basis for the refractory period (Figure 5-6). However, evidence for a direct interaction between InaD PDZ5 and PLC-β remains elusive (see Methods, Figure 5-11) and the possibility exists that other target proteins in the visual signaling pathway might associate with PDZ5. Future work in identifying and characterizing real-time localization of PDZ5's binding partners *in vivo* will be required to address this issue.

The refractory period and inactivation.

Loss of the refractory period clarifies aspects of the *inaD*^{C645S} phenotype described in chapter four – the intensity-dependent inactivation defect observed in

Figure 5-6 A model for generation of the refractory period. During continuous light stimulation, individual microvilli are producing trains of electrical responses (quantum bumps) and therefore cycling between signaling permissive states (black/blue) and refractory states (red). The transition is controlled by the dynamic behavior of InaD-PDZ5. While it is in a reduced, binding-competent state (left and right), PLC-β is properly localized to the InaD complex and signaling proceeds efficiently. When PDZ5 is in an oxidized, binding-incompetent state (middle), PLC-β is transiently mislocalized and signaling becomes refractory.

macroscopic flash responses (Figure 4-4). For low intensity flashes, each microvillus very rarely receives multiple photons. Thus, loss of the refractory period has no consequence and *inaD*^{C645S} mutants show no defects (Figure 4-4A, top panel). As stimulus intensity increases, multiple rhodopsins will be activated per microvillus and now the refractory period becomes of functional significance. Rhodopsin activation will still produce an initial quantum bump with normal latency and shape but without a refractory period, signaling from other simultaneously activated rhodopsins would be expected to stimulate additional channel activation in the period before they are shut off. Integrated over many microvilli, such responses would produce a slow inactivation of the macroscopic response (Figure 4-4A, lower panels).

Data from chapter four also suggested that inactivation in *inaD*^{C645S} mutants is biphasic in nature (Figure 4-5), similar to the macroscopic phenotype seen in arrestin hypomorphs (*arr2*^{3}) (Ranganathan and Stevens, 1995). In both mutants, the second phase is due to persistent signaling activity – in *arr2*^{3}, the activated rhodopsin lifetime is prolonged while in *inaD*^{C645S} the rhodopsin lifetime is effectively prolonged (when multiple rhodopsins are activated) because no refractory period limits their signaling. The data then support the idea that the refractory period plays an important role in maintaining fast deactivation at high light intensity. As previously suggested (Hardie and Raghu, 2001), the refractory period allows signal shutoff to be determined by downstream events such as rapid channel inactivation without having to wait for potentially slower upstream events such as arrestin binding and GTPase activity.

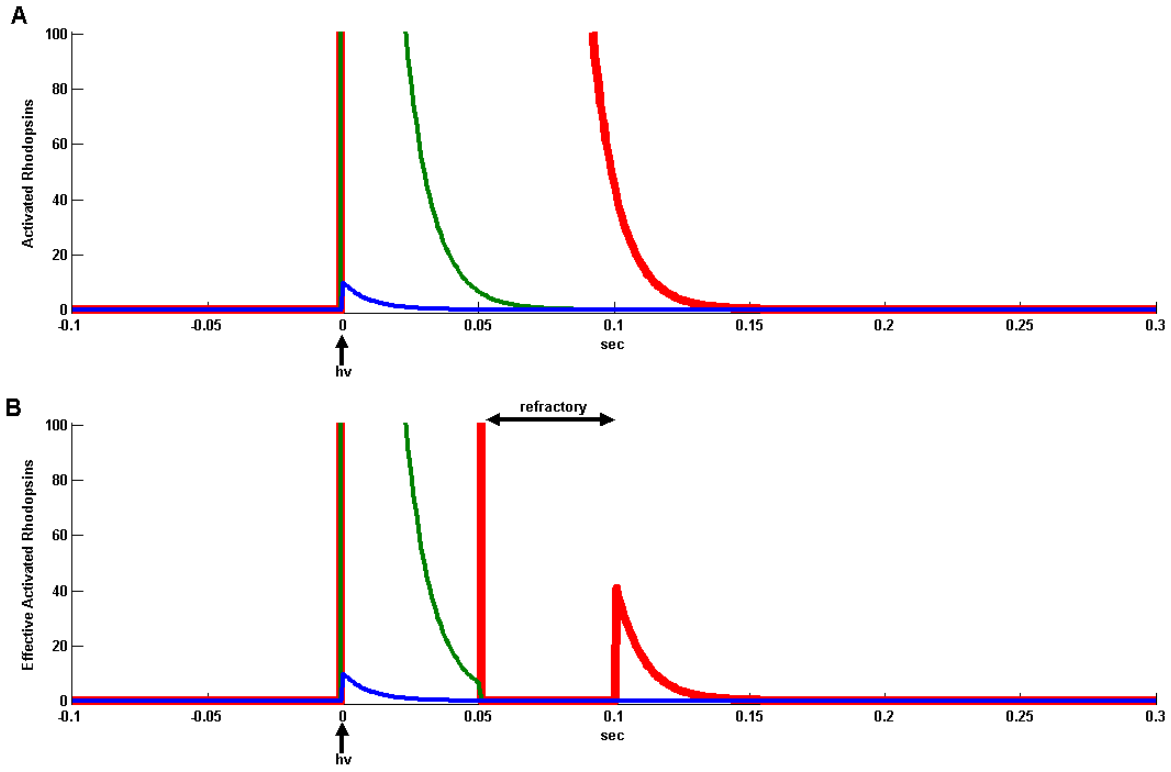

Figure 5-7 A model of activated and effective rhodopsin lifetime. (A) A plot of number of activated rhodopsins versus time. At time = 0, either 10 (blue), 1000 (green) or $1x10^6$ (red) molecules of rhodopsin are simultaneously activated. After activation, rhodopsins decay according to a single exponential (here, τ=100/sec). (B) A plot of number of effective activated rhodopsins versus time; colors and decay are the same as in (A). A refractory period is imposed between 50 and 100msec. At low photon fluxes (blue and green curves), no activated rhodopsins remain after the refractory period. However, at very high fluxes (red curve), a small population of rhodopsins will still be active after 100msec and continue to signal.

Should inactivation of the wild-type macroscopic flash response also be biphasic in nature? At low light intensities, the refractory period should limit signaling from excess rhodopsins; thus, rates of rhodopsin inactivation will play no role in channel inactivation and the response decay should have one phase. However, if the flash intensity is raised high enough, there should be enough activated rhodopsins per

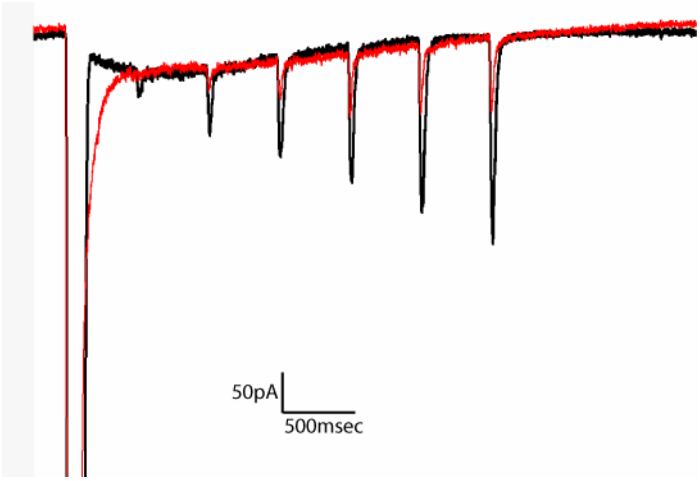

Figure 5-8 A closeup of the adapting flash response from Figure 4-6B. The wild-type response is in black and the *inaD*^{C645S} response is in red. The mutant response shows biphasic inactivation as discussed earlier (Figure 4-5); however, at this intensity, the wild-type response also shows a biphasic response convolved with a refractory period (causing the brief dip in activity).

microvilli such that some have not inactivated even after the refractory period has ended (see Figure 5-7 for an illustration). Thus, at very high photon fluxes, we expect that a wild-type cell might illustrate a biphasic response. A careful examination of Figure 4-6B, in which cells were submitted to adapting flashes of very high intensity, is consistent with this model (Figure 5-8). Ignoring the subsequent responses to test flashes, the wild-type response (black) to the adapting flash displays an initial phase of fast inactivation, followed by a dip in activity (presumably representing the refractory period), and finally a second phase of slow inactivation that closely matches the second phase from the *inaD*^{C645S} response (in red). It's noteworthy that the mutant response does not have the dip in channel activity, consistent with a loss of the refractory period.

A model for the bump train

The bump trains observed in the *arr2*^{3} phenotype are reminiscent of an oscillatory signal; instead of having continuous channel activity in response to continuous rhodopsin activation, microvilli generate individual bumps spaced by segments of channel silence. This is in stark contrast to the *arr2*^{3} phenotype of the vertebrate visual system; here, the single photon response is an elongated slowly decaying quantum bump (Chen et al., 1999; Xu et al., 1997). These results suggest that producing a quantum bump (including activation and inactivation of the TRP channels) is the fundamental activity of a wild-type microvillus; and this activity, once triggered, will produce distinct quantum bumps (with proper shutoff) while rhodopsin remains active. Such a response is reminiscent of a van der Pol relaxation oscillator (Strogatz, 1994), and can be modeled as such (see below).

Considering the signaling pathway of *Drosophila* phototransduction, we realize that the interactions between the TRP channel, Ca^{2+}, and PKC form a closed feedback loop that is capable of producing oscillations during an *arr2*^{3} single photon response (Figure 5-9A). As discussed in chapter one, opening of TRP channels leads to Ca^{2+} entry which triggers positive feedback and opening of more TRP channels (Henderson et al., 2000; Ranganathan et al., 1991). Once sufficient Ca^{2+} has entered, PKC molecules will be activated which feedback phosphorylate and close the TRP channels (Popescu et al., 2006). During a wild-

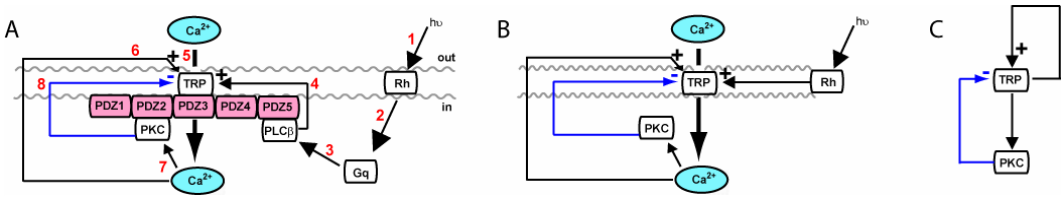

Figure 5-9 Modeling the visual response. (A) Schematic of *Drosophila* visual transduction as described in chapter one. (B) Simplified schematic of the quantum bump "generator." Initial TRP channel opening (initiated by rhodopsin signaling) allows Ca^{2+} entry which triggers positive feedback (to open more TRP channels) and activates PKC. PKC feedback phosphorylates TRP, facilitating channel closure. (C) Simplified schematic for quantum bump generation. If Ca^{2+} is assumed to equilibrate quickly, the system can be viewed as TRP channels activating positive feedback on themselves, and negative feedback via activation of PKC.

type single photon response, channels do not open again as there is no signal from rhodopsin (via Gq and PLC-β) to trigger another bump; it has been deactivated by arrestin. However, in an *arr2*[3] cell, continuous rhodopsin activation should elicit another bump once enough Ca^{2+} has been pumped out of the cell such that PKC molecules can deactivate; once enough PKC molecules have inactivated, TRP channels may open again and begin the next quantum bump. Thus, we can simplify "generation" of the quantum bump to an interaction between Ca^{2+}, TRP and PKC which is triggered by an initial channel opening via the rhodopsin-Gq-PLC pathway (Figure 5-9B).

If we assume that Ca^{2+} equilibrates quickly (relative to the rates of TRP channel and PKC activation and inactivation), our model can be further simplified to a two dimensional system (Figure 5-9C). Here, TRP channels directly activate themselves (via Ca^{2+} influx), as well as activate PKC (via Ca^{2+} influx); PKC then inactivates the TRP channel. This simplification allows us to visualize the system

behavior in two-dimensions. We parameterize the system using the following set of differential equations:

$$\frac{dTRP}{dt} = \alpha(N_{TRP} - TRP)(\beta + \frac{k_1 TRP^n}{1 + k_2 TRP^n}) - k_3 TRP - k_4 PKC \cdot TRP$$

$$\frac{dPKC}{dt} = k_5 TRP(N_{PKC} - PKC) - k_6 PKC$$

Here, N_{TRP} and N_{PKC} represent total numbers of TRP and PKC molecules respectively, while *TRP* and *PKC* refer to numbers of the activated species. α and β parameterize activation of TRP channels via Rh→Gq→PLC-β signaling and are assumed to be constant for an *arr2*[3] single photon response. k_1 and k_2 parameterize a Hill function representing positive feedback of TRP onto itself. k_3 is the rate constant for first order *TRP* decay, while k_4 is the rate constant for TRP decay via PKC mediated negative feedback. k_5 and k_6 represent activation and decay constants, respectively, for PKC. Lastly, *t* represents time.

While we do not know which set of parameters correspond to the *in vivo* situation, we can find multiple sets of parameters consistent with the *arr2*[3] single photon response. The dynamic behavior of the system can then be visualized using nullcline analysis, whereby a fixed point with a stable oscillation is formed at the intersection between the *TRP* and *PKC* nullclines (Figure 5-10A). The non-linearity encoded by the Hill function for TRP positive feedback generates the inversion in the TRP nullcline which makes this oscillation possible, similar to a van der Pol oscillator (Strogatz, 1994). Solving the system of equations

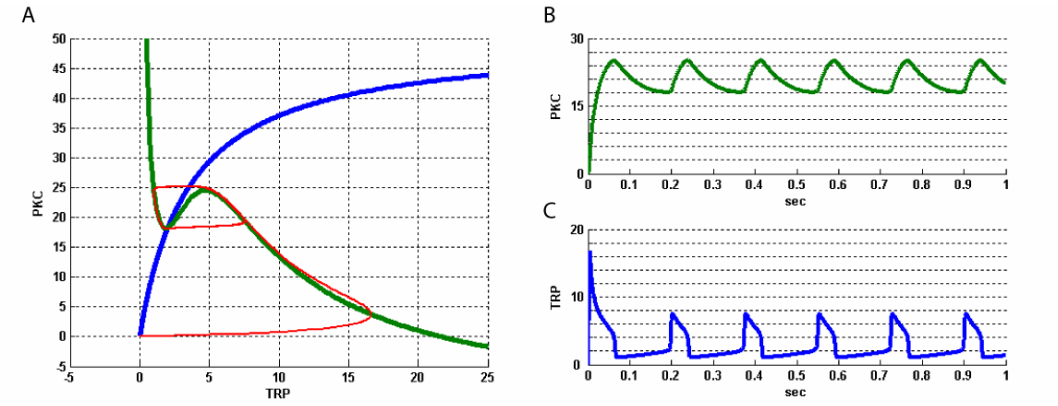

Figure 5-10 Nullcline analysis of the TRP, PKC interaction. (A) The intersection of the *TRP* nullcline ($\frac{dTRP}{dt} = 0$, green) and the *PKC* nullcline ($\frac{dPKC}{dt} = 0$, blue) creates a fixed point with a stable oscillation. A trajectory, starting from the dark state (*TRP*=*PKC*=0), is plotted in red. (B-C) *PKC* (green, B) and *TRP* (blue, C) values are plotted versus time. Both show oscillatory behavior; in addition, *TRP* shows spikes of activity separated by periods of inactivity reminiscent of the *arr2*^{3} phenotype.

numerically reveals the behavior illustrated in Figure 5-10B and C; both *PKC* and *TRP* show oscillatory behavior. In particular, *TRP* behavior shows bursts of channel opening separated by periods of silence – similar to the bump trains seen in the *arr2*^{3} phenotype (Figure 5-5A). The initial bump is larger, reflecting the system starting far from the fixed point (i.e., at *TRP*=*PKC*=0), and having to traverse to high TRP levels before settling into the oscillatory region (Figure 5-10A, redline). Lastly, the oscillation period in this system is constant (unlike the *arr2*^{3} phenotype); however, the direct inclusion of noise into the model or the use of a stochastic stimulation can lead to successive periods with variable lengths.

In summary then, the topology of the *Drosophila* visual signaling pathway suggests that bump trains may arise from a combination of successive positive

and negative feedback on the TRP channel. Much of the oscillatory behavior can be recapitulated in a simplified two-dimensional non-linear system with an appropriate choice of parameters. How these parameters are related to the *in vivo* situation is unclear and remains an important area of future study. The parameter set shown here does make one clear prediction – that PKC also undergoes oscillatory behavior (Figure 5-10B) (around a relatively high value) during a quantum bump train; it will be interesting to test this *in vivo*, as well as the potential oscillatory behavior of other molecules.

Interestingly, we were able to model bump trains with refractory periods **without** invoking a transitioning InaD; this is in stark contrast to our results that the PDZ5 disulfide is intimately involved in generation of the refractory period. Our initial model (Figure 5-6) suggests that PDZ5 controls the relative values of α and β (i.e., activation of TRP channels via Rhodpsin$\rightarrow$Gq$\rightarrow$PLC-β signaling). Allowing these values to change with time will likely allow oscillations to be more robust to biological noise; in addition, it may allow quantum bump shape to be determined independently of the refractory period (which does not appear to be the case in our current model). Future work will address these issues.

Methods

Electrophysiology

Whole-cell path clamp on isolated photoreceptors was performed as described previously (Ranganathan et al., 1991). Briefly, flies were dark-reared for >12 hour and their retinas were dissected under dim red light in 125mM $CsCl_2$, 10mM HEPES, 30mM sucrose, pH7.1. The retinas were gently triturated into bath solution (120mM NaCl, 5mM KCl, 10mM HEPES, 4mM $MgCl_2$, 24mM proline, 5mM alanine, 1.5mM $CaCl_2$, pH7.1) and were imaged via Hoffman interference contrast on an inverted light microscope (Olympus IX70). Recordings were performed using fiber-filled borosilicate pipettes pulled using a Sutter P-97 (Sutter Instruments) and fire polished to a final resistance of 4-6 MΩ. Electrode solution was 140mM K-gluconate, 10mM HEPES, 2mM $MgSO_4$, 1mM NAD, 4mM MgATP, 0.5mM NaGTP, 0.5mM EGTA, pH7.1. Reversal potentials were between -40 and -70mV; series resistance was typically 10-20 MΩ and was routinely compensated to 75%. No series compensation was used during quantum bump recordings.

Light responses were elicited by a 3nsec flash of 580nm light from a dye-stirred VSL-337-ND-S nitrogen laser (Laser Science, Inc.) controlled by a PCI-DIO32HS board (National Instruments). Unattenuated intensity corresponds to ~10^4 effective photons per flash; light was filtered using neutral density filters (Oriel). Quantum bumps were collected using laser flashes at intensities which generated responses at less than 30% success rate; typically $\log(I/I_0) < -5.0$. Light responses for the stationary fluctuation analysis and synchronization experiments were elicited with constant white light from a Xenon arc lamp (Lambda LS (Sutter); unattenuated intensity ~60 lux), fitted with a *Smart*Shutter (Sutter). Light was filtered using neutral density filters (Oriel). Currents were amplified using an Axopatch 200B (Axon Instruments) and low-pass filtered at 100

or 200Hz (LPF-8, Warner Instrument). Data were collected and digitized via a PCI-6052E DAQ board (National Instruments) using custom software.

Stationary fluctuation analysis was performed as previously described (Johnson and Pak, 1986; Juusola and Hardie, 2001; Wu and Pak, 1978); all calculations were performed in MatLab 7.0 (Mathworks Inc.). In brief, whole-cell recordings were collected from dark-adapted cells without series compensation. Data were recorded either in the dark or upon stimulation with 10 seconds of constant white light at intensities varying from $\log(I/I_0) = -8.5$ to $\log(I/I_0) = -6.0$ in steps of 0.5 log units. Data from the last 2 seconds of each exposure were used to extract average bump parameters using Campbell's theorem for rectangular shot processes, which relates the mean (μ) and variance (σ^2) of the observed current (after subtracting the background (dark) mean and variance) to three parameters – the bump amplitude (*a*), the bump duration (*T*), and the rate of bump generation (λ):

$$\mu = a\lambda T$$
$$\sigma^2 = a^2\lambda T$$

The amplitude, *a*, can then be calculated directly from the ratio of the variance to the mean. The bump duration, *T*, can be estimated from the spectral density function as described previously (Johnson and Pak, 1986; Juusola and Hardie, 2001; Wu and Pak, 1978); briefly, the experimental power spectrum is fit to a normalized single Lorentzian:

$$k\left(\frac{1}{1+(2\pi\tau f)^2}\right)^{n+1}$$

where *f* represents frequency; *k*, τ, *n* are parameters to be fit. *T* and λ can then be calculated as

$$T = \tau \frac{(n!)^2 2^{2n+1}}{(2n!)} \text{ and } \lambda = \frac{\mu}{aT}$$

Isothermal Titration Calorimetry

A peptide consisting of the C-terminal seven amino acids of NorpA PLC-β (Acetyl-NH_2-GKTEFYA-COOH) was titrated (8uL injections of a 1mM peptide stock) against ~2mL of recombinant PDZ5 (or PDZ1) protein (100uM) in 50mM Tris, 100mM NaCl, pH7.5. For some experiments, dithiothreitol (DTT) was supplemented to 100mM to fully reduce PDZ5. Experiments were performed at 20°C in a VP-ITC instrument (Microcal, Inc.) Representative titrations are shown in Figure 5-11.

Figure 5-11 InaD-PDZ5 does not bind the C-terminus of NorpA. Binding experiments using isothermal titration calorimetry of recombinant oxidized PDZ5 (A), reduced PDZ5 (B), $PDZ5^{Cys645Ser}$ (C), and PDZ1 (D) against a peptide from the C-terminal 7 residues of NorpA PLC-β (see Methods for details). No significant heat was liberated during any of these titrations indicating that none of these proteins interacted with the PLC-β C-terminus.

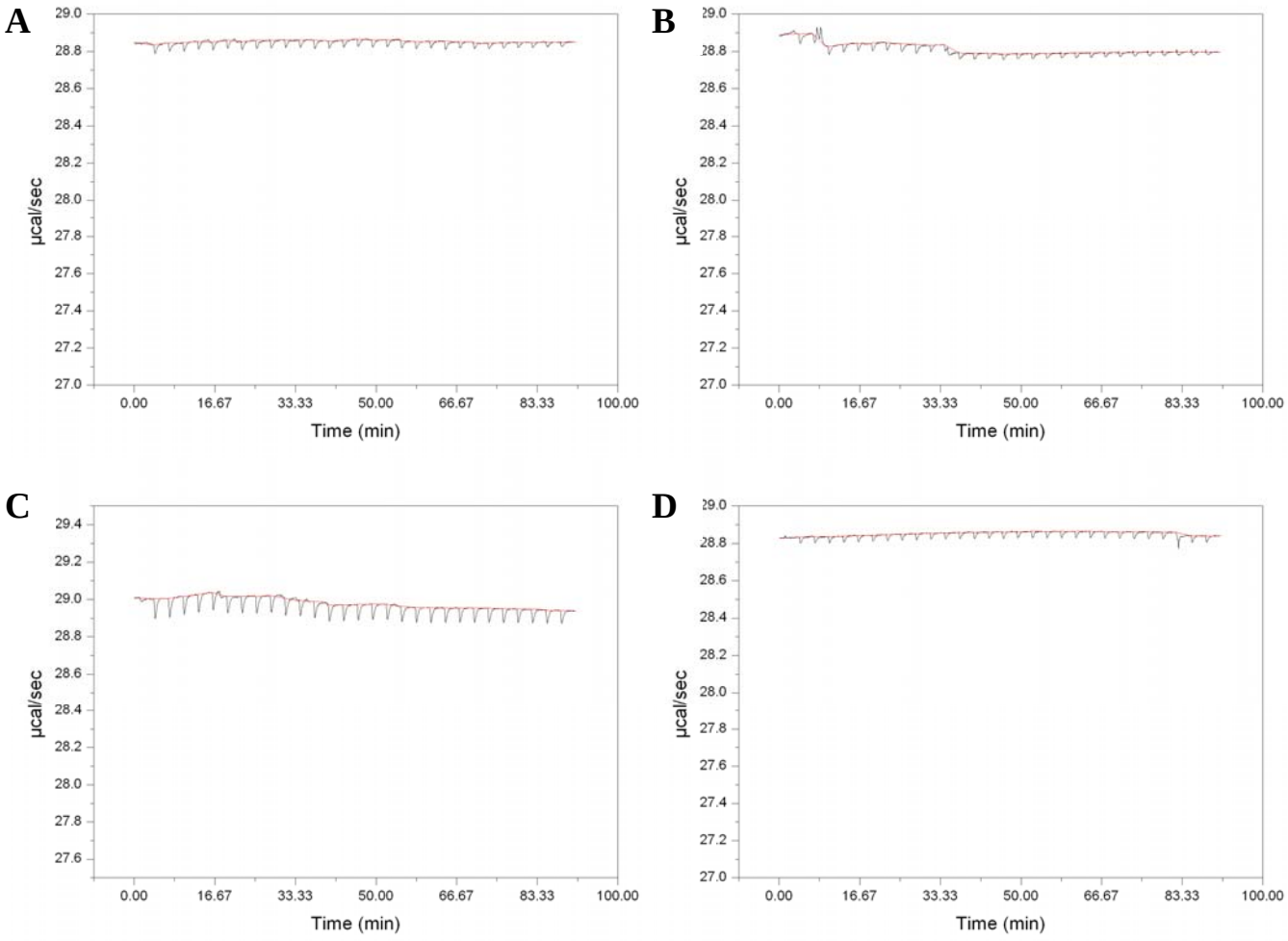
A
B
C
D
µcal/sec
Time (min)
0.00
16.67
33.33
50.00
66.67
83.33
100.00

References

Chen, C. K., Burns, M. E., Spencer, M., Niemi, G. A., Chen, J., Hurley, J. B., Baylor, D. A., and Simon, M. I. (1999). Abnormal photoresponses and light-induced apoptosis in rods lacking rhodopsin kinase. Proc Natl Acad Sci U S A *96*, 3718-3722.

Dolph, P. J., Man-Son-Hing, H., Yarfitz, S., Colley, N. J., Deer, J. R., Spencer, M., Hurley, J. B., and Zuker, C. S. (1994). An eye-specific G beta subunit essential for termination of the phototransduction cascade. Nature *370*, 59-61.

Dolph, P. J., Ranganathan, R., Colley, N. J., Hardy, R. W., Socolich, M., and Zuker, C. S. (1993). Arrestin function in inactivation of G protein-coupled receptor rhodopsin in vivo. Science *260*, 1910-1916.

Hardie, R. C. (2001). Phototransduction in Drosophila melanogaster. J Exp Biol *204*, 3403-3409.

Hardie, R. C., and Raghu, P. (2001). Visual transduction in Drosophila. Nature *413*, 186-193.

Henderson, S. R., Reuss, H., and Hardie, R. C. (2000). Single photon responses in Drosophila photoreceptors and their regulation by Ca2+. J Physiol *524 Pt 1*, 179-194.

Johnson, E. C., and Pak, W. L. (1986). Electrophysiological study of Drosophila rhodopsin mutants. J Gen Physiol *88*, 651-673.

Juusola, M., and Hardie, R. C. (2001). Light adaptation in Drosophila photoreceptors: I. Response dynamics and signaling efficiency at 25 degrees C. J Gen Physiol *117*, 3-25.

Popescu, D. C., Ham, A. J., and Shieh, B. H. (2006). Scaffolding protein INAD regulates deactivation of vision by promoting phosphorylation of transient receptor potential by eye protein kinase C in Drosophila. J Neurosci *26*, 8570-8577.

Ranganathan, R., Harris, G. L., Stevens, C. F., and Zuker, C. S. (1991). A Drosophila mutant defective in extracellular calcium-dependent photoreceptor deactivation and rapid desensitization. Nature *354*, 230-232.

Ranganathan, R., and Stevens, C. F. (1995). Arrestin binding determines the rate of inactivation of the G protein-coupled receptor rhodopsin in vivo. Cell *81*, 841-848.

Scott, K., Sun, Y., Beckingham, K., and Zuker, C. S. (1997). Calmodulin regulation of Drosophila light-activated channels and receptor function mediates termination of the light response in vivo. Cell *91*, 375-383.

Scott, K., and Zuker, C. S. (1998). Assembly of the Drosophila phototransduction cascade into a signalling complex shapes elementary responses. Nature *395*, 805-808.

Smith, D. P., Ranganathan, R., Hardy, R. W., Marx, J., Tsuchida, T., and Zuker, C. S. (1991). Photoreceptor deactivation and retinal degeneration mediated by a photoreceptor-specific protein kinase C. Science *254*, 1478-1484.

Strogatz, S. (1994). Nonlinear Dynamics and Chaos (Cambridge: Westview Press).

Tsunoda, S., Sierralta, J., Sun, Y., Bodner, R., Suzuki, E., Becker, A., Socolich, M., and Zuker, C. S. (1997). A multivalent PDZ-domain protein assembles signalling complexes in a G-protein-coupled cascade. Nature *388*, 243-249.

Wong, F., and Knight, B. W. (1980). Adapting-bump model for eccentric cells of Limulus. J Gen Physiol *76*, 539-557.

Wu, C. F., and Pak, W. L. (1978). Light-induced voltage noise in the photoreceptor of Drosophila melanogaster. J Gen Physiol *71*, 249-268.

Xu, J., Dodd, R. L., Makino, C. L., Simon, M. I., Baylor, D. A., and Chen, J. (1997). Prolonged photoresponses in transgenic mouse rods lacking arrestin. Nature *389*, 505-509.

Chapter Six
Conclusions

The InaD scaffold has served as a primary model system for defining the principles of organized signaling in cells (Scott and Zuker, 1998). Previous work has established the concept of a "transducisome" (Tsunoda et al., 1997) or "signalplex" (Montell, 1998) – essentially a pre-ordered macromolecular complex that carries out a series of signaling reactions with great speed and specificity. Here, we extend this concept by showing that InaD is a dynamic scaffold, undergoing cycles of intramolecular disulfide bond formation in one PDZ domain. Crystallographic studies define this conformational switch at atomic resolution, showing that PDZ5 adopts a canonical PDZ-like structure in the reduced state and a novel structure in the oxidized state in which the binding pocket is distorted. To our knowledge, this work provides the first example of such large scale conformational switching in the PDZ domain, and presents the possibility that other members of this large family of scaffolding modules may also be engaged in dynamic conformational changes. Most importantly, we show a clear biological role for the disulfide-mediated conformational switch in InaD: the light-dependent transient formation of the oxidized state in PDZ5 triggers a refractory period after a single photon response without which cells display excess signaling. Thus, InaD acts more like a dynamic machine than a passive scaffold, controlling reactions that shape the visual response through stimulus-dependent conformational change.

How does light absorption lead to conformational switching in InaD *in vivo*? Formation of the PDZ5 disulfide appears to be regulated by a light-dependent protein

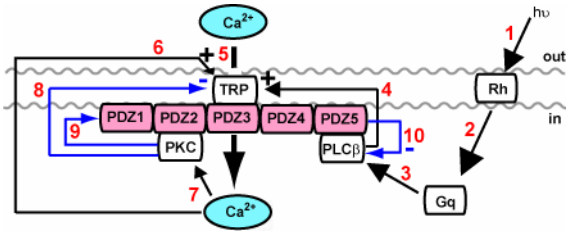

Figure 6-1 Visual signaling in *Drosophila* at the microvillar membrane. Photon absorption by rhodopsin (1) sequentially activates Gqα (2) and PLC-β (3), leading to activation of TRP cation channels (4). Calcium influx (5) activates positive feedback mechanisms, resulting in further TRP channel opening (6). Calcium also activates the eye-specific kinase (eye-PKC, 7) which feedback phosphorylates the TRP channel (stimulating channel closure, 8) and the InaD scaffold (9). Phosphorylation of InaD triggers a reduced→oxidized transition in PDZ5 which negatively regulates PLC-β (through unbinding, 10) allowing the microvillus to enter a refractory, signaling-incompetent state. Return to a signaling permissive state is likely dictated by dephosphorylation of InaD (allowing rebinding of PLC-β) via the action of currently unidentified phosphatases.

kinase, eye-PKC, that feedback phosphorylates the InaD scaffold itself. A plausible model is that the light-dependence of the InaD conformational switch is due to an allosteric effect within InaD rather than due to a change in environmental redox potential. In this scenario, the redox potential of the PDZ5 disulfide is a function of one or more eye-PKC phosphorylation events in InaD; thus, the probability of InaD to exist in the oxidized state is set by the relative rates of eye-PKC activity and opposing phosphatase activities. Many other scaffolding proteins are known to undergo phosphorylation or other post-translational modifications to tune pathway output. For instance, phosphorylation of Ste5 down –regulates the mating response in yeast (Bhattacharyya et al., 2006a) and phosphorylation of Rim1α is required for presynaptic long-term potentiation in embryonic cerebellar neurons (Lonart et al., 2003). How these modifications affect these scaffolds at a structural level is not known. Further work on

InaD phosphorylation and its role in controlling PDZ5 structure and function may contribute a valuable model for understanding the mechanistic basis for feedback regulation of scaffolding proteins in general.

Thus, we propose our final model (Figure 6-1). Light stimulation triggers rhodopsin, Gq, and PLC-β activation, leading to opening of TRP channels. Calcium influx activates positive feedback mechanisms (currently unknown) to stimulate further channel opening, as well as negative feedback mechanisms via activation of PKC. PKC phosphorylates the TRP channel (triggering channel closure) as well as the InaD scaffold. Phosphorylation of InaD triggers PDZ5 to transition from a reduced to an oxidized state; functionally, this causes PLC-β to dissociate from the macromolecular complex, thereby decreasing the efficiency of signaling and sending the microvillus into a refractory state. Return to a signaling-permissive state is likely dictated by the action of phosphatases (currently unidentified) which dephosphorylate InaD, allowing PDZ5 to return to the reduced state and PLC-β to rebind. Of course, many aspects of this model remain untested and future work will focus on examining these issues.

Data from chapters four and five indicate that the refractory period allows channel signaling from individual microvilli to occur in spikes or bump trains, as opposed to continuous channel activity. This response clearly has a role in maintaining fast shutoff of signaling in response to a decline in light levels – the refractory period allows deactivation kinetics to be determined by channel inactivation as opposed to rhodopsin inactivation or GTPase activity. In addition, the ability to signal in spikes may offer an additional advantage for information processing by the photoreceptor cell. The photoreceptor's function is to transfer visual information from the environment to the

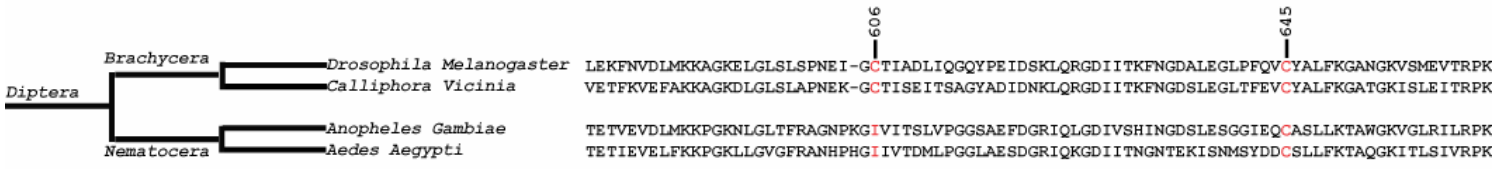

Figure 6-2 Sequences of the PDZ5 orthologs from currently available *Dipteran* genomic databases. Positions 606 and 645 (*Drosophila* numbering) are shown in red. Note that having dual cysteines at positions 606 and 645 is only conserved in the *Brachycera* suborder, and not in the *Nematocera* suborder.

large monopolar cell, and spike trains provide a large capacity for information transfer (MacKay and McCulloch, 1952). These two roles for a refractory period are likely related - natural visual input often contains large, sudden fluctuations in intensity resulting in sparse but intense firing events (Field, 1987; Niven et al., 2004; Ruderman and Bialek, 1994; Tolhurst et al., 1992; van Hateren, 1997; van Hateren and Snippe, 2001). Thus, an important avenue of future work will be to test how the refractory period affects the ability of the photoreceptor to process information; and whether the effect (if any) differs between naturalistic input and white-noise input.

While the core feature of signaling and scaffolding discussed in this thesis are conserved from flying insects to mammals, the specific mechanism discovered here is not: the PDZ5 disulfide appears to be present only in the *Brachycera* suborder of flies (Figure 6-2). This suborder is specific to the fast-flying insects; other flies (such as the *Nematocera* suborder, including *Anopheles* and *Aedes*) display mostly sluggish flying behavior and are nocturnal (Laughlin and Weckstrom, 1993; Osorio, 2007); in addition, they have structurally distinct photoreceptors (Seifert and Smolua, 1990; Zelhof et al., 2006) and do not possess cysteines 606 and 645 in their scaffolding protein. We suspect that the use of the PDZ5 disulfide offers a specific advantage to flight at fast speeds where high frequency visual signals must be processed into aerodynamic decisions. The invertebrate eye has been shown to be an extremely evolvable system with specialization occurring at the family and species level, and even between different sexes of the same

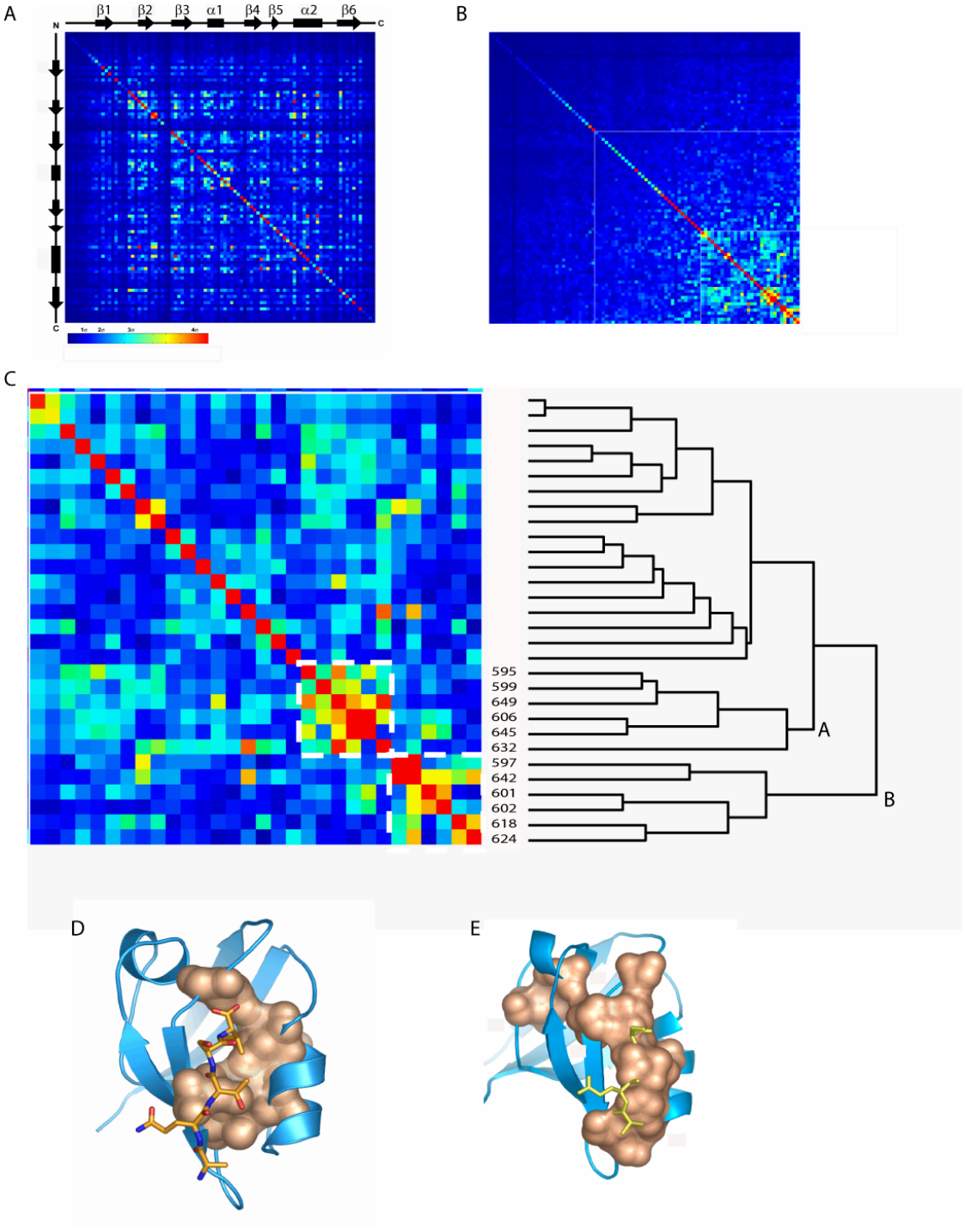
A
β1 β2 β3 α1 β4 β5 α2 β6
N
C
B
C
595
599
649
606
645
632
597
642
601
602
618
624
A
B
D
E

species (Franceschini et al., 1981; Hornstein et al., 2000; Laughlin and Weckstrom, 1993; O'Carroll et al., 1996). Much of this specialization has been attributed to changes in the impedance of the photoreceptor membrane, which is matched to the timescales of the relevant visual input via the combinatorial use of a set of distinctive potassium channels (Laughlin and Weckstrom, 1993). This modular approach allows a species to choose the appropriate set of channels for its behavioral needs. Adaptive changes in the phototransduction cascade are also present, but, here, the underlying molecular mechanism has not been elucidated. Perhaps these changes are encoded in the sequences of the visual scaffolds? A scaffolding protein, which coordinates the organization of the key signaling components, seems ideally suited to serve as a "control" center for the system; thus, we propose that modification of scaffolds provides an attractive way to evolve new features into a signaling pathway without changing its core constituents.

Figure 6-3 Statistical Coupling Analysis of the PDZ domain family. (A) Matrix of statistical coupling values for the PDZ domain family (see Methods). Rows and columns represent PDZ positions (N-terminal to C-terminal as shown by the secondary structure diagram). Each pixel represents the coupling value between the residues for that column and row. Pixels are colored according to the number of standard deviations greater than the mean coupling value in accordance with the color bar shown. (B) Matrix from (A) is sorted using hierarchical clustering. (C) Close-up of the bottom right-hand corner of the matrix from (B), representing the highly co-evolving residues. Positions 606 and 645 are highly co-evolving with one another. In addition, two independent clusters are observed: cluster A (residues 595, 599, 649, 606, 645 and 632) and cluster B (residues 597, 642, 601, 602, 618 and 624). (D) Cluster A is mapped as space-filling residues onto the structure of PSD95-PDZ3 (coordinates 1BE9). Stick bonds show the co-crystallized peptide. (E) Same as (D), except cluster B is mapped as space-filling residues.

The notion that modification of scaffolds might underlie adaptive fitness to specialized selection pressures presumes that proteins (and their individual domains) retain a basic plasticity for the emergence of novel functional mechanisms. As it is well known, scaffolds are often composed of modular units (e.g., PDZ domains, SH3 domains, pY motifs) – and this modularity has been hypothesized to be an important component of the evolvability of the system (Bhattacharyya et al., 2006b; Dueber et al., 2003; Park et al., 2003) In fact, modularity may even be a requirement for a system evolving in a changing environment (Kashtan and Alon, 2005). As such, InaD's composition of five PDZ domains suggests an inherent modularity to its function, analogous to the photoreceptor membrane's decomposition into a set of distinct K+ channels. It will be interesting to test whether these five domains are truly modular, i.e., how they interact with each other functionally and structurally.

However, within the PDZ5 module, how might this disulfide switch have evolved from the typical PDZ domain that does not show such significant conformational changes? Interestingly, an analysis of correlated evolution in the PDZ family indicates that though cysteines at positions 606 and 645 are highly unusual, these two positions are at the heart of a small network of mutually evolving and physically interacting amino acids that is deeply conserved in the PDZ family (Figure 6-3). Interestingly, there are two conserved networks of co-evolving residues in the PDZ family: the 1st (cluster A) containing positions 606 and 645 (along with 595, 599, 649, 632) which dominates the interaction surface between the α2 helix and the β sandwich (Figure 6-3D); the 2nd (cluster B) containing positions 597, 642, 601, 602, 618 and 624 which connects the α1 helix and the binding groove and has been shown to be involved in ligand specificity in

the PDZ domain family (Sharma, 2004). The results suggest that evolution of the PDZ module may also occur in a modular manner – with mutations in cluster A controlling the interaction between the α2 helix and the β sandwich, and mutations in cluster B controlling ligand specificity. Thus, the conformational switch in PDZ5 may be a relatively subtle variation on a conserved motif in the PDZ family. The ability to examine PDZ domain function from atomic structure to organismal behavior will underlie the testing of these models for the evolution of protein domains.

Methods

Co-evolution analysis

Statistical coupling values were calculated essentially as previously described (Lockless and Ranganathan, 1999) with a modified method (Sharma and Ranganathan, in preparation). Briefly, perturbations were made to a multiple sequence alignment (by removing each sequence individually) and the ΔΔE value for each residue was calculated as described (Lockless and Ranganathan, 1999). Coupling values were then calculated as the conservation-weighted correlation coefficient between ΔΔE values for pairs of residues in response to multiple perturbations.

References

Bhattacharyya, R. P., Remenyi, A., Good, M. C., Bashor, C. J., Falick, A. M., and Lim, W. A. (2006a). The Ste5 scaffold allosterically modulates signaling output of the yeast mating pathway. Science *311*, 822-826.

Bhattacharyya, R. P., Remenyi, A., Yeh, B. J., and Lim, W. A. (2006b). Domains, motifs, and scaffolds: the role of modular interactions in the evolution and wiring of cell signaling circuits. Annu Rev Biochem *75*, 655-680.

Dueber, J. E., Yeh, B. J., Chak, K., and Lim, W. A. (2003). Reprogramming control of an allosteric signaling switch through modular recombination. Science *301*, 1904-1908.

Field, D. J. (1987). Relations between the statistics of natural images and the response properties of cortical cells. J Opt Soc Am A *4*, 2379-2394.

Franceschini, N., Hardie, R., Ribi, W., and Kirschfeld, K. (1981). Sexual dimorphism in a photoreceptor. Nature *291*, 241-244.

Hornstein, E. P., O'Carroll, D. C., Anderson, J. C., and Laughlin, S. B. (2000). Sexual dimorphism matches photoreceptor performance to behavioural requirements. Proc Biol Sci *267*, 2111-2117.

Kashtan, N., and Alon, U. (2005). Spontaneous evolution of modularity and network motifs. Proc Natl Acad Sci U S A *102*, 13773-13778.

Laughlin, S. B., and Weckstrom, M. (1993). Fast and slow photoreceptors-a comparative study of the functional diversity of coding and conductances in the Diptera. J Comp Physiol *172*, 593-609.

Lockless, S. W., and Ranganathan, R. (1999). Evolutionarily conserved pathways of energetic connectivity in protein families. Science *286*, 295-299.

Lonart, G., Schoch, S., Kaeser, P. S., Larkin, C. J., Sudhof, T. C., and Linden, D. J. (2003). Phosphorylation of RIM1alpha by PKA triggers presynaptic long-term potentiation at cerebellar parallel fiber synapses. Cell *115*, 49-60.

MacKay, D. M., and McCulloch, W. S. (1952). The Limiting Information Capacity of a Neuronal Link. Bulletin of Mathematical Biophysics *14*, 127.

Montell, C. (1998). TRP trapped in fly signaling web. Curr Opin Neurobiol *8*, 389-397.

Niven, J. E., Vahasoyrinki, M., Juusola, M., and French, A. S. (2004). Interactions between light-induced currents, voltage-gated currents, and input signal properties in Drosophila photoreceptors. J Neurophysiol *91*, 2696-2706.

O'Carroll, D. C., Bidweii, N. J., Laughlin, S. B., and Warrant, E. J. (1996). Insect motion detectors matched to visual ecology. Nature *382*, 63-66.

Osorio, D. (2007). Spam and the evolution of the fly's eye. Bioessays *29*, 111-115.

Park, S. H., Zarrinpar, A., and Lim, W. A. (2003). Rewiring MAP kinase pathways using alternative scaffold assembly mechanisms. Science *299*, 1061-1064.

Ruderman, D. L., and Bialek, W. (1994). Statistics of natural images: Scaling in the woods. Phys Rev Lett *73*, 814-817.

Scott, K., and Zuker, C. S. (1998). Assembly of the Drosophila phototransduction cascade into a signalling complex shapes elementary responses. Nature *395*, 805-808.

Seifert, P., and Smolua, U. (1990). Adaptive structural changes indicate an evolutionary progression towards the open rhabdom in diptera. J Evol Biol *3*, 225-242.

Sharma, R. (2004) Logic and mechanism of an evolutionarily conserved interaction in PDZ domains, University of Texas Southwestern Medical Center, Dallas.

Tolhurst, D. J., Tadmor, Y., and Chao, T. (1992). Amplitude spectra of natural images. Ophthalmic Physiol Opt *12*, 229-232.

Tsunoda, S., Sierralta, J., Sun, Y., Bodner, R., Suzuki, E., Becker, A., Socolich, M., and Zuker, C. S. (1997). A multivalent PDZ-domain protein assembles signalling complexes in a G-protein-coupled cascade. Nature *388*, 243-249.

van Hateren, J. H. (1997). Processing of natural time series of intensities by the visual system of the blowfly. Vision Res *37*, 3407-3416.

van Hateren, J. H., and Snippe, H. P. (2001). Information theoretical evaluation of parametric models of gain control in blowfly photoreceptor cells. Vision Res *41*, 1851-1865.

Zelhof, A. C., Hardy, R. W., Becker, A., and Zuker, C. S. (2006). Transforming the architecture of compound eyes. Nature *443*, 696-699.